Bioactive coating for titanium based bone anchored implants

Doctoral thesis by
Matthias Johannes Frank

Department of Biomaterials
Institute of Clinical Dentistry
Faculty of Dentistry
University of Oslo
Norway
2013

"There is no authority who decides what is a good idea."

Richard P. Feynman

PREFACE

TABLE OF CONTENT

LIST OF PUBLICATIONS

This thesis is based in the following papers, which will be referred to by their Roman numerals in the text.

Paper I   Matthias J. Frank[*], Martin S. Walter[*], S. Petter Lyngstadaas, Erich Wintermantel and Håvard J. Haugen, Hydrogen content in titanium and a titanium-zirconium alloy after acid etching, Materials Science and Engineering: C, 2013, 33, 1282-1288.

Paper II   Matthias J. Frank, Martin S. Walter, S. Petter Lyngstadaas and Håvard J. Haugen. Polarization of modified titanium and titanium-zirconium creates nano-structures while hydride formation is modulated. 2013.
                 Revised version accepted in Applied Surface Science, DOI: 10.1016/j.apsusc.2013.04.059.

Paper III   Matthias J. Frank, Martin S. Walter, Marina Rubert, Bernd Thiede, Marta Monjo, Janne E. Reseland, Håvard J. Haugen, and S. Petter Lyngstadaas. Novel integrated technique for bioactive coating of metal implant materials. 2013.
                 In submission.

Paper IV   Matthias J. Frank, Martin S. Walter, Hanna Tiainen, Marina Rubert, Marta Monjo, S. Petter Lyngstadaas and Håvard J. Haugen. Bioactive coating of metal implant materials with strontium. 2013.
                 Revised version accepted in Materials Science: Materials in Medicine, DOI: 10.1007/s10856-013-5007-1; 2013.

Paper V   Matthias J. Frank, Martin S. Walter, Marta Monjo, Sebastian Geißler, Maria Satué, Hans Jacob Rønold, Jan Eirik Ellingsen, Johann Caspar Wohlfahrt, Janne E. Reseland, S. Petter Lyngstadaas and Håvard J. Haugen. Effect of bioactively coated titanium-zirconium alloy with enamel matrix derivate and strontium on bone growth in rabbits. 2013.
                 Manuscript.

All publications were reproduced with kind permission of the respective journal.

---

[*] *First and second author contributed equally to this study.*

1   INTRODUCTION

Teeth are important tools for processing food, act as a sensory organ and determine the appearance of humans and other vertebrates. Tooth-loss due to age, diseases or accidents does not only lower our personal comfort but may even be life-threatening. Thus, tooth replacement in order to restore tooth-function is not a new idea. The first known dental implants that were fully integrated in the bone were made from nacre by the Maya over 2000 years ago.[1] Anyhow, this knowledge has not been used for a long time, as partial, complete, fixed, or removable dentures were state of the art for restoring teeth-function for decades. This changed when Brånemark introduced screw shaped titanium implants for the bone.[2,3] Today, endosseous dental implants are preferred over dental prostheses for esthetical reasons, increased patient comfort and superior function.[4] The ongoing demographic change towards an increasingly aging society contributes to the rising demand for tooth replacement.[5] Current screw shaped endosseous dental implants are commonly made from titanium and its alloys. Titanium based materials are preferred for use as an implant due to their excellent mechanical properties, corrosion resistance, and biocompatibility.[6-8]

Biocompatibility was defined by Williams as "the ability of a material to perform with an appropriate host response in a specific application."[9] In a definition that is more specific for bone implants, biocompatibility can be classified in six categories. According to those categories an implant is either bioincompatible, biocompatible, bioinert, bioactive, bioinductive, or bioconductive.[10] In the case of endosseous dental implants, a bioactive behavior is desired. According to the aforementioned bone-specific definition, a bioactive implant shows positive interaction with differentiation of the tissue that leads to bonding and adhesion of the bone in the peri-implant region.[10] Since the integration of an implant takes place at the bone-implant interface, the implant`s material, shape, surface morphology, surface topography, and surface chemistry largely affect the biological response to any implant. On the other side, the quality and quantity of the bone at the implantation site, the surgical procedure, unique patient variables and mechanical loading of the implant significantly affect the short- and long-term success of an endosseous dental implant.[11-16]

1.1   Bone formation and bone remodeling

Since endosseous implants are placed in bone, it is important to understand the mechanism involved in bone formation and bone remodeling. Generally, all bone is made from osteoblasts while osteoclasts are responsible for bone resorption. During bone remodeling both cells are needed in order to resorb the current bone and to generate new bone thereafter. While osteoblasts derive from mesenchymal stem cells, osteoclasts derive from hematopoietic stem cells.[17] By influencing the signaling pathways during the expression of different genes, biomolecules can influence bone formation and bone remodeling by promoting specific cell differentiation. Moreover, the gene expression can be assessed in order to determine the influence of a biomaterial on cell differentiation.[18-20] Typically, osteocalcin (OC), bone morphogenetic protein-2 (BMP-2), alkaline phosphatase (ALP), and collagen type 1 (Coll-1) are related to bone formation and osteoblast proliferation, differentiation and matrix maturation.[21,22] Markers like proton-

ATPase (H$^+$-ATP), tartrate-resistant acid phosphatase (TRAP), calcitonin receptor (Calc-R) are generally related to osteoclast differentiation and function.[23] Inflammatory markers like the pro-inflammatory tumor necrosis factor-alpha (TNF-α), interleukin 6 (IL-6), and the anti-inflamatory interleukin 10 (IL-10) are commonly used to assess the reaction of the immune system to an implant.[24]

1.2   Peri-implant bone healing

In order to understand the working principle of an endosseous implant, the underlying principles of implant fixation in the bone have to be understood. When an implant is placed in bone, the primary stability is provided by the implant`s shape and surface topography. That is the reason why a screw-shape is preferred for endosseous dental implants.

Contact and distance osteogenisis are the two possible ways of peri-implant bone healing. Contact osteogenisis is characterized by bone forming on the implant surface first that leads to bone apposition to the implant surface. In contrast, during distance osteogenisis, bone forms first on the old bone in the peri-implant region and then approximates the implant surface and eventually surrounds it. In most cases, peri-implant bone healing is a combination of both mechanisms whereas the prevailing mechanism determines an integration or encapsulation of the implant in the bone tissue.[25]

Placement of an implant in bone leads to unavoidable damage of blood vessels at the implantation site. This leads to the formation of a blood clot in the peri-implant region and adsorption of proteins from the surrounding blood and tissue fluids at the implant`s surface. Thereafter, inflammatory and connective tissue cells approach the implant`s surface alongside of matrix proteins that are adsorbed at the implant surface. This allows adhesion of osteogenic cells to the implant`s surface and formation of connected bone tissue on the surface.[14,25] This phase determines if bone will form in contact to the implant (contact osteogenisis) or if the implant becomes encapsulated by bone tissue (distance osteogenisis).[25]

It is critical for the initial mechanical stabilization of an implant and the mechanism of bone formation what type of bone an implant is placed in. The bone type is often pooled in the general term "bone quality" among other qualitative properties of the bone at the implant site.[25] The two major kinds of bone are the spongy trabecular bone and the compact cortical bone.[26] Yet, cortical and trabecular bone do not only differ in their general structure but also in their healing behavior. While peri-implant healing of cortical bone is achieved exclusively by lamellar remodeling that typically leads to distance osteogenisis, trabecular bone may rapidly develop new bone tissue by attracting osteogenic cells and favors contact osteogenisis.[25] Generally, all bone is synthesized by osteoblasts. Once those have been embedded into bone as unmovable osteocytes, other osteogenic cells are needed for appending further additions to the bone. Thus, the cells that are already bond in the existing bone matrix may no longer influence the ongoing process of bone-healing at the bone-implant interface.[25]

Originally, implants were only placed in the compact cortical bone that provided adequate initial fixation. The compact design of the cortical bone provides a good ground for physically interlocking with the threads of a screw shaped endosseous implant. Anyhow, lamellar remodeling of the cortical bone at the peri-implant interface may lead to long-term implant

failure, as implant is not integrated in the bone. Such an encapsulation of the implant by the surrounding tissue can be classified as bioinert behavior according to the abovementioned bone-specific definition of biocompatibility.[10]

Over the recent years, implants have also commonly been placed in posterior sites with reduced cortical bone. This leads to decreased initial implant stability and may result in early implant failure.[25,27-29] In contrast to reduced initial stability, trabecular bone provides a rapid healing by attracting osteogenic cells to the implantation site during bone-healing. Thus the initially inferior properties of the trabecular bone may be compensated by its active growth towards the implant surface.[10,25,26]

1.3   Current endosseous dental implants

Modifications of the surface micro- and nano-topography have been subject of extended research in improving osseointegration of endosseous dental implants. Studies have shown that implants with increased surface roughness promoted bone healing and formation of a stable interface between mineralized bone and the surface of the implant.[30-34] A moderately rough surface with a surface roughness between 1.16 µm and 3 µm has been shown to be optimal for bone implants.[35-39]

Many dental implants available on the market today feature such a moderately rough surface. Screw shaped dental implants like TiOBlast® (Astra Tech AB, Sweden), TiUnite™ (Nobel Biocare, Sweden), and SLA® (Institut Straumann AG, Switzerland) have shown clinical success for over 10 years.[39] Moreover, such moderately rough implants may be placed under more challenging conditions than implants with a turned surface.[39] While the surface roughness of most implants remained mostly unchanged during recent implant developments, the focus was shifted to enhancing the surface chemistry of an implant.

Modifications of the surface chemistry can hardly be achieved without simultaneously influencing its surface morphology. Usually, the surface of commercially pure titanium is covered by a 2 nm to 6 nm thick oxide layer. This oxide layer forms spontaneously when titanium comes into contact with oxygen.[40] Previous studies have used anodic oxidation to increase oxide layer thickness on titanium implants more than tenfold in quest for better biological performance. Anyhow, this did hardly improve hard tissue healing.[41-43] Etching in various acids has been shown to alter the surface`s micro- and nano-topography but also to change the surface chemistry.[11,44,45] Acid etching demonstrated to enhance titanium`s surface reactivity by increasing surface hydride levels.[45-47] Recent studies have suggested a possible relation between a surface`s hydrogen content and its *in vivo* performance.[48,49]

While improving the performance of dental implants, the moderately rough surface of many implants has been subject to some modifications. The SLActive® (Institut Straumann AG, Switzerland) implant surface e.g. is a modified design of the original SLA® surface. The surface energy and wettability of the original sand-blasted and acid-etched (SBAE) SLA® surface has been improved by reducing environmental carbon contamination. The reactive surface created by the etching process was maintained by handling of the implants under protective cover gas and storing them in saline solution.[50,51] This surface modification is not limited to commercially pure grade IV titanium (Ti), but has successfully been used for titanium-zirconium alloy (TiZr). The Roxolid™ SLActive® implant system (Institut Straumann AG, Switzerland) is such a TiZr alloy

with an optimized version (SLActive®) of the SBAE surface. This alloy has shown an *in vivo* performance comparable or even superior to the performance of Ti SLActive® implants.[52,53] The advantage of the TiZr alloy is its increased fracture toughness and corrosion resistance over commercially pure Ti.[7,8] This allows the production of implants with smaller diameters that are more suitable for use in critical implantation sites, such as in the front mandible where bone is scarce.[53] Another approach that was taken in the OsseoSpeed™ system (Astra Tech AB, Sweden) used etching in hydrofluoric acid for surface-etching. This surface not only demonstrated elevated surface hydrogen levels but also additional traces of fluorine (F) on the surface. Implants with such a fluorine-modified surface exhibited enhanced bone integration.[34,54-56] Although, novel materials could contribute to improve the implant`s mechanical properties and novel surface-modifications increased the clinical success of dental implants, the requirements a patient must fulfill in order to be eligible for an endosseous dental implant have not been improved significantly.

Despite the respectable success of most implants systems, there have been recent reports about long-term bone resorption and infections around current implants that lead to peri-implantitis and challenge the use of those implants.[29,57,58] Moreover, some patients are still not eligible for an endosseous dental implant. Challenges lie in patients who e.g. experienced radiation therapy, have poor oral hygiene, or are extensive smokers. These patient groups still show significantly lower success rates for early implant stability when compared to patients without the aforementioned conditions. General bone quality and quantity are also a frequent reason for early dental implant failure.[27-29] By contrast, other potential risks like e.g. diabetes can already be reduced by controlling the state of the disease.[59] Thus the current, bioinert implants shall be refined to actively support peri-implant bone healing. Besides improved long term stability, a bioactive surface may also provide increased primary stability when considering the results presented by Puleo and Nanci, who showed that bone formation extending away from the implant generally was 30% faster than bone formation towards the implant.[14]

1.4   Quest for a bioactive implant-surface

In the quest for an improved endosseous implant surface it is not intended to create a whole new implant surface but to refine existing implant surfaces utilizing their advantages like the general screw-shaped design and the moderately rough surface that have demonstrated a history of clinical success in providing primary implant stability.[60-64] With the intention of helping patients who are not yet eligible for placement of an endosseous dental implant and in order to improve long-term stability, a biomedical surface modification that actively supports bone healing at the bone-implant interface is desired. A bioactive coating of the surface is preferred over possible systemic administration of implant-supplementary bone healing agents or drugs due to the local effect of a coating on bone healing directly at the implantation site. Another advantage of a coating with a local effect is that it requires a significantly decreased amount of the active agent compared to systemically administered supplements. This may also reduce or avert undesired adverse reactions of the active agent.[65-67] Thus, the holy grail of ongoing research is the biomedical modification of the implant surface by coating of the implant surface with biomolecules that actively support bone healing or even possess osseoinductive properties. Although large efforts have been made over the recent decades to create such a bioactive surface,

no prevailing technique has been reported that could create an implant with bioactive properties that was suitable for commercial implant production nor has any modification demonstrated increased long term success over existing solutions. Coating with calcium phosphate has been subject to extensive research due to its similarity to the multi-substituted hydroxyapatite bone is made of.[68-71] Other coatings used e.g. Sr-substituted Ca-phosphate,[72] sol–gel coatings containing different bioactive particles of glass, glass-ceramic or hydroxyapatite[73], coating by soaking in bone morphogenetic protein-2,[74,75] or coating with peptides and extracellular matrix proteins.[76] Most surface coatings rather adsorb the coating onto the surface instead of creating a link between the surface and the coating.[77]
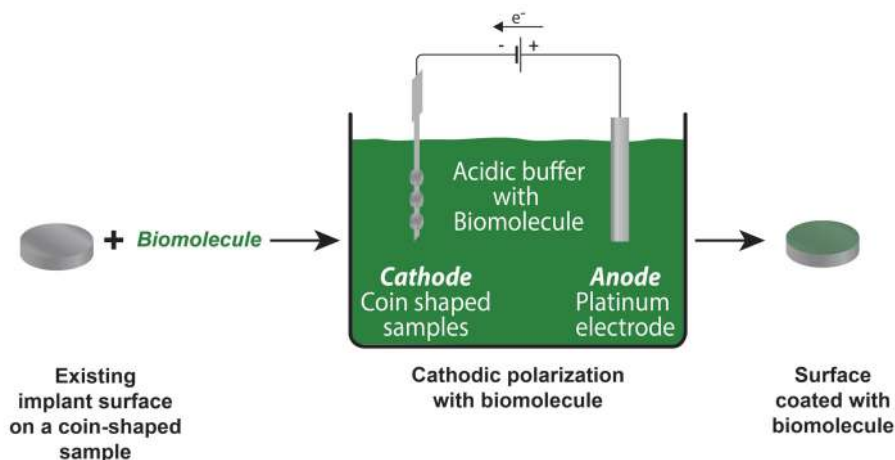
Figure 1.1   Schematic illustration of the electric polarization process suggested by Lyngstadaas and Ellingsen[78] for creating a hydride layer on the surface which may be used for attaching charged biomolecules to the surface. The illustration shows coin-shaped samples like they were used in this study.

Lyngstadaas and Ellingsen suggested to use an electric polarization process for creating a hydride layer on the surface which may be used for attaching charged biomolecules to the surface (Figure 1.1).[78] The advantage of such an electro-coating process over techniques like plasma coating or soaking in saturated solution is the creation of a direct link between the material`s hydride layer and the biomolecule without an additional linking layer. Previous studies showed that cathodic polarization in an acidic solution was successfully used to increase surface hydrogen levels.[79,80] A would-be biomolecule for use in such an electro-coating of the surface by polarization must be ionizeable and should ideally support bone attachment, peri-implant bone healing, induce peri-implant osteogenisis or have some other long term improving effect on an implant`s performance.

Enamel matrix derivate (EMD) was selected as one candidate biomolecule for the surface coating. EMD is a protein-mixture that is composed of multiple enamel extracellular matrix proteins of which more than 95% are amelogenins whereas less than the remaining 5% are proline-rich non-amelogenin derived peptides derived mainly from enamelin.[81-84] EMD has shown promising results in supporting periodontal bone regeneration.[85-87] Other studies have shown an angiogenic

effect of EMD.[87] The potential of EMD for use in bone regeneration and hence implantology and the significant positive influence of amelogenins on wound healing and bone formation has been suggested.[83,88,89] For completeness, it should be mentioned that some studies have reported varying results regarding the direct role of amelogenin in bone formation.[90,91] EMD is also the active component of the commercially available product Emdogain® (Institut Straumann AG, Basel, Switzerland). Emdogain® basically consists of EMD that has been combined with a *propylene glycol alginate* carrier-gel for making it applicable for clinical use.[84,92] Emdogain® has shown favorable success in periodontal treatment.[93-96] As the major components in EMD have been reported to have ampholytic properties, is stable and soluble at high temperatures and low pH, it appeared well suited for use in an electro-coating process.[97-100] Moreover, Emdogain® has been classified as a medical device by the Food and Drug Administration (FDA) in the USA.[101] Thus, a surface coating of an existing dental implant system with EMD would most likely be classifiable as the combination of two existing devices in the potential case of such a product, which has large implications on the marked approval process of such an implant with the FDA and on the costs involved.

Strontium (Sr) was selected as an alternative biomolecule for coating the surface. Although technically strontium is not a biomolecule but an alkaline earth metal, it was considered as a biomolecule in this study for its bioactive properties. The beneficial effect of Sr in the process of bone remodeling has been subject to several studies.[102,103] Strontium has a physical and chemical similarity to calcium, which is the major component of hydroxyapatite in bone.[104] It has been suggested by several *in vitro* and *in vivo* studies that Sr affects bone resorption and bone formation by reducing pre-osteoclast differentiation and osteoclast function and survival. At the same time bone formation is supported by activation of pre-osteoblast replication and by osteoblast differentiation and survival.[102,103] As Sr is an alkaline earth metal, it may be ionized for use in an electro-coating process.

This thesis chose to use a highly active SBAE surface with comparably high hydrogen levels and relatively low oxide levels because such a surface may further facilitate an electro-coating process for actively attaching the biomolecules EMD and Sr to the hydride layer by use of the method suggested by Lyngstadaas and Ellingsen.[78]

2   DESIGN OF THE RESEARCH WORK

2.1   Hypothesis

The general hypothesis was that a hydrogen-rich, sand-blasted and acid-etched titanium based surface may provide an appropriate substrate for linker-free attachment of biomolecules in an integrated cathodic polarization process without hampering the integrity, bioavailability and bioactivity of the named biomolecules. The specific sub-hypothesis was that such a coated surface can be used to improve implant performance.

2.2   Aim of research

Based on the proposed hypotheses, the main aim of this thesis was to demonstrate that SBAE surfaces of grade IV titanium and titanium-zirconium alloy can be coated with the biomolecules EMD and Sr using a cathodic polarization process. Furthermore, the de facto "bioactivity" of the different surface coatings was to be evaluated by assessing their *in vitro* and *in vivo* performance.

The main aim was further divided into the following sub-aims:

1. Assessment of the base materials` hydrogen content and surface topography (Paper I).
2. Identification of viable process parameters for a surface coating based on the development of the hydrogen layer during cathodic polarization in order to maximize coating efficiency and to minimize process time (Paper II).
3. Demonstration of an effective surface coating with EMD (Paper III) and Sr (Paper IV)
4. Demonstration of bio-availability and maintained function of the surface coatings with EMD (Paper III) and Sr (Paper IV) in *in vitro* studies.
5. Assessment of the biological response in bone to the EMD and Sr coated implant surfaces in a verified animal model (Paper V).

The flowchart presented in Figure 2.1 illustrates the design of this thesis. The flowchart clarifies how each sub-aim contributed to accomplishing the general aim of research. The flowchart also suggested a possible step for follow up research to the work presented in this thesis by transferring the established process to actual implants and their specific requirements.
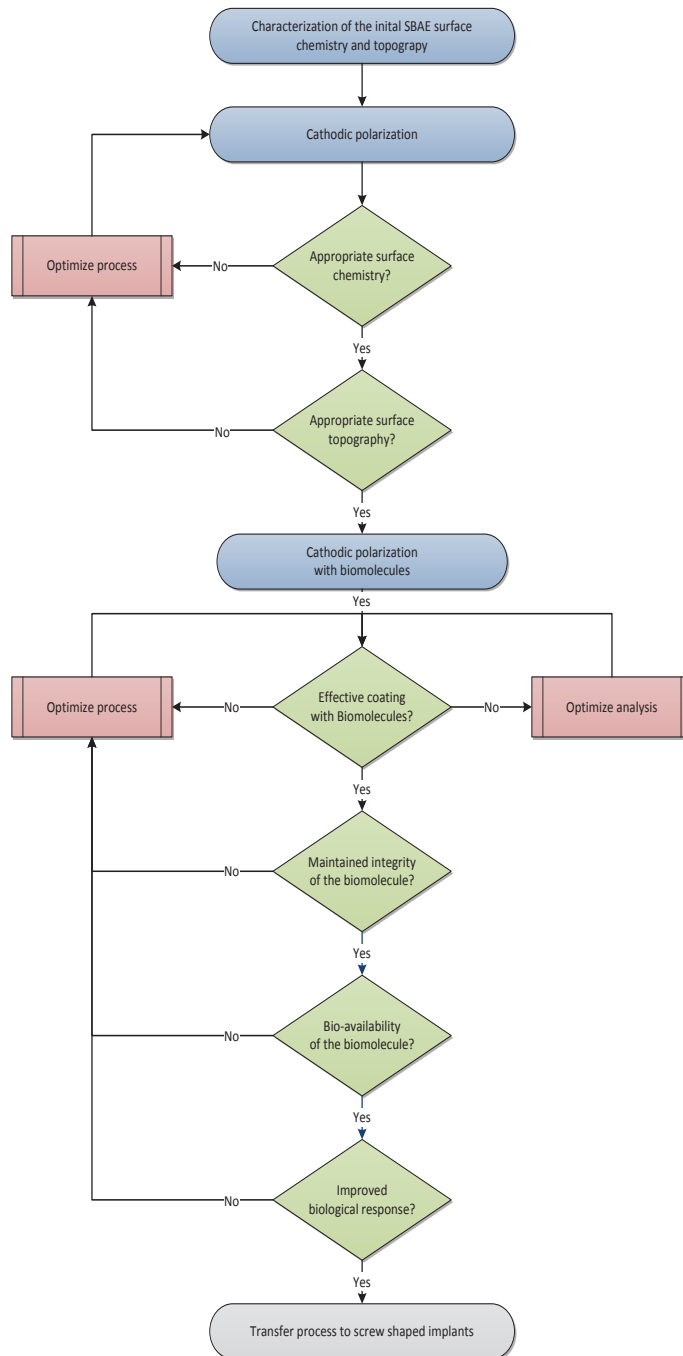
Figure 2.1   Design of the research process to pursue the aim of research is illustrated in vertical direction. In addition to the steps assessed in this thesis, the flowchart envisioned the next step to follow up the work of this thesis towards the ultimate goal this research shall lead to, by transferring the coating process to screw shaped implants.

3 EXPERIMENTAL DESIGN

This chapter intended to discuss methods used in this thesis by providing the reasons for selecting a specific method with regards to the aim of research. Moreover, this chapter discussed how each method performed during the experiments and how the results were interpreted. All specific details about the equipment, materials, and specific settings used were provided in the "materials and methods" section of each individual paper (Papers I-V).

3.1 Study materials

This study used commercially pure grade IV titanium (Ti) and a titanium-zirconium (TiZr) alloy containing 13%–17% of Zr (Figure 3.1). The TiZr alloy is commercially known as Roxolid® (Institut Straumann AG). The SBAE surface was prepared according to the same procedures used for creating the commercially available Straumann SLActive® surface. Surfaces were sand-blasted with large-grit (0.25 mm–0.5 mm) aluminum oxide particles and acid-etched in a mixture of hydrochloric and sulfuric acid at 125°C–130°C for 5 minutes. Thereafter, samples were handled under nitrogen cover gas and stored in 0.9% NaCl solution in order to avoid carbon contamination and to maintain the reactivity of the surface (Figure 3.2). This surface modification has been previously described and discussed in other studies.[45,50]
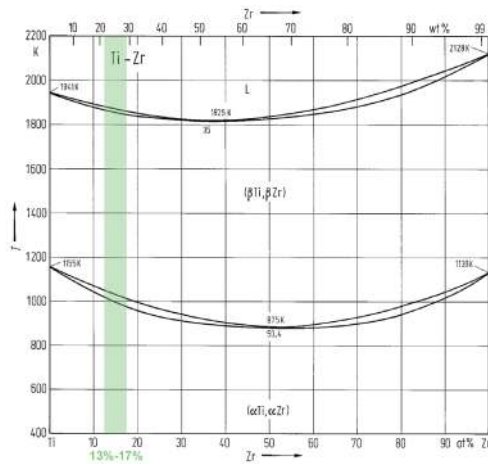
Figure 3.1   The titanium-zirconium system (Ti-Zr). The region of the alloy used in this study, between 13% and 17%, was highlighted in the figure (green region) (Figure was adapted from Predel[105]).
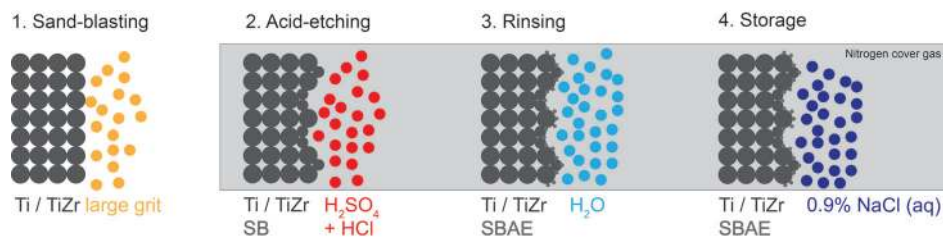
Figure 3.2   Production process of the SBAE surface for Ti and TiZr. In step 1 the material was sand-blasted with large-grit aluminum oxide. In a second step, the surface was acid-etched in a mixture of sulfuric and hydrochloric acid. After acid-etching, the surface was handled under nitrogen cover gas while it was rinsed with water (step 3) and thereafter stored in saline solution (step 4).

This study used coin-shaped samples with a diameter of either 4.5 mm (Papers I-IV) or 6.25 mm (Paper V) and a height of 2 mm. The special coin-shape of the samples required a manual production of the samples as opposed to the production of the screw-shaped implants, which are produced in a largely automated process. For this reason, the surface used in this study was not called SLActive® but SBAE. The coin-shaped samples used in this thesis were only sand-blasted and acid-etched from the front and on the sides. The surface at the backside of the coins was kept smooth. Moreover, the backside of the coin contained a central, threaded hole that was used for mounting the coins during polarization and for detachment in the animal study.

Coin-shaped samples were chosen in order to facilitate access to the surface for further analysis. In contrast to a screw shaped dental implant, which has a cylindrical, threaded shape, coins provided a leveled surface that was fairly easy to access. Despite the advantage of the geometry for the purpose of surface analysis, the use of coin shaped implants also involved certain limitations. As coins have been produced for research purposes, there was no highly automated production process available for creating the SBAE surface. Although everything was performed to a standardized procedure that was a handcrafted version of the SLActive® production, the human factor could not be neglected as a source of intra-batch and inner-batch variations of the SBAE coins. SIMS analysis of the hydrogen content of the custom made coins from the same production batch for TiZr SBAE revealed significant deviations for some coins (Figure 3.3).
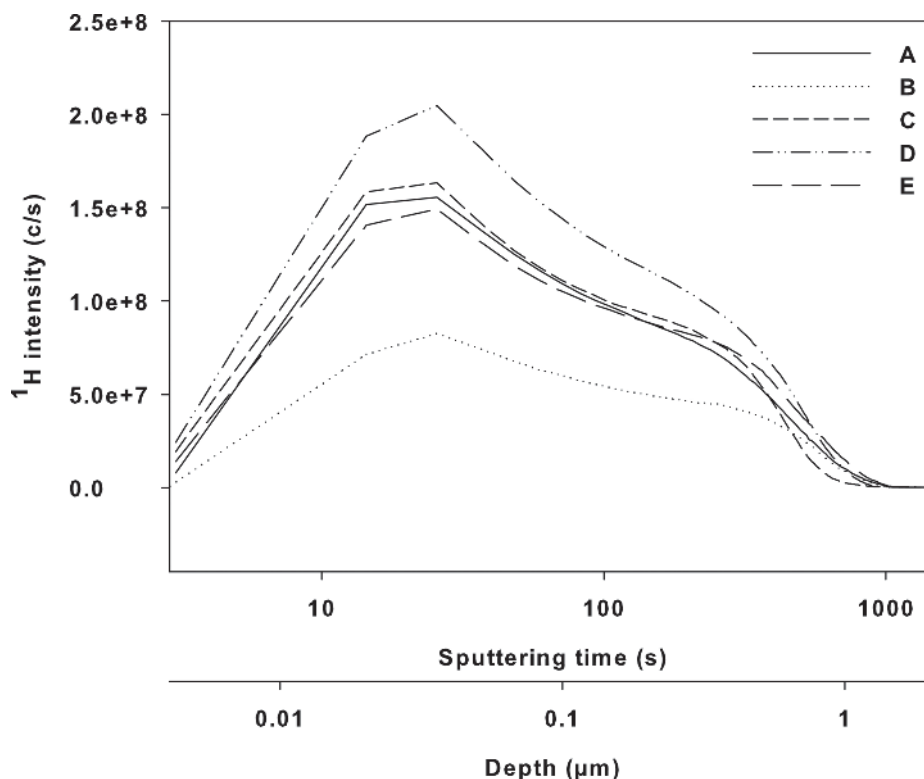
Figure 3.3 SIMS ^{1}H depth profiles from a measurement on five individual TiZr SBAE coins from the same production batch (A-E). Sample B and D revealed significantly different hydrogen levels.

Another difference between screw-shaped dental implants and the coin-shaped samples was their packing. While screw-shaped dental implants are commonly packed in individual tubes, the coins were provided in batches of up to ten coins inside a single vial. Multiple coins per vial lead to coin to coin interaction during transport and storage of the coins. As a result of the interaction between the coins, some coins revealed large scratches that were clearly visible to the naked eye. In addition to these large scratches, the coins also revealed small scratches at the micro-level that were only visible when using magnification. Besides the local alteration of the surface`s topography and morphology, the scratches may also have had an influence on the chemistry of the SBAE surface. Scratching of the surface may have abraded the hydrogen layer. If Ti, or TiZr respectively, was laid open by abrasion of the hydride layer, the open spot was expected to have oxidized immediately when in contact with oxygen. Such a change in surface chemistry was believed to have influenced the polarization process. It has been shown that the electrical conductivity and the polarization resistance of pure titanium, titanium-oxide, titanium-hydride, and titanium-alloys are very different.[106-109] The oxygen layer at the scratch may potentially have been thicker than it was observed for the oxide layer on top of a hydride layer (Paper I).[79] If the surface was not oxidized, the hydride layer could still have been damaged and the naked Ti or TiZr would have reacted differently to the polarization process. In this case, the absence of a hydrogen layer would even allow hydrogen diffusion into the material (Paper II). Moreover, this

spot would most likely have been the point with the least polarization resistance.[110,111] Although this has not been observed during the experiments conducted for this thesis, this may potentially lead to local pitting corrosion. In summary, the scratches observed for some samples may be a reason for inconsistencies experienced during measuring repeated surface coatings. Not all scratches were visible to the naked eye, hence only the coins that were clearly damaged by scratches could be removed when the coins were screened before each experiment in order to reduce the variability of the substrate.

3.2   The electro-coating process

Electro-coating of the study materials was done by a cathodic polarization process (Figure 1.1, Figure 3.4 A). The study materials were mounted as the cathode while a platinum (Pt) electrode acted as the anode. While a buffer made of acetic acid and sodium-acetate was used for coating with EMD (Paper III), the sodium-acetate was replaced by strontium-acetate for the Sr-coating (Paper IV). Table 3.1 summarizes all groups that were used in this thesis. The specific details of the buffers used for surface coating have been described in the respective papers.

Table 3.1   Summary of all groups that were used in this thesis. The group names were used in combination with the material names like e.g. Ti SBAE and TiZr SBAE.

Group	Surface modification
SBAE	Sand-blasted and acid-etched surface that was comparable to the Straumann SLActive® surface
pol	Polarized only group 2 M Acetic acid and sodium-acetate buffer, pH=3
EMD	EMD-coated group 2 M Acetic acid and sodium-acetate buffer with 0.01mg/ml EMD, pH=3
Sr	Sr-coated group 0.25 M Acetic acid and Sr-acetate buffer, pH=5
Sr+NaCl	Sr-coated group with additional NaCl in the buffer 0.25 M Acetic acid and Sr-acetate buffer with 0.1M NaCl, pH=5
Sr+NaF	Sr-coated group with additional NaF in the buffer 0.25 M Acetic acid and Sr-acetate buffer with 0.1M NaF, pH=5
Sr+HFp	Sr-coated group with pickling in 0.2% HF for 2 min before electro-coating 0.25 M Acetic acid and Sr-acetate buffer, pH=5

This study used two different setups for polarization. The first setup consisted of a power supply with a single output channel. All coins were mounted on a long, rectangular titanium electrode as it has been used in this studies described by Lamolle et al.[44] The electrode had holes that allowed mounting the coins "back to back" with the sample holder in between the coins by using the threaded holes on the back of each coin and a threaded pin to connect them (Figure 3.4 B). A fine-meshed Pt-cylinder was used as the counter electrode for this setup. This setup was set to a constant output current according to the total surface area that was submerged into the buffer. The

studies conducted in Papers I–IV have been coated using this setup. More specific details about the hardware used in this setup may be found in Papers I–IV.

Although this setup had the advantage of a comparably simple setup for polarizing the samples, it did not allow any adjustments of the current to the specific resistance of a single sample. With respect to the variability in the substrate described earlier (section 3.1), this setup did not compensate for diverse electrical resistance of the samples. Another downside of using a titanium sample holder for mounting the coins was the polarization and coating of the sample holder itself. Although the sample holder should have had a higher polarization resistance due to the thicker oxide layer on pure titanium than on a SBAE surface, it could not be excluded that the sample holder leaked more electricity than accounted for by the initial calculation of the current density.
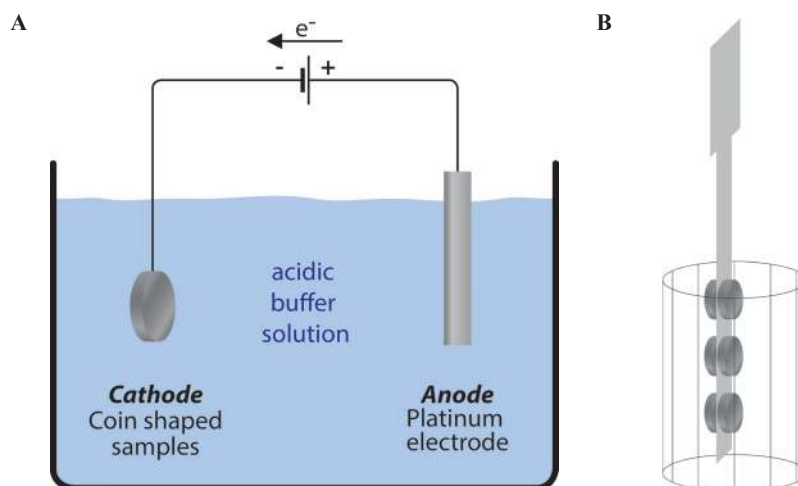
Figure 3.4   A: Schematic illustration of the cathodic electro-coating setup. Coin-shaped samples were mounted as the cathode, while a platinum-electrode was used as the anode for polarization in an acidic buffer.

B: Schematic drawing of the electrode used for the conventional coating setup that coated all samples on a single electric output channel. The coins were mounted back-to-back with the titanium sample holder in between and placed inside a fine-meshed platinum cylinder that acted as the counter electrode during polarization.

The second setup used in this study was a custom-made power source based on LabVIEW (National Instruments, Austin, TX, USA) hardware and software (Paper V) that provided sophisticated options to provide a stable output current (Figure 3.5 A). This was achieved by implementing a proportional–integral–derivative (PID) controller that adjusted the output current according to the desired current in a feedback loop. Moreover, this setup was equipped with eight separate output channels. This allowed coating of each sample on an individual electric channel and hence a more precise control of the output current and the potential for each individual sample. This was also desirable due to the aforementioned differences between the hydrogen content of a sample within a batch and the resulting influence of the surface chemistry on the

surface`s conductivity and the resulting change in electric resistance during the process. This setup was combined with a sample holder that allowed mounting each coin on an individual output channel. A custom-made titanium mounting-pin was used for retaining the coins in the buffer (Figure 3.5 B). This mounting-pin provided a cylindrical handling piece at its top end that could also be used for connecting a crocodile clamp to it that connected the sample to the electric-setup. Moreover, the pin had a long neck for sliding on a protective polytetrafluoroethylene (PTFE) cap that was placed over the side face and the top of the coin. The threads for connecting the coin, by the threaded hole at the back of the coin, were located at the lower end of the mounting-pin (Figure 3.5 C). As this setup was developed during the course of this thesis to improve reproducibility, it could only be used for the experiments conducted during the development of the setup and was first deployed for the *in vivo* study conducted in Paper V.

The advantage of this second polarization setup was its ability to provide an individual output current solely to the front face of the sample coins. The absence of a shared sample holder and use of the protective PTFE cap eliminated potential leakage of current and focused the polarization and coating with biomolecules on the desired front face of the coin.
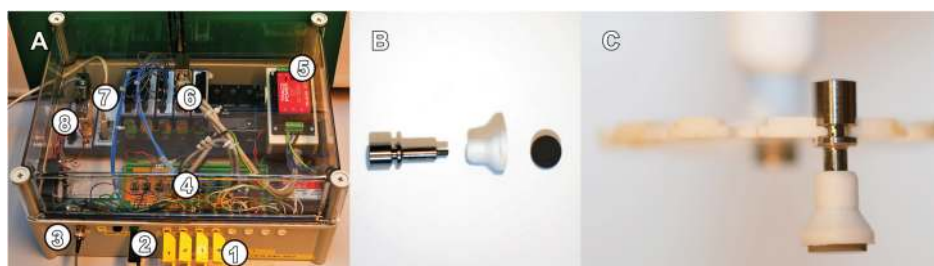
Figure 3.5   (A) shows the newly developed coating setup that was custom-made based on National Instruments Hardware and Software components. The image shows 4 of the 8 individual channels (1), the counter-electrode (2) and the pH electrode (3) connected to the box at the front panel. The main components of this setup were the amplifiers (4), the power source (5), the NationalInstruments controller (6), the Ethernet connection (7) to the controlling computer, and the pH electrode connector (8).
The custom-made threated Ti-pin, the PTFE cover cap and a sample coin where displayed in (B). The three parts were assembled and mounted on the PTFE sample holder in (C).

During the testing phase for the advanced coating setup, the influence of the electrode design became evident. "The principle of making the electric field lines spatially uniform over the surface of the sample" has been shown to be valid for the production of porous silicon.[112] The size of the electrode and the distance of the counter electrode and the sample have also been shown to have a large influence on the homogeneity of an electro-chemical surface modification.[112,113] Observations made during the experiments with another biomolecule that allowed visual confirmation of the coating by coloring the surface[114] showed a similar effect of the electrode shape and distance onto the coating by revealing a coloring of the samples after coating. When placing the electrode and the sample face to face while covering specific spots on the electrode with an electrically non-conductive material, the homogeneity of the coating could be influenced. In detail, the spots on the sample that were directly facing the covered spots showed less or no coloration after coating while the parts that were facing the electrically conductive parts of the

electrode were colored. Although the effects of the electrode design and distance to the sample were not investigated any further during the work for this thesis, some basic standards were defined based on these principles and observations in order to achieve an improved homogeneity of the coating. In detail, the electrode was designed in the shape of a cylindrical mesh in order to provide an electric field that was as homogeneous as possible. Moreover, the lateral and vertical spacing between samples and counter electrode was standardized by position marks for alignment on each element of the coating setup. The influence of the electrode design provides large room for improving the electro-coating process described in this thesis as the research conducted on electro-etching illustrates by the steady improvements that are made in this field.[115]

Besides the design of the electrode, the buffer has an influence on the electric field during the coating process. The conductivity of the buffer had impact on the movement of the ions in the buffer. As the process intended to bind charged biomolecules to the surface, the resistance of the buffer should be minimized for alleviated ion-movement. Experiments that used additional sodium chloride (1 wt.% NaCl) in the buffer appeared to show increased biomolecule content for EMD. By contrast, the opposite effect was observed during Sr-coating (Paper IV) with additional NaCl but without NaF in the buffer. It appeared that Sr-ions competed with NaCl and formed $SrCl_2$ that prevented Sr from attaching to the sample`s surface. The effect of the conductivity of the buffer was not investigated to a larger extend but it appeared to provide additional potential for optimizing the electro-coating process.

3.3   Characterization of the surface topography and morphology

Figure 3.6   Illustration of a selection of important surface topography and functional parameters (S_a, S_{ku}, S_{ku}, and S_{ci}) that were assessed by profilometry.

3.3.1   Assessment of the surface micro-topography and micro-morphology

The effect of the surface modification on the topography was characterized by optical imaging profilometry. An optical imaging profiler consists of a confocal microscope that takes an image of one focal pane at a time and combines all images of a measurement to one three-dimensional topographical image. The advantage of this technique was the high depth resolution, as each pane was in focus when the image was recorded. While a normal confocal microscope uses plane white light, the profilometer used in this study (PLμ 2300, Sensofar-Tech S.L., Terrassa, Spain) was equipped with a blue light source. The precision of an image was only limited by the objective used. Although an objective with a large magnification allowed a more precise assessment of the surface topography, it also limited the field of view at the same time. As a consequence, a multitude of overlapping images had to be recorded in order to cover a larger part of the surface. For increased precision, this study analyzed at least three different areas for each sample. Another

advantage of the optical profilometer was the ability to run a detailed analyzes of the surface obtained afterwards. The advanced topography software Sensomap 4.1 Plus (Sensofar-Tech S.L., Terrassa, Spain) for dimensional and surface state metrology was used to calculate up to 44 different surface topography parameters and functional parameters. Only a fraction of these parameters were of particular interest in this study as they have been reported to have an influence on the biocompatibility of an implant.[116] The parameters selected for further analysis were the surface roughness (S_a), the surface skewness (S_{sk}), the surface kurtosis (S_{ku}), the surface core fluid retention index (S_{ci}) and the developed interfacial area ratio (S_{dr}). As illustrated in Figure 3.6, the S_a describes how much a surface deviates from the mean plane. A positive S_{sk} refers to peaks emerging as elevations from a relatively flat surface whereas a negative S_{sk} refers to wide plateaus that are eroded by deep valleys. The S_{ku} describes if a surface is either leptokurtic ($S_{ku}>3$) or platykurtic ($S_{ku}<3$) whereas the S_{ci} describes the spacing between the peaks on the surface. In detail, a high S_{ci} refers to large gaps between the peaks and a low S_{ci} refers to small or no gaps between the peaks. The S_{dr} provides information about the percental enlargement of the surface area due to roughness in percent when comparing it to a completely flat reference area.

Analysis of the surface topography was of particular interest for the electro-coating, as it provided the S_{dr} of the original SBAE surface which is crucial for taking the surface enlargement caused by the surface roughness of the sample into account for polarization. The total surface area of a sample (A_{Sample}) was calculated from its geometrical surface area and the S_{dr} acquired by optical imaging profilometry. The set current (I_{SET}) for the electro coating was then calculated from the total surface area of the sample (A_{Sample}) and the desired current density ($CD_{Desired}$) (Equation 3.1). The advantage of using a current density instead of a fixed output current is the scalability of the process to different samples. This makes it much easier to transfer the process e.g. to a screw shaped implant with a significantly larger surface than the test coins used in this study for future use.

Equation 3.1
$$I_{SET}(mA) = A_{Sample}(cm^2) * CD_{Desired}(mA/cm^2)$$

Unfortunately profilometry was also subject to certain limitations. Although the profilometer performed well at assessing the surface topography of a surface, it was not capable of detecting undercuts or certain changes to the surface-morphology. The reason for this was believed to have been the 50XEPI confocal-objective (NIKON, Tokyo, Japan) that was not capable of assessing slopes steeper than 42°. Even the more powerful 150XEPI confocal-objective (NIKON, Tokyo, Japan) was only capable of analyzing surface slopes of up to 71°.[117] As a result of this insufficiency, a statistical evaluation of the surface parameters often revealed no significant differences between the groups, although the SEM showed significant visible differences (Paper I-IV).

A surface`s micro-topography and micro-morphology may alternatively be assessed by an atomic force microscope (AFM) that uses a cantilever with a detector tip and records the movements of the tip caused by the sample surface. Although this technique has frequently been used in our laboratory and is well established in the field of biomedical research[34,116,118], it could not be

deployed for the rough SBAE surface. A stylus profilometer assesses the surface micro-topography in a similar way as an AFM and was thus also not compatible with the rough SBAE surface as well.
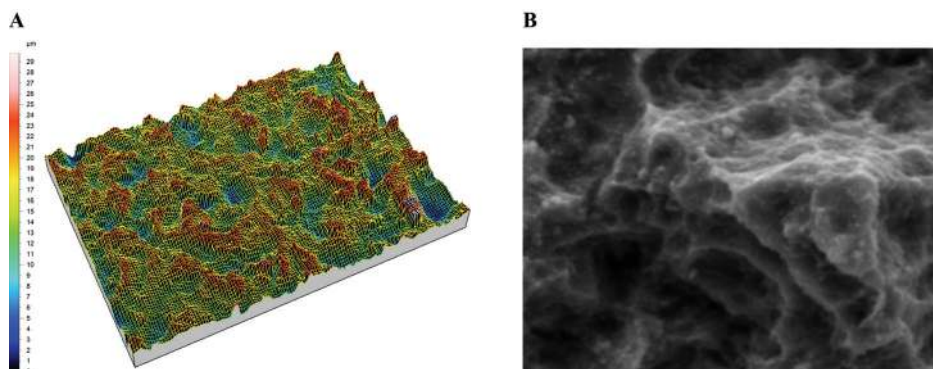
Figure 3.7   A: Three dimensional topographical image of a TiZr SBAE surface acquired by optical imaging profilometry.

B: Visual image of a TiZr SBAE surface (Paper II) acquired by scanning electron microscopy.

3.3.2   *Assessment of the surface nano-topography and nano-morphology*

Scanning electron microscopy (SEM) was used for visualizing the surface topography and morphology. The SEM provided high-resolution 2D images by using a focused, high-energy electron beam for raster scanning the surface of a specimen. All images in this study were taken on a Quanta 200 FEG (FEI Hillsboro, Oregon, USA) field-emission SEM (FE-SEM) with a Schottky field emission gun for high spatial resolution (Paper I-IV).

The comparably rough surface of the SBAE samples posed a challenge with regards to acquiring images with an adequate depth of field resolution and a suitable enough contrast. The ideal combination of spot size, working distance and acceleration voltage for use with SBAE surfaces had to be defined. The best results were achieved using a spot size of 3μm–5μm, a working distance of 5mm–7mm and an acceleration voltage of 8kV–10kV. Although the images were only two-dimensional, the high depth of field and the 45° angled stage used for imaging made them appear almost three-dimensional. This quasi-3D effect and the high resolution of the SEM allowed a very precise evaluation of the surface topography and morphology at the micro-level and at the nano-level. Moreover, the SEM was capable of displaying undercuts that could not be assessed by the profilometer.

Assessment of a surface`s nano-topography and nano-morphology may usually be done by AFM but could not be used for the rough SBAE surface as aforementioned in section 3.3.1.

3.4   Characterization of the surface chemistry

Assessment of the surface chemistry was performed in order to detect the effect of the surface modifications to the surface chemistry and to trace the chemical components of a biomolecule on the coated surface. As it was proposed in the hypothesis, the SBAE surface was believed to provide an adequate basis for attaching charged biomolecules by means of a cathodic polarization process, as it was suggested by Lyngstadaas and Ellingsen.[78] For this reason, the initial surface of the SBAE samples was assessed with a particular focus on hydrogen content (Paper I). Subsequently, the effect of the polarization process on the surfaces` hydrogen content was assessed in order to identify suitable process parameters for the polarization process (Paper II). After the process parameters had been defined, the actual surface modification was done with the biomolecules EMD (Paper III) and Sr (Paper IV), which were described in the introduction (section 1.4). Assessment of the surface chemistry was necessary for evaluating the success of the surface modification. Chemically, EMD consists of carbon, oxygen, hydrogen, nitrogen, silicon, and sulfur (Paper III). Thus, this study used a combination of methods that are suitable for detecting those elements like Secondary ion mass spectroscopy (SIMS) and X-ray photoelectron spectroscopy (XPS). By contrast, Sr is an element by itself that may be detected directly by XPS (Paper IV).

3.4.1   *Secondary ion mass spectroscopy (SIMS)*

SIMS was used for analyzing the chemical composition of a sample by tracing specific isotopes of an element. All SIMS analyzes were performed on an IMS 7f (Cameca, Paris, France). In order to trace light elements like hydrogen, the specimen was located in an ultra-high vacuum chamber over night to eliminate the presence of hydrogen in the sample chamber. During the SIMS analysis, a focused primary ion beam of Cs^+-ions was used to sputter the surface. When the primary ion beam hit the surface, it ejected so called "secondary ions" from the specimen. In a sequential order, secondary ions were passed to an electrostatic sector analyzer to select ions by their electric energy and thereafter to a magnetic sector analyzer to separate them by their individual ion-mass before they hit the detector, which recorded the specific intensity.[119,120]

The detector used for measuring the intensity of a secondary-ion degrades over time and has to be recalibrated prior to a measurement to ensure a sufficient sensitivity.[120] This procedure posed a challenge in comparing measurements deriving from different experiments to each other, as the recorded count intensity was relative to the calibration of the detector. A comparison of SIMS measurements from different experiments could be done by calibrating the intensity of a measurement to the intensity of an isotope with a concentration that was either known or identical for all samples. As the base material of samples within the same batch should not have had any differences in the ratio of the ^{46}Ti isotope, the baseline intensity of this isotope could be used for comparing different measurements to each other.

Over the course of a SIMS measurement, the primary ion beam continuously denudes the surface and a profile of the measured intensity at the given sputtering time is recorded. By measuring the total depth of the crater, the sputtering time can be converted to the actual depth of the measurement. Anyhow, a transformation of the time profile to depth profile would require a

consistent sputtering rate of the specimen. Each specimen usually carried carbon contaminations on the oxygen layer on the outer surface. This oxide layer sat on top of the hydride layer created by the SBAE procedure (Paper I). Once the hydride layer was removed, only the metal, Ti or TiZr, remained. As the oxide, hydride and pure metal have differing mechanical properties, the sputtering rate changed during the course of a measurement dependent on the layer that was currently sputtered. As a result, all specimen analyzed by SIMS were displayed as time profiles and an approximated depth scale that was based on the assumption of a constant sputtering rate was added for displaying purposes (Figure 3.3).

Although a depth profile of a specimen may be created by XPS in an iterative combination of XPS measurements and sputtering of the surface to assess it layer by layer, the XPS available for the measurements conducted during this thesis did not provide the ability to sputter the surface (section 3.4.2).

SIMS was mainly used for characterizing a surface`s hydrogen content of the samples. As hydrogen is a comparably light element it is particularly difficult to detect or even quantify by most techniques.[121] While this study used SIMS, the hydrogen content of a sample may also be assessed e.g. by thermo-gravimetric analysis mass spectrometry (TGA-MS)[122], X-ray diffraction (XRD)[123], or Elastic recoil detection analysis (ERDA)[121,124], scanning tunneling microscopy (STM)[125,126], or resonance nuclear reaction analysis (RNRA)[124]. Although TGA-MS may provide the total hydrogen amount of a specimen, it cannot provide information about the positioning of the hydrogen like a hydrogen depth profile from the SIMS. In a comparable way, XRD only provides information about the hydrogen on the very first few atomic layers of a sample as it does not create a hydrogen depth profile. On the other hand, XRD does provide information about the phase composition of the surface which cannot be assessed by a SIMS (compare section 3.4.3). ERDA and RNRA are methods that are related to SIMS in the working principle of Rutherford backscattering and in creating a depth profile. This study used a SIMS, as it was easily available, affordable within the budged of this project, and comparably fast. Moreover, our laboratory was experienced with this technique.[79,116]

3.4.2   X-ray photoelectron spectroscopy (XPS)

In XPS, monochromatic soft x-rays irradiate a solid in an ultra-high vacuum in order to provoke electrons to be emitted from the specimen. These electrons can be analyzed by their energy to plot the number of detected electrons per energy interval over their binding energy. As each element possesses a unique peak in the energy spectrum, it is possible to assess the chemical composition of a specimen. XPS may also be used for quantifying the detected elements or compounds by assessing the relative peak height and the peak area. Anyhow, XPS analysis is limited to a few top layers of atoms on a specimen`s surface due to the limited free path of an electron in a solid specimen.[127] XPS analysis was carried out on an Axis Ultra[DLD] XP spectrometer (Kratos Analytical Limited, Manchester, United Kingdom). The specific settings of the instruments were provided in the individual papers (Paper I-IV).

XPS was used for assessing the chemical composition and the specific bindings of the components on the surface. The ability to identify specific compounds made it possible to identify

EMD-specific bonds (Paper III) or Sr (Paper IV) on the surface of a specimen. Figure 4.5 shows the detail spectra for the Sr 3d peak from Paper IV. As XPS analysis was limited to the outer surface of a specimen, it could not be used to assess the depth profile of a specimen. Moreover, hydrogen could not be detected by XPS.[128] Thus, this study used SIMS for assessing the hydrogen content of a sample and for recording depth profiles of an isotope (Papers I-III). The downside of a rough surface is that it generally increases the scattering of x-rays similar to the effect in the SEM and thus creates more noise in a measurement. Alternatively a rough surface may lead to partial shading of the surface. It appeared that the rough surface did not significantly affect the XPS measurements conducted for this study as all elements that were assumed to be on the surface could be observed (Papers I-IV). Anyhow, averaging of repeated measurements is a possible solution for this challenge solution[129,130]

Alternatively to XPS, Sr may have been assessed by SIMS, transmission electron microscopy (TEM), Raman spectroscopy, Fourier transform infrared spectroscopy (FTIR), or Auger electron spectroscopy. The advantage of XPS over SIMS is the higher resolution on the assessed layer and the ability to determine the binding state of an atom like it was done in Paper IV. Techniques like Raman spectroscopy or FRIR may be used to assess the chemical bond of an atom by exciting it with monochromatic light (compare section 3.5.3). Although these techniques should work independently of the surface roughness, the results from the FTIR were not satisfactory and the method for Raman was not available and it would have been more costly to set up the complex available instrument with an unknown outcome then using the very precise XPS.

3.4.3   X-ray diffraction (XRD)

X-ray diffraction (XRD) was used to analyze the phase composition of TiZr SBAE before cathodic polarization and after polarization (Paper II) in order to assess the effect of the polarization process on the phase of the hydride. In XRD, an x-ray is diffracted by the atoms of the specimen into multiple directions. The angle and intensity of the diffracted x-ray reveals the crystalline structure and the spacing of the atoms in a single unit of the crystalline system. The advantage of this technique when e.g. compared to TEM is that XRD does not require any preparation of the specimen. Other alternatives to XRD are low energy electron diffraction (LEED) and reflection high energy electron diffraction (RHEED) which are limited to surfaces and cannot analyze the bulk material.[131]

3.5   Assessment of the biomolecule after coating

While chemical analysis of the surface by XPS may have been a feasible method for proving an effective coating with Sr (Paper IV), it could only indicate the presence of EMD by revealing the presence of its elementary composition (Paper III). Thus, other methods were deployed in order to assess the integrity of EMD after coating. Fourier transform infrared (FTIR) analysis, dot blotting, and matrix-assisted laser desorption/ionization time of flight mass spectrometry (MALDI-TOF MS) have shown good success in analyzing EMD in previous studies.[132] Thus, those methods were investigated for potential use in confirming EMD and its integrity after electro-coating.

In order to analyze the biomolecule by MALDI-TOF MS or dot blot, the biomolecule had to be detached from the surface. At first, this posed a certain challenge itself, as the EMD-coating was not intended to be removed easily from the surface again. This task was approached by a series of experiments that involved different solvents. Basic and pH neutral solutions, like water, showed no success in detaching EMD from the coated samples. Eventually, pure acetic acid, a solution made of 40% acetonitrile and 0.3% trifluoric acid (ACN+TFA), and 1M NaOH were successfully used for detaching EMD from the surface. Moreover, the solutions appeared to maintain the integrity of EMD as it was shown in the MALDI and dot blot results. Since ACN+TFA is a solution that is commonly used in combination with MALDI measurements, it was chosen as a release medium for this technique by placing the coins in ACN+TFA for 24 hours at 8°C (Paper III). For the dot blot, EMD was detached from the coated coins by placing each coin in 0.5 ml of 1 M sodium hydroxide (NaOH) for 24 hours at 8°C.

3.5.1   Matrix-assisted laser desorption/ionization time of flight mass spectroscopy

Matrix-assisted laser desorption/ionization time of flight mass spectroscopy (MALDI-TOF MS) uses a matrix that is mixed with the specimen in a liquid state. Thereafter the sample, consisting of the specimen-matrix mixture is placed on a MALDI plate and dried up before the MALDI plate is placed in a vacuum sample chamber for analysis. MALDI-TOF MS uses a pulsed laser for exciting the matrix of the sample and thus volatilizing the sample. Once the sample has been vaporized, it is passed through a linear time of flight analyzer that imparts all molecules to an identical translational kinetic energy. In a free field drift tube all molecules of the sample travel the same distance to the detector. Hence, the smaller, lighter ions travel faster and hit the detector first. The detected signals can be combined to a mass spectrum as a function of time (Figure 4.3).[133] The frequency and intensity of the laser pulses alongside the length of irradiation influence the intensity of a measurement by determining the amount of sample that becomes volatilized.

Although MALDI-TOF MS provided decent results in identifying the components of EMD after coating and sequencing pure EMD (Paper III), the samples had to be destructed for analysis. For this reason, alternative methods, like FTIR for a possible destruction-free analysis of EMD on the surface were evaluated. Anyhow, MALDI-TOF MS was reliable in confirming the integrity of EMD after coating.

3.5.2   Immuno dot blot

Immuno dot blot was performed in order to confirm the integrity and quantify EMD before the animal study (Figure 4.3 D). As MALDI could only confirm the integrity of EMD after coating, dot blot was a very efficient and comparably fast method for quantifying EMD. After releasing EMD off the surface like it was described earlier, every sample was blotted twice on a membrane (Bio-Rad Laboratories Ltd., Herts, UK), one test group and one control group without the primary antibody as a control to test for nonspecific cross reactivity or false positive signals. Along the samples, pure EMD diluted 1:5 from 5000 ng/ml to 5 ng/ml in 0.1% acetic acid was blotted in order to create a reference curve for quantification. A Millipore SNAP i.d. protein detection

system (Millipore Corporation, Billercia, MA, USA) was used for the blotting. TBS containing 0.1% Tween-20 (TBST) was used as a blank negative control sample for both groups. The membrane blocked with TBS and 0.1% casein for 1 hour. The primary EMD-antibody (sheep-anti EMD; Mölnlycke Health Care AB, Gothenburg, Sweden) was applied in TBS 1:100 for group A while group B was kept in pure TBS for 1 hour. Both groups were washed three times in TBST for 3 minutes. The secondary EMD-antibody (rabbit anti-sheep HPPOX; Southern Biotech, Birmingham, AL, USA) was diluted in TBS (1:1000) and applied to both groups for 1 hour. Both groups were washed three times in TBST for 3 minutes and once in deionized water for another 3 minutes. A 3,3-diaminobenzidine-based (DAB, Sigma-Aldrich, St. Louis, MO, USA) horseradish peroxidase reaction product (0.3 g/l DAB, 0.03% H_2O_2, and 0.03% $NiCl_2$ in 50 mM $(NH_4)HCO_3$) was used to stain the EMD proteins. A Kodak Gel Logic 212 imaging system (Eastman Kodak Company, Rochester, NY, USA) was used to examine the dot blot and to assess the concentration of EMD of each sample by the intensity of the staining relative to the blotted standard.

Dot blot may have been replaced by techniques like SDS-Page, western blotting, chromatography, or gel electrophoresis. Anyhow, the procedure for detecting EMD by Immuno dot blot has been well established in our laboratory and was hence selected for quantifying EMD.[132,134,135]

3.5.3   Fourier transform infrared spectroscopy (FTIR)

Fourier transform infrared (FTIR) spectroscopy uses light in the infrared (IR) region to excite the specimen in order to induce a change of the vibrational and rotational state of its molecules. The vibrational state of a molecule can be a symmetric stretching, an asymmetric stretching, a deformational vibration, or a combination of the stretching mechanisms.[136] The specific vibrational frequency of a molecule defines which frequency of the IR light is absorbed. This optical signal is detected by a detector and processed by the machine as a digital signal of the signal strength as a function of the optical path difference, the so called interferogram. Fourier transform of the interferogram is used to create a single beam spectrum of the specimen. In order to separate the background from the specimen, the unmodified SBAE background of the respective material was measured and subtracted from the spectrum of a modified sample. The resulting difference spectrum showed only the surface modification.

This study used a Spectrum 400 FT-IR/FT-NIR spectrometer (PerkinElmer, Waltham, MA, USA) with an attenuated total reflectance (ATR) sampling tool for liquid or powder state samples and a diffuse reflectance (DR) sampling tool for coin shaped samples. The spectrum of a sample constituted of eight individual measurements with a resolution of 8 cm^{-1}. The background was subtracted for all samples. The difference spectrum of a coin sample was normalized and processed by the Kubelka-Munk algorithm. Individual peaks were quantified by Beer`s law.

FTIR analysis was considered as an alternative method for analyzing EMD directly on the coins (Figure 3.8). However, preliminary test on the sample coins revealed large interferences of the surface roughness with the measurement (results not shown). Thus FTIR was rejected as a

method for assessing the surface coating and MALDI was selected to be the experimental method to identify the integrity of EMD after coating (Paper III).

Raman could have been used as an alternative to FTIR. While the working principle of Raman and FTIR are very similar, they use light at a different wavelength to excite the specimen. As mentioned above, FTIR uses light in the infrared region, whereas Raman uses light in the region of visible light.[136] Raman was not evaluated to detect EMD as the available instrument was comparably complex to set up and because MALDI-TOF MS, XPS and dot blot had already shown sufficient results that made assessment by Raman obsolete. Anyhow, Raman may be interesting as a screening technique for quality control in a potential production process if this coating should be transferred to screw shaped implants that are produced industrially.
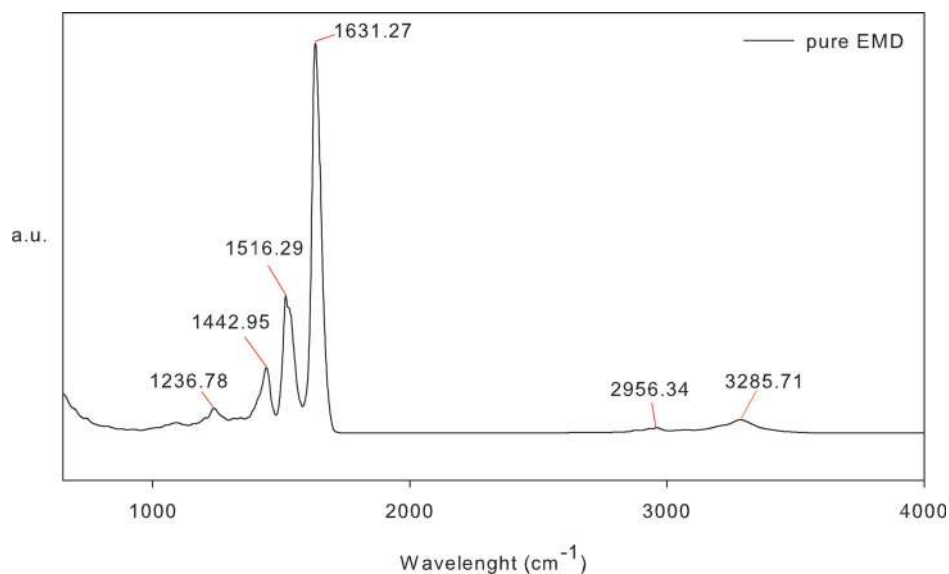
Figure 3.8   FTIR spectrum of pure, lyophilized EMD with its characteristic peaks.

3.5.4   Atomic absorption spectroscopy

Atomic absorption spectroscopy (AAS) was considered for determining the Sr content of a sample for the study conducted in Paper IV. An AAnalyst 400 (PerkinElmer Inc., Waltham, MA, USA) was used with a strontium lumina hollow cathode lamp. The flame was fueled by a mixture of pressurized air and acetylene gas. Samples were prepared by releasing Sr off the coated coins in a mixture containing 40% acetonitrile and 0.3% trifluoric acid (ACN+TFA, compare Paper III) for 24 hours. A total of 1% lanthanum chloride was added to each sample as a strontium release agent. A standard curve was recorded by preparing a standard solution containing 5ppm of Sr.

AAS is a relatively accurate technique for quantifying Sr once the standard curve has been recorded. The challenge with AAS was releasing Sr off the surface. Although release in ACN+TFA showed Sr, these results showed a large deviation. As the amount of Sr coated onto a

surface by cathodic polarization was varying quite significantly depending on the buffer or F contaminations on the sample`s surface this might have been the reason for the differences observed. On the other hand, it was also possible that ACN+TFA was not the ideal medium for achieving a total wash-down of Sr from the surface. As the XPS showed accurate and stable results for quantifying Sr, AAS was not further pursued as an alternative. Anyhow, this might be a more cost-effective method compared to XPS for quantifying Sr.

Other alternatives for detecting and quantifying Sr on the surface were energy-dispersive X-ray spectroscopy (EDX), FTIR, inductively coupled plasma mass spectrometry (ICP-MS)[137]. EDX is easy to use, fairly quick, inexpensive and capable of detecting elements like Sr on the surface of a specimen. Anyhow, EDX does not reveal any information about the binding state of an element and is not as precise as an XPS. Thus, EDX could be used as a mean for quick screenings in between experiments but was not used for analysis of the samples in this thesis. Although ICP-MS is favorable over AAS for its increased precision and sensitivity, it was not available at our laboratory and thus not evaluated. As ICP-MS would have required a liquid sample just like AAS, the same challenges in washing the complete coating off the coated surface would have to be solved in order to deploy this technique as well.

3.6   Cell study

This thesis used *in vitro* experiments to evaluate the biological performance of the surface modifications in comparison to the untreated surface. The use of *in vitro* experiments provided a cost effective screening of the effect of the different surface modifications on the biological response. Such a screening is indispensable with regards to ethical desires and legal requirements for avoiding unnecessary *in vivo* experiments. All *in vitro* experiments conducted for this thesis were performed on the murine, osteoblast like MC3T3-E1 cell line. Although permanent cell lines generally have a reduced similarity to the *in vivo* situation when compared to primary cells, it has been shown that MC3T3-E1 cells possess a high potential for cell proliferation and differentiation that is comparable to the *in vivo* development of murine bone.[20,138,139] This cell line has been established as a viable choice in biomedical research as it expresses many characteristics of the osteoblast phenotype. Moreover, this model provided the possibility of easily identifying the different development stages of the cells.[20,139,140] It has been shown that the time related differentiation of the MC3T3-E1 could be assigned to the development stages cell proliferation, matrix maturation, and mineralization of the cell cycle. In this development, high gene expression of Coll-1 marked the proliferation phase, a steep rise in ALP expression marked the matrix maturation phase, and rising OC expression indicated the mineralization phase of the cell cycle (Figure 3.9).[20,139] This knowledge about the characteristic expression of the different markers allowed a very specific evaluation of the influence of the surface coating on cell development (Paper III, Paper IV).

Although this model is well established, it must be kept in mind that the culturing history of the cells, like the number of biological replicas and the passage number, has a significant influence on the expression of the cells.[141] The cell experiments performed in for this thesis did not exhibit any signs of cell-deterioration, as pre-screenings showed changes in the expression of the different markers (results not shown).
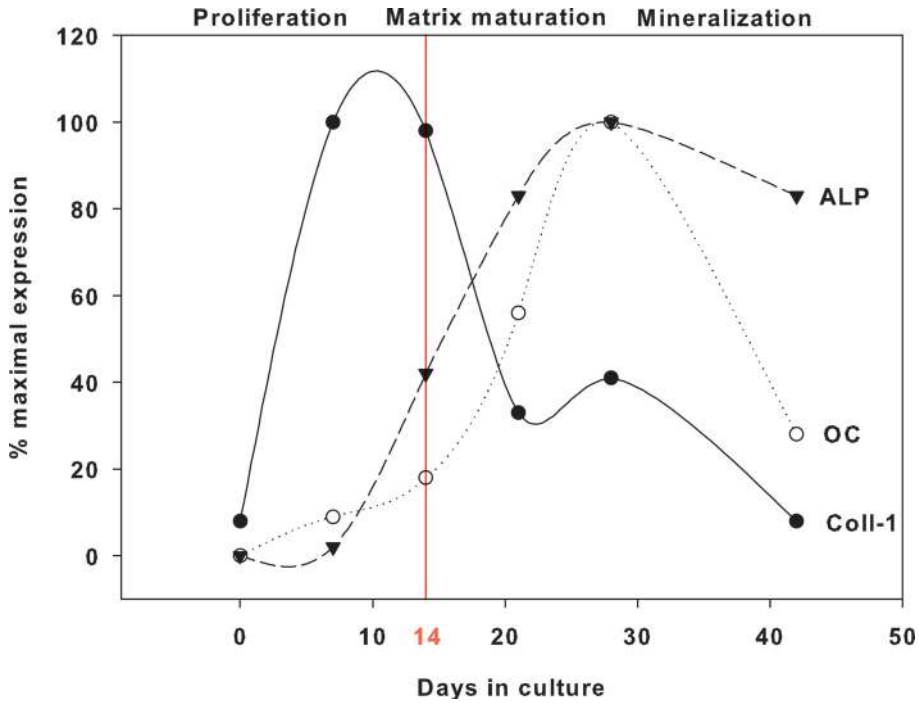
Figure 3.9   Time related differentiated stages of MC3T3-E1 cells based on the results presented by Monjo et al.[20] Peak levels of Coll-1 gene expression marked the proliferation phase; A steep development of ALP gene expression marked the matrix maturation phase while rising expression of OC indicated the mineralization phase of the cell cycle. The 14 days marker (red line) shows the time point used in the studies conducted for this thesis (Paper III, Paper IV).

Lactate dehydrogenase (LDH) is an intracellular enzyme that is released to the culture medium when the cell membrane becomes disrupted and is thus correlated to cell death. Hence LDH activity as a marker of cell-viability is commonly assessed in cell studies. As the total number of cells was not assessed during the cell studies conducted in Papers III & IV, the LDH activity could not be normalized according to the total number of cells. The results from LDH activity assessment corresponding to the cells studies presented in Papers III & IV is presented in Figure 3.10.
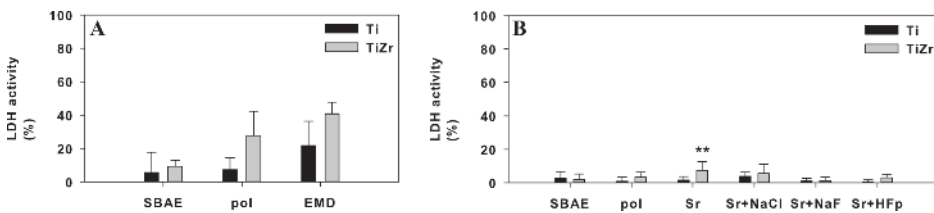
Figure 3.10   Lactate dehydrogenase (LDH) activity as a marker of cell-viability from the studies on EMD in Paper III (A) and on Sr in Paper IV (B). Data are displayed as the mean values with standard error of the mean relative to cells cultured on a plastic control. Student t-test revealed significant (*p≤ 0.05) and highly

significant (**p≤ 0.01) differences for the highlighted groups against SBAE.

3.7   Animal study

The ethical responsibility in medical research demands the detailed knowledge that may be acquired by *in vivo* studies prior to human trials. Legislation has established mechanisms that shall ensure animal welfare and reduce the number of animals used for experiments to a minimum. The key components of these efforts are often summarized as the "three R" that have been proposed by Russell and Burch in 1959, namely: reduction, refinement, and replacement. Various techniques, like SIMS, XPS, or MALDI-TOF MS, have been used in this study in order to refine the coating process and the surface coating. The *in vitro* experiments (Paper III & IV) have been a valuable replacement for animal trials by indicating a positive influence of both surface coatings on the biological response. Since animal trials involve high costs, the number of samples was further reduced due to budgetary restrictions and furthermore for reducing animal trails in general. TiZr was selected as the only material to be tested in an animal trial since it provided a more versatile potential for deployment due to its enhanced material properties over Ti. Eventually, the groups TiZr SBAE, TiZr pol, TiZr Sr+NaF, and TiZr EMD were chosen for testing the biological response to the surface in a situation that provided the full complexity of a living organism *in vivo* (Paper V).

3.7.1   Selection of the animal model

The model used in this thesis was selected as our laboratory had extensive experience with the use of this model.[18,19,142-146] Moreover, the *in vivo* findings of this model have been shown to be transferable to the clinical performance of a screw shaped implant as the fluorine modified OsseoSpeed[TM] surface (Astra Tech AB) has been developed by use of this model.[54,147] All details about this model have been described in Paper V.

3.7.2   Selection of animals

The *in vivo* study performed in Paper V was done with rabbits as they are comparably easy to handle and provided a bone mineral density (BMD) that is comparable to the human BMD.[148] On the other hand, the rabbit`s bone structure is generally very dissimilar to the human bone structure and has a much faster bone turnover than humans which may be a challenge for projecting results collected in a rabbit study onto the biological response of a human.[148-151] Rabbits are comparably small animals and thus easy to handle and to house.[149] Moreover, our department provided an extensive knowledgebase on the rabbit model selected for the animal study. These advantages overruled the disadvantages of the rabbit in animal trials like the reduced number of implants that may be used with a rabbit in comparison to sheep, goats, pigs, or dogs that allow twice as many samples as a rabbit.

The *Gray Bastard Chinchilla* (GBC) rabbit was selected for the studies presented in Paper V instead of the *New Zealand White* (NZW) rabbit that had been used in earlier studies done at our department.[18,19,152] This decision was made by the animal facilities at the Norwegian School of

Veterinary Science as the NZW rabbits have shown aggressive behavior in our previous studies, when the rabbits are housed non-caged in groups. Previously the NZW rabbits were kept in cages during the experiment, but new regulations did not allow for this practice anymore.
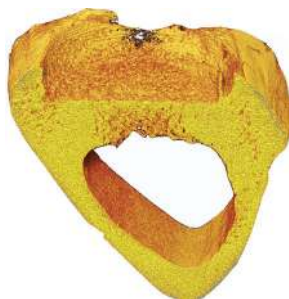
Figure 3.11 µCT image of a TiZr Sr implant side after 8 weeks healing time. As the coin diameter (6.2 mm) was larger than the width of the rabbit`s tibia, the coin was enclosed by a callus on the sides that`s clearly visible by the porous, newly formed bone. Moreover, the bone rim that formed in between the coin and the protective PTFE cap is clearly visible on the right side of the spot where the coin was positioned.

The GBC rabbit used in this study did not have a tibia as large as the NZW rabbit used in earlier studies. [18,19,152] As a result, sometimes the tibia did not provide enough space for placing an implant with a diameter of 6.2 mm and lead to the formation of a callus around the overlappings of the implant (Figure 3.11). Such a callus formation was not desired and offered an opportunity for refining the experimental model. A reduction of the coin diameter to a size that would be suitable to the NZW rabbit`s tibia may be a possible solution. Whatsoever, a smaller coin diameter would reduce the total area for bone attachment under the coin exponentially and may thus have implications on the use of a central defect under the coin.

3.7.3 Animal surgical procedure

During surgery, some shortcomings of the model introduced by Rønold et al. became obvious.[152] This model did not standardize the position of the coins on the tibia. Thus, it was suggested to refine the model by introducing a reference point that shall have a standardized distance to the drilling guide. An anatomical position like the knee may be such a reference point for setting a position distal of the knee that shall be used for the first hole of the drilling guide.

Another observation that offers potential for improvement was made during euthanasia of the rabbits. After the tibia bone had been laid open, the protective PTFE cap (Paper V) was removed by use of pressurized air. Anyhow, this method did not appear to work for all cover caps, as the callus that sometimes had formed around them was comparably large. Moreover, the bone rim between the coin and the cover cap (explained in detail in section 3.7.4) applied additional shear forces onto the cover cap and hindered the removal of the cover cap. As a result, a scalpel had to be used in order to remove the cover cap. Use of a scalpel induced lateral forces into the coin and leads to coin loosening prior to the tensile removal test. This influence could not be quantified and lead thus to a modification of the removal force. As the callus was part of this problem, the

solutions suggested earlier (section 3.7.2) for avoiding callus formation may already provide a solution to this issue. Moreover, the bone rim shall be avoided as discussed in detail in the next section (3.7.4). Rønold et al. have observed a similar effect of possible implant loosening during the removal of the PTFE cover cap even without the bone-rim between the coin and the cover cap.[146]

3.7.4   Tensile removal force test

A tensile removal test was performed for all groups included in the animal study that was presented in Paper V. Evaluation of the bone-to-implant contact strength using a removal tensile test was performed 4 and 8 weeks after the surgery. The tibial bone with the samples was fixated in a specially designed rig that gave total stabilization of the bone and allowed perpendicular adjustment of the sample to the tensile test load during the test procedure.[142] The tensile tests were performed with a Zwicki Materials testing machine (Zwick-Roell, Ulm, Germany) fitted with a calibrated load-cell of 100 N. Cross-head speed range was set to 1.0 mm/min. The load was applied until loosening of the implant and recorded on a force (N) versus strain (%) plot. The samples were connected to the tensile testing machine by a threaded pin with a ball-head that was attached to a 300 mm long wire connecting it to the load-cell. The set-up was then adjusted to be in line and perpendicular with the load-cell using a laser alignment tool in order to minimize the influence of shear forces. Detailed information concerning this removal tensile test have been published by Rønold et al.[142]
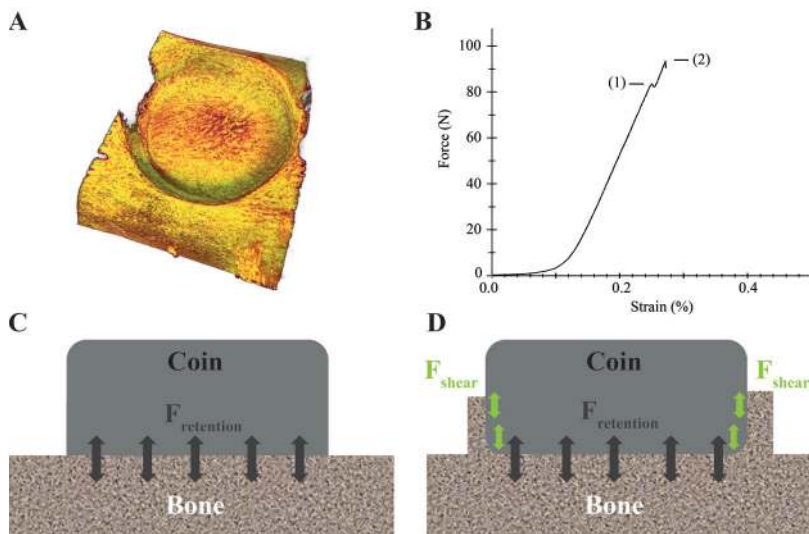
Figure 3.12   µCT image of a wound site after coin removal showed a bone-rim that grew between the coin and the PTFE cover cap (A). The force vs. strain plot from the tensile test showed two plateaus (as marked (1) and (2)) for most samples (B). Ideally, the coin would only be attached to the bone on the frontal area and thus only experience retention forces (C). In this study, a bone-rim that attached to the side of the coins caused additional shear forces that could not be distinguished from the retention forces in a tensile test with a perpendicular load (D).

The results of the tensile removal force test were surprising, as there was not one clear pull-out force but two breaking points for most implants (the results of the tensile test were presented in section 4.4.3 of this thesis). The coin model was originally designed by Rønold et al. in order to test the retention created solely by the reaction between bone and the implant`s surface.[142] While the model used in this study used test coins and PTFE caps as they had been used by Rønold et al., there appeared to be a difference in bone growth towards the surface of the coin. Rønold et al. defined the annulment of friction on the side faces of the coins as critical for solely assessing the retention force.[153] In contrast to the studies by Rønold et al., the study at hand observed bone that had grown in between the protective PTFE cap and the coin (Figure 3.8 A). It was believed that this bone attached to the side of the coins and created shear forces in addition to the retention forces that were intended to be evaluated (Figure 3.8 C, D). The perpendicular tensile test could not distinguish between the two forces but could only measure a single removal force.

The observations made during the tensile removal force test offered the potential for eliminating sources of error with the model used. Comparison of the coins used for this study and the study conducted by Rønold et al. revealed differences in the production process that were believed to have been responsible for the bone growth inside the gap between the PTFE cap and the coin. While Rønold et al. had embedded their coins in silicon during sand-blasting in order to protect the side faces of the coin, no such protection was used in this study during creation of the SBAE surface or further surface modification of the coins.[142] Even though the PTFE caps enclosed the coins as close-fitting as possible, the moderately rough surface appeared to provide a sufficient gap for bone to grow into the gap. Concluding it was advised to use protective embedding for the side faces of the coins during surface modification and PTFE caps with a tight fit to prevent a gap that allows bone growth to the side faces of the coin.

3.7.5 *Wound fluid and bone tissue analysis*

Wound fluid was taken from the wound sites after coin removal and analysis for LDH activity, ALP activity, and total protein content. This was done in order to assess any toxic effect the coating may have had. The bone tissue, meaning cells, proteins, and fluids, that remained on the coins after coin removal was analyzed for total RNA content and the expression of bone formation related markers (OC, BMP-2, and Coll-1), bone resorption related markers (H^+-ARP, TRAP, and Calc-R), and inflammation related markers (TNF-α, IL-6, and IL-10). Although IL-6 has been suggested to be a marker that is related to osteoclastogenesis in bone[154,155], it was regarded as an inflammatory marker[24] because the bone-tissue analysis conducted in Paper V did not grind or dissolve bone-tissue for analysis but analyzed the fluids secreted from or remaining on the bone tissue. The combination of the information provided by the expression of bone formation related markers, bone resorption related markers, and inflammation related markers made it possible to evaluate the biological response of the tissue to the different surface modifications used in Paper V. The selected markers were used as they have been shown to be reliable for evaluating bone healing.[18,19]

The disadvantage of using a rabbit model (Paper V) was that there are no antibodies available for rabbits that allow assessment of the protein instead of mRNA expression of the markers, which would be the ideal object to analyze. This is due to the fact, that rabbit antibodies are commonly used for creating protein detection kits for a multitude of other animals. Hence antibody cross reactivity of the secondary antibody would not allow a precise detection of the proteins. The disadvantage of using mRNA expression instead of proteins is the inability to distinguish where the gene expression derived from. Thus, the expression of a gene is only necessary but not a sufficient condition for the ultimate amount of a protein due to post transcriptional and post translational effects.[156,157]

3.7.6   Micro-computed tomography analysis

Micro-computed tomography (μCT) was chosen for analysis of the bone after implant removal as it provided imaging that is comparable to a traditional histology cross-section but also the possibility of collecting parametric data about the bone tissue. Moreover, a μCT scan is much faster than the longsome process of creating a histological slide, imaging and analyzing the slide.

The μCT was used for evaluating the volumetric bone mineral density (BMD) of bone defects and to analyze the 3D architectural parameters of the bone structure within the tibial cortical bone defect. A Skyscan 1172 (Bruker MicroCT, Kontich, Belgium) μCT was used for the measurements presented in Paper V. The μCT operated almost like a regular CT scanner, with the difference that the sample is rotated in a μCT whereas the scanner rotates around the sample in a regular CT. The scanner takes a multitude of images while the sample is rotated 360 degrees. The computer then calculates a single, 2D image, from all images taken for one pane during a full rotation of the sample. In order to assess the parametric values of the bone, the computer combined the 2D images of all panes into one 3D image of the scan (Figure 3.11, Figure 3.12 A). This 3D image may be used for further analysis by selecting specific volumes of interest inside the image and having the computer calculate a multitude of parameters that provide information about the development of the bone within the entire defect region. Moreover, an image of an individual 2D pane may be analyzed by the same means that are commonly used for analysis of histological cross-sections.

4   SUMMARY OF KEY FINDINGS

This chapter intended to summarize the key findings of the different experiments conducted during this thesis and to show additional results that were not presented in the papers. All detailed results that have already been described in Papers I-V.

4.1   The SBAE surface

Paper I revealed that TiZr SBAE had an increased hydrogen content compared to Ti SBAE. Zirconium appeared to enhance hydride formation in this titanium alloy when etched in acid. The hypothesis was proposed in Paper I that zirconium mainly catalyzed the hydrogen absorption in the TiZr alloy. Comparison of the surface topography between Ti SBAE and TiZr SBAE revealed significant differences on the micro- and nano-scale. Still, both materials` micro-topography values were within the range that had been described as optimal for bone-anchored implants in various studies.[36-38] Assessment of the nano-topography revealed large numbers of spherical structures for TiZr SBAE, whereas Ti SBAE only showed very few of these structures (Figure 4.1 A, E). The source of these nano-structures remained unclear, but was believed to have been associated with the influence of Zr on hydride formation during the etching process. The results presented in Paper II for the same SBAE surfaces could confirm the findings presented in Paper I (Figure 4.2 B).

Based on the hydrogen content and the surface topography it was proposed in Paper I that Ti SBAE and TiZr SBAE provided an adequate surface for use in a cathodic polarization process in order to maximize the efficiency of the process in terms of process time and biomolecule coating. This was in agreement with the first 1st aim in the aim of research of this thesis.
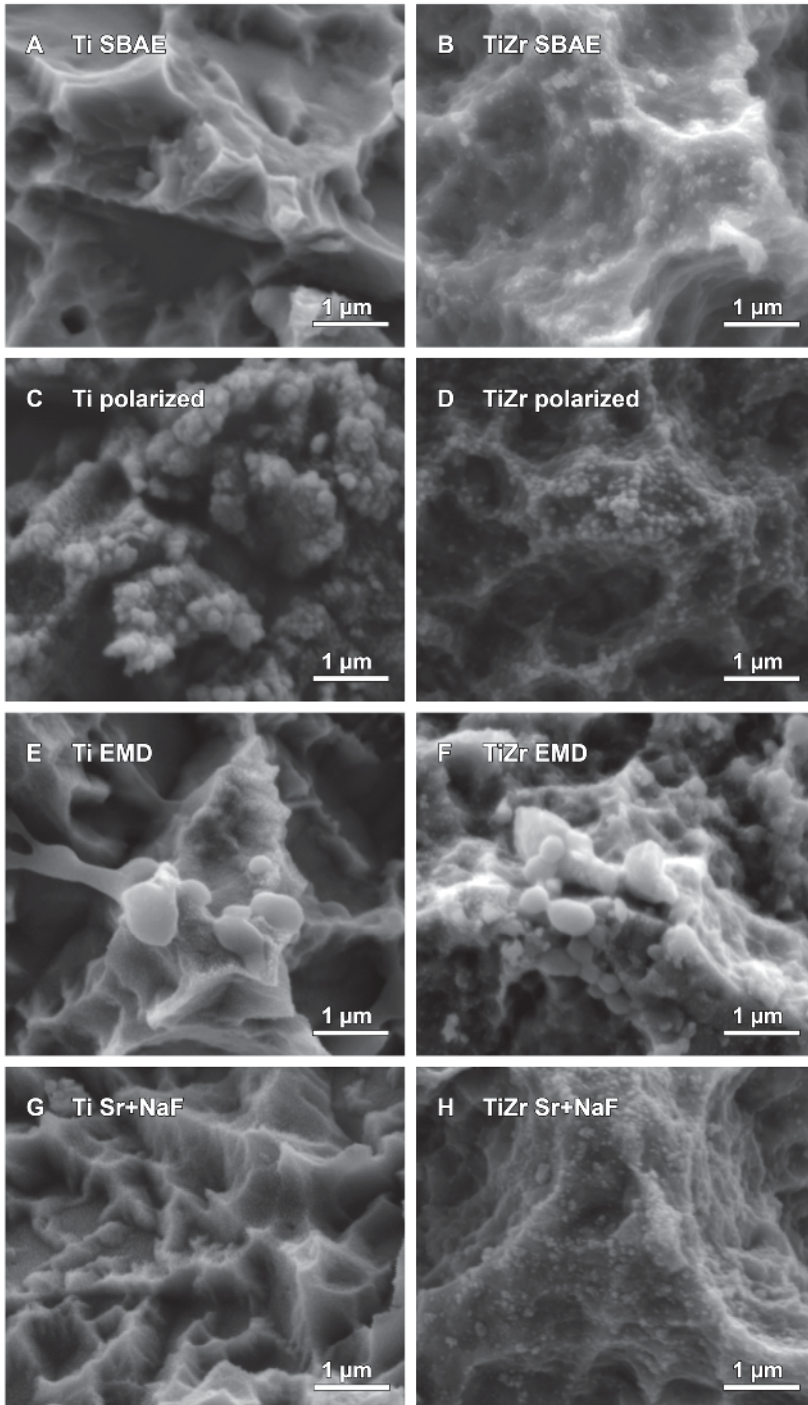
Figure 4.1   FE- SEM images of SBAE (A, B), polarized (C, D), EMD-coated (E, F), and Sr-coated (G, H) surfaces
for Ti and TiZr at 50k magnification (Papers I-IV).

4.2 Cathodic polarization of SBAE surfaces

Paper II examined the influence of cathodic reduction of TiZr SBAE and Ti SBAE in acidic solution. The results presented in Paper II showed a continuous, cyclic buildup and breakdown of surface hydrogen levels. It was hypothesized in Paper II that such a cyclic development may provide a possibility to speed up a process that actively attaches charged biomolecules to the surface by allowing relatively short process times. Anyhow, Paper II also showed that polarization did not seem to be a suitable method for increasing total hydrogen content on SBAE surfaces as further hydride creation seemed to be suppressed. The proposed hypothesis in Paper II was that the hydrogen layer already present on the SBAE surface from the preceding hot acid-etching appeared to modulate hydride creation. Analysis of the surface topography after cathodic polarization showed that the surface of both materials was altered by creation of nano-nodules, nano-spheres and flower shaped micro-structures on the surface (Figure 4.1 B, F).

Paper II showed that cathodic polarization of SBAE surfaces can be used for modifying the hydrogen layer on Ti SBAE and TiZr SBAE surfaces while offering the possibility of increasing the polarization time efficiency compared to not chemically modified surfaces. Thus the 2nd sub-aim of the general aim of research of this thesis could be accomplished successfully.
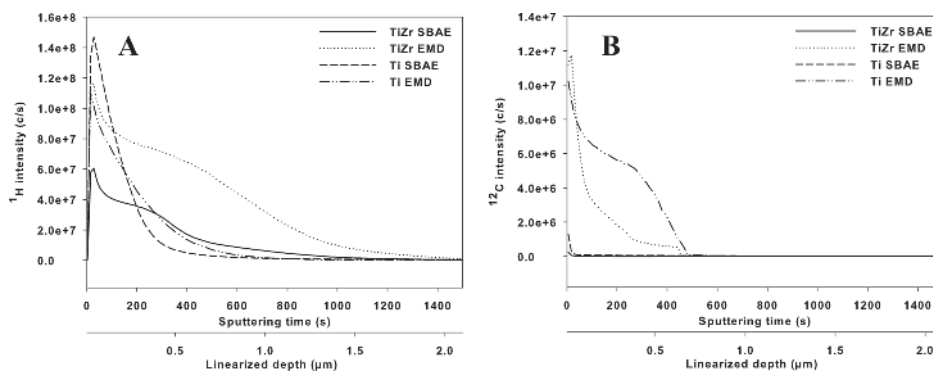
Figure 4.2   SIMS depth profiles of the ^{1}H (A) and ^{12}C (B) isotopes for SBAE and EMD-coated samples (Figure modified from Paper III).

4.3   Biomedical modification of the SBAE surfaces

Paper III and Paper IV have shown that a cathodic polarization process can be used for coating EMD (Paper III) and Sr (Paper IV) onto titanium-zirconium alloy and grade IV titanium surfaces while maintaining the integrity and bio-availability of the biomolecules.
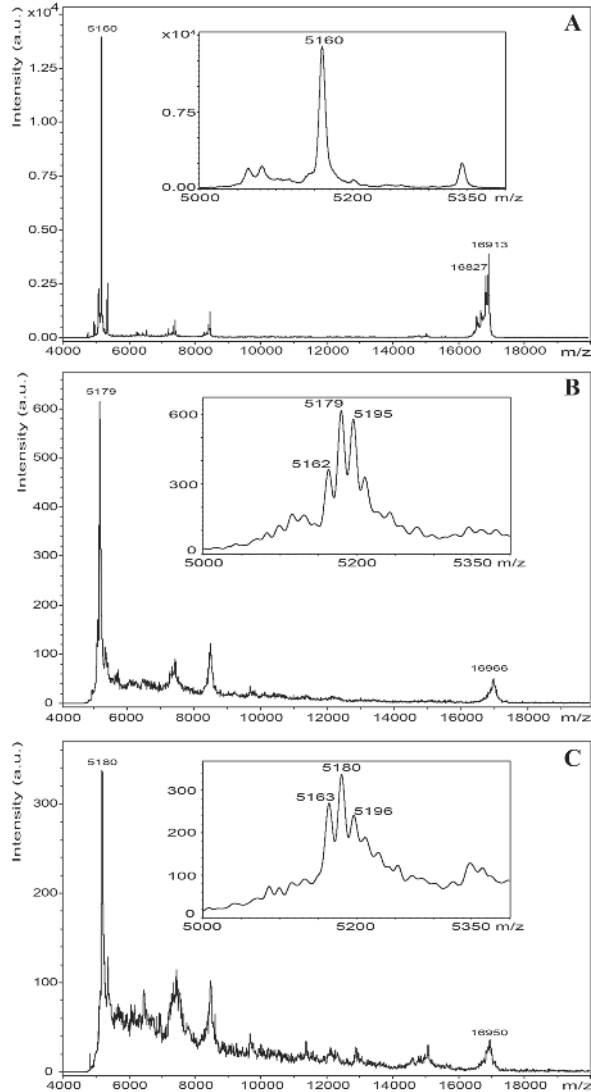
Figure 4.3   MALDI spectra of pure EMD (A), TiZr EMD (B), and Ti EMD (C). All graphs include an enlarged version of the region between 5000 m/z and 5400 m/z. (Figure taken from Paper III).

EMD coated surfaces presented in Paper III were analyzed by SIMS in order to verify coating with EMD by tracing EMD related carbon on the surface. Carbon depth profiles acquired by SIMS revealed an incorporation of carbon into the surface that was believed to be EMD related (Figure 4.2 A-C). Moreover, XPS analysis revealed the presence of EMD specific components and a change of EMD-related binding states of carbon and oxygen that had roughly doubled in comparison to the uncoated samples. EMD-coated surfaces of both materials showed a shift in the binding state of the carbon towards a distribution of C-C, C=C, and C-O/C-N bonds comparable to the distribution observed for pure EMD. Coated surfaces also revealed EMD related nitrogen, silicon, and sulfur on the surface after coating. Decreased Ti and Zr levels observed in XPS indicated a masking of surface after polarization as it had previously been described by Morra et al. for a different surface coating.[158] Analysis of the surface topography by SEM imaging showed spherical structures of EMD on the surface of both materials after coating (Figure 4.1 C, G) that were comparable to structures of EMD that had been reported by other authors.[89,159] Main components of EMD could be verified to be intact after coating by MALDI-TOF MS analysis of the 5 kDa and 16 kDa peaks that have also been reported for EMD by other studies (Figure 4.3).[84,132,160,161]

After the cell study presented Paper III it was desired to quantify the amount of EMD prior to the animal study presented in Paper V. Hence, dot blot was used to quantify EMD on TiZr EMD coins (Figure 4.4). The specific reaction of the primary antibody in the test group confirmed that EMD was on the surface in measurable amounts, while the control group confirmed that this was not due to false positives or nonspecific cross reactivity. This was in agreement with the results from the MALDI presented in Paper III. Comparison of the results from the coated samples to results of the EMD standard revealed an average of 77.0±19.2 ng of EMD per TiZr EMD coin.
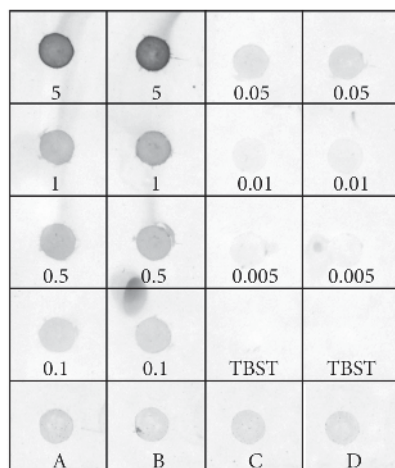
Figure 4.4 Dot-blot quantification of EMD released from TiZr EMD samples. The labels inside the grid refer to the EMD standard (in ng/ml), TBST for the blank negative control, and TiZr EMD samples A-D.

Coating with Sr and different F-modifications presented in Paper IV revealed that F appeared to support the attachment of Sr to the surface, when F was present in the buffer during polarization. By contrast, when F was already absorbed to the surface before polarization, it appeared to hinder Sr-attachment. It was hypothesized that the presence of F in the buffer led to the formation of SrF_2 that was adsorbed to the surface (Figure 4.5). SEM images of the surface revealed nano-structures for the Sr+NaF group but no differences compared to the SBAE groups for all other Sr-coatings (Figure 4.1 D, H).
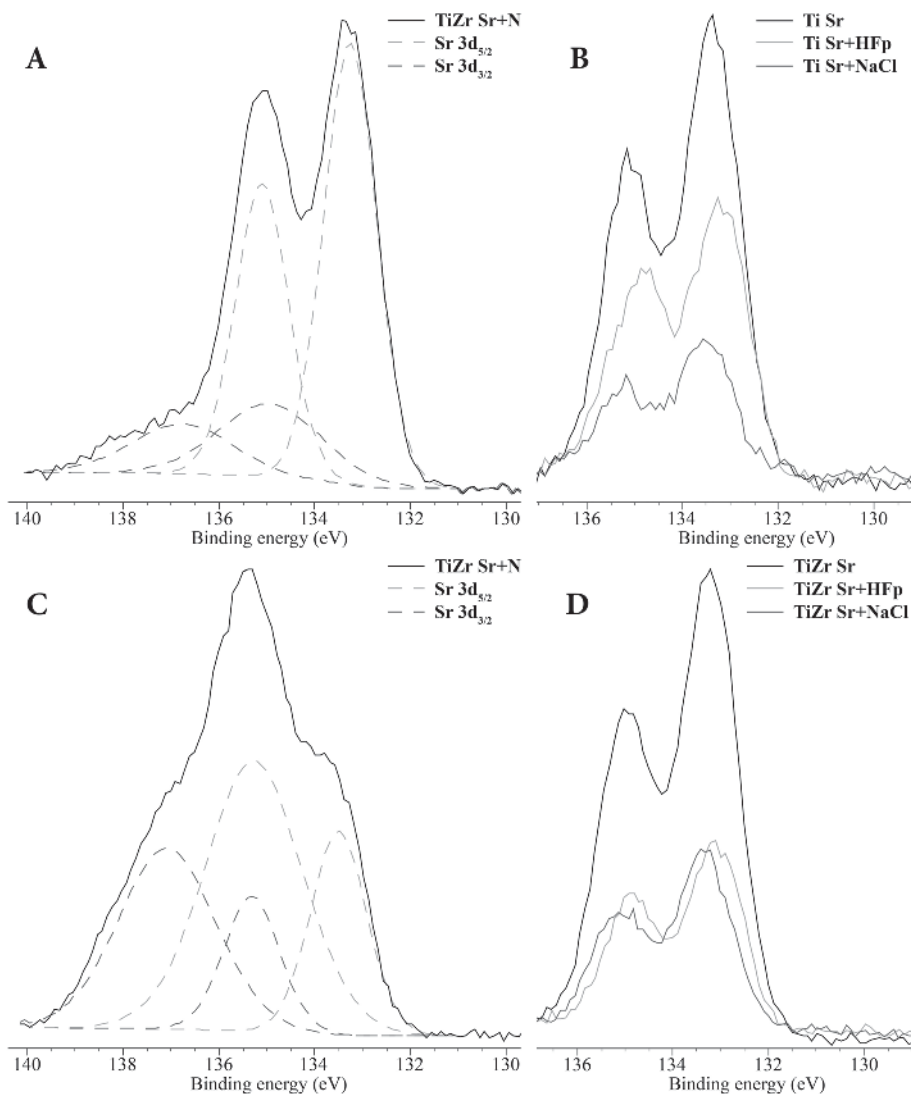
Figure 4.5   XPS detail spectra of the Sr 3d peak with the peak position (eV) on the x-axis and the relative peak intensity on the y-axis (a.u.). The groups polarized with Sr+NaF (A, C) revealed a second Sr $3d_{5/2}$ and a second Sr $3d_{3/2}$ peak, whereas there was only one Sr $3d_{5/2}$ and one Sr $3d_{3/2}$ peak for all other groups (B, D). (Figure taken from Paper IV)

4.4   Bio-availability and function of the biomolecules on the coated surfaces

4.4.1   Cell studies

The bio-availability of the biomolecules was tested in cell studies with the osteoclastic, murine MC3T3-E1 cells for EMD (Paper III) and Sr (Paper IV) for coated Ti and TiZr surfaces.

EMD coated surfaces showed promising results for an improved biological response by enhanced ALP activity and increased Coll-1 expression as it was expected for EMD-modified surfaces.[86,162,163] Assessment of the LDH activity showed that the EMD-coated surfaces was not toxic to the cells. Paper III concluded that this was a sign of earlier cell differentiation and thus confirmed that EMD was bio-available and maintained its function in creating an active surface.

Sr-coatings with different alterations of the coating procedure (Table 3.1) presented in Paper IV suggested marginally earlier cell differentiation for Sr+NaF and Sr+HFp modified surfaces in comparison to the respective SBAE surface. It was concluded that there appeared to be an ideal ratio of SrF_2 and SrO on the surface that triggered the improved biological response. In detail, the Sr+NaF group showed decreased Coll-1 expression and increased ALP and OC expression. At the same time LDH activity assessment revealed that the coating was not toxic to the cells. It was believed that the mechanism involved in the improved cell response was the protection of the surface from contaminations by a small amount of SrF_2 while a larger amount of SrO activated the surface and provided bio-available Sr.

4.4.2   Animal study

The rabbit study conducted in Paper V assessed the bio-response to TiZr EMD and TiZr Sr+NaF coin-shaped implants in a validated rabbit model.

μCT analysis showed EMD induced a lower bone surface density, bone surface to volume ratio and intersection surface than the SBAE, pol and Sr groups, which was in agreement with the long-term effect that has been reported for EMD.[164,165] Moreover, EMD had lower inflammation markers (TNF-α, IL-6, and IL-10) and lower cytotoxicity for both time points compared to TiZr SBAE. ALP activity in the wound fluid was higher in the EMD group compared to pol and Sr groups after 8 weeks

TiZr Sr+NaF implants showed no significant differences of the bone formation, bone resorption, and inflammation related markers compared to TiZr SBAE in the analysis of wound fluids and bone tissue gene expression. Moreover, μCT evaluation showed no significant effect of the coating on the quality or quantity of the bone in the central defect under the coin for TiZr Sr+NaF implants.

It was believed that a possible beneficial effect of the individual surface coatings could not be clearly quantified due to shortcomings of the animal model for evaluating the desired effect of the biomolecules. The SBAE surface has been shown to work comparatively well *in vivo*[52,53] for healthy bone. Thus, a model that uses an implantation site of minor bone quality of bone quality

may be better suited for showing a significant effect of the coating compared to the SBAE surface.

4.4.3   Tensile removal test of the animal study

A tensile removal test was performed during the animal study presented in Paper V that was not included in the manuscript since the results may have been misleading as it has been described in section 3.7.4. Hence, the groups presented here are the same groups that have been described in Paper V. After the PTFE caps had been removed from the implants, bone was revealed that had grown in between the sample coin and the protective PTFE cap. Figure 3.8 A shows a μCT image of this bone that was visible as a rim on the surface after removal of the coin. The tensile removal force test revealed unexpected results as the force vs. strain plot recorded during the test did not reveal a single maximum removal force but the plot showed two plateaus for many samples (Figure 3.8 B). During the recording of the measurement, both points in the plot could be recognized by the sound of breaking bone. It could not be detected whether the bone one the side of the coin or the bone grown into the face side of the coin had been detached (Figure 3.8 C, D). As the load could still be increased significantly for most samples, the maximum force recorded was selected for further evaluation. Only the pol group revealed a significant difference (p<0.05) against the SBAE group after 8 weeks (Figure 4.6 B). No other significant differences could be detected, nor was there observed any clear trend.
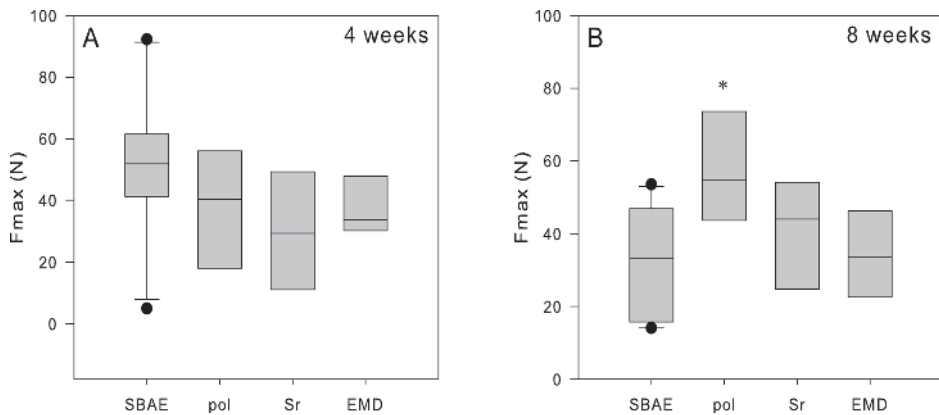
Figure 4.6   Maximum forces recorded in tensile removal test after 4 weeks (A) and 8 weeks (B) for all four groups (n=8). Box plots represent the median with interquartile range. The SBAE group had a larger sample size (n=10) and was thus displayed with the 5% and 95% percentile. The pol group showed significantly higher (*p<0.05) pull-out forces after 8 weeks than the SBAE group. No other significant differences were observed.

5 DISCUSSION

The ultimate goal of biomedical surface modification is to help patients who are not eligible for an endosseous dental implant yet for various reasons and to improve long-term implant stability.[27-29] The conception of bioactive surface modification is creating a surface that is bioactive in the bone or may even be osseoinductive. As it was described in section 1.4 of this thesis, EMD and Sr have indicated such a bioactive effect in a multitude of studies. This thesis aimed at demonstrating a coating of Ti SBAE and TiZr SBAE with EMD and Sr by a polarization process and assessing the biological response to the different surface coatings *in vitro* and partially *in vivo*. This chapter intended to put the results of Paper I-V into perspective in order to discuss the aim of this thesis and to support or reject the general hypothesis. All methodological considerations and matters regarding observations that were made during the course of this thesis and have not been presented in Papers I-V have been discussed in section 3 of this thesis.

5.1 Considerations on the surface coatings

5.1.1 *The SBAE surface as a basis for surface coating*

The reason for using a SBAE surface, which was comparable to the Straumann SLActive® surface that is currently available for dental implants, was the idea of improving a surface that has already shown a history of clinical success.[39] A moderately rough SBAE surface provides adequate primary stability by mechanical interlocking of the surface roughness in bone. A bioactive surface coating is not intended to create such a primary stability but is much more aiming at supporting peri-implant bone healing that may ultimately lead to an improved long-term stability of the implant.

The results presented in Paper I showed that Ti SBAE and TiZr SBAE already have comparably high hydrogen levels and a surface topography that is in the range that has previously been reported to be ideal for endosseous dental implants.[35-39] This marked a successful completion of the 1st sub-aim of this thesis.

5.1.2 *Cathodic polarization of the SBAE surface*

The effect of cathodic polarization to the SBAE surfaces in acidic solution has demonstrated a cyclic development of the surface hydride layer as it has been shown in Paper II. As it was proposed in the general hypothesis, this was believed to provide an appropriate basis for attaching charged biomolecules and could conceivably speed up overall process time. The results of Paper II allowed a selection of process parameters that promised an ideal balance of hydrogen build-up and short process times. Ti SBAE and TiZr SBAE demonstrated a different development of the surface hydrogen levels during cathodic polarization (Paper II) in acidic solution. This was the reason for selecting a differing current density for coating the biomolecules (Paper III & IV) onto Ti (1.65 mA/cm²) and onto TiZr (0.54 mA/cm²) as the selected current densities have shown the most promising development of the surface hydrogen levels with a focus on reduced process times (Paper II). The selection of the individual current density for each material was based on the theory that hydride creation was more favorable than overall hydride levels on the surface since it

was believed that the biomolecules would attach to the hydride layer during creation of the hydride layer.

Moreover, the polarized surfaces have been shown to maintain a surface roughness comparable to the roughness of the original SBAE surfaces. As a modification of the surface morphology was not the aim of the surface coating, the unchanged micro-morphology was considered as a positive outcome of the surface modification. It was believed that maintaining the moderately rough surface of the original SBAE surface should provide a similar primary stability of the electro-coated surface as the original SBAE surface. This hypothesis was based on the principle of mechanical interlocking of the implant surface with the bone, since the surface roughness of polarized surfaces was comparable to the SBAE surface and was also in the range between 1.16 μm and 3 μm that has been shown to be optimal for endosseous implants in other studies.[36-39]

While the micro-topography of polarized surfaces remained unchanged after cathodic polarization, the influence on the surfaces` nano-morphology and nano-topography was different for the individual materials and specific surface-coatings with EMD and Sr (Papers III & IV). The detailed effect of the individual coating on each material was illustrated in Figure 4.1 and has been discussed in Papers I-IV. The general trend was observed that the polarization appeared to have a significantly stronger effect on the nano-topography and nano-morphology of Ti compared to TiZr. While the increased polarization resistance of Ti-alloys, like TiZr, is usually related to a generally increased biocompatibility, it similarly affects the influence of the electro-coating process on the different materials.[166] Thus, it was reasoned that the larger influence of the process on Ti was a direct result of the increased corrosion resistance of TiZr compared to Ti.[7,8] It was believed that this was also the reason for the different hydrogen development of the surface at comparable current densities that lead to the selection of specific processing parameters for each material.

In summary, Paper II could identify suitable process parameters for coating the surface with biomolecules at reasonably short process time, as it was proposed in the 2nd sub-aim of this thesis.

5.1.3   Coating of the SBAE surfaces with EMD and Sr

Surface coatings with EMD (Paper III) and Sr (Paper IV) by cathodic polarization have been shown to effectively attach EMD and Sr to Ti SBAE and TiZr SBAE while maintaining the micro-topography and micro-morphology of the original SBAE surfaces. As above-mentioned, each specific coating had a unique influence on the nano-topography and nano-morphology of a surface (Figure 4.1).

The effective coating of the surface with EMD has been described in Paper III. As aforementioned, EMD is a protein-mixture of several components. Although analysis of the surface by XPS and analysis of the coating by MALDI could confirm major components of EMD for the surface, the question still remained regarding which components did not attach to the surface. This thesis could not identify which components besides amelogenin (Paper III) of the EMD were actually attached to the surface. Still, it shall be mentioned again that less than 5% of EMD consist non-amelogenin.[81-84] It has been established that the major part of EMD, the amelogenins, ionizes when in an acidic environment like the acidic buffer used for surface

coating in this thesis.[97-99] In reversing the argument, the components that did not ionize should not have attached to the surface alongside the ionized components during the surface coating. It has been shown that not all components of EMD are required in order to unfold the effect EMD has on bone; ongoing research has taken up this idea and is investigating the possibility of removing unnecessary components from EMD or even synthesizing the active components of EMD.[167-172] Thus it was concluded that the surface coating with the major components of EMD should already enhance biological reaction to the surface and should therefore be investigated further in an *in vitro* study.

Coating with Sr by cathodic polarization appeared to be intuitively easy to perform due to its solubility, temperature resistance, light resistance, and long term stability. As an earth alkali metal, Sr ionizes easily and recombines into new compounds. Anyhow, the results of Paper IV showed that Sr-attachment was influenced by the presence of additional ions and by the location of those ions. F in particular appeared to have a significant effect on the amount of Sr that could be attached to the surface by cathodic polarization when present in the buffer solution (Paper IV). This mechanism was additionally influenced by the base material, as TiZr showed larger amounts of SrF_2 than Ti for the Sr+NaF group. The presence of F in the buffer attached SrF_2 to the surface in addition to Sr that was bond to the surface as part of a Sr-oxide-compound. Such Sr-oxide-compounds were also observed for coatings without F in the buffer (Figure 4.5). As XPS analysis of the Sr-coated surfaces showed fairly low amounts of Sr on the surface (Paper IV), an increase in Sr surface coverage appeared desirable. For this reason, the Sr-coating with additional F in the buffer (Sr+NaF) was selected for the surface coating used in the animal study (Paper V). This decision was driven by the desire of all parties involved in this project to maximize Sr-content of the surface against the knowledge that SrF_2 is insoluble in aqueous solution[173] and would most likely stay attached to the surface. In this regard, attachment of SrF_2 to the surface would not provide bio-available Sr in an *in vitro* or *in vivo* situation. Yet, Paper IV proposed the hypothesis that a small amount of additional SrF_2 maintained the surface`s bio-activity by protecting it from undesired contaminations. Moreover, Sr+NaF modification had an effect on the nano-topography of the surface (Paper IV, Figure 4.1). Anyhow, a modification of the surface coating by coating with Sr without additional F in the buffer in order to avoid the formation of SrF_2 on the surface has been shown to be a viable option for coating of the surface with Sr that is bound as bio-available and active SrO. Paper IV also suggested to use protective cover gas like it is used for the original SBAE surface in order to maintain the surface`s reactivity.

It has been shown in Paper III and Paper IV that EMD and Sr can be coated to Ti SBAE and TiZr SBAE surfaces by cathodic polarization. Thus the 3rd sub-aim of the general aim of research of this thesis could be successfully accomplished.

5.2   Considerations on the bioactivity of the coated surfaces

5.2.1   Bioactivity of EMD- and Sr-coated surfaces

EMD coated surfaces have shown enhanced cell differentiation over SBAE surfaces in the cell study and thus confirmed that EMD was bio-available, intact, and maintained its bioactivity (Paper III). The rabbit study (Paper V) showed that EMD-coated surface performed at least as well as the SBAE or pol surface in healthy bone. At the same time EMD coated TiZr showed a

trend towards lower inflammatory response and lower cytotoxicity *in vivo*. The Sr-NaF coated surface has been shown to provide bio-available Sr and earlier cell differentiation compared to the SBAE surface *in vitro* (Paper IV). Moreover, this surface coating performed as well as the SBAE surface *in vivo*.

As it has been discussed in Paper V, it was believed that the animal model was not capable of quantifying the effect of the surface coating with regard to the desired effect of the coating. Taken into consideration the motivation for the surface coating, a model that would provide an implantation side with poor bone quality or reduced bone quantity would be preferable in order to assess the effect of the individual biomolecules on bone healing. It was believed that a beneficial effect of the biomolecules on bone healing could not be observed for healthy bone.

Although the animal study showed diverse results, the bio-availability and maintained function could be confirmed in the cell study. This was subject of the 4th sub-aim of this thesis. Moreover, the biological response to the coated surfaces was assessed in a rabbit study as it was proposed in the 5th sub-aim of this thesis. As TiZr EMD and TiZr Sr+NaF performed as well as TiZr SBAE in the rabbit study, this did neither support nor confute the proposed hypothesis that the coated surfaces may be bioactive in the bone.

5.2.2   *Considerations on the tensile removal test*

Although the validity of the findings of the tensile removal test may be appealed as the shear forces could not be distinguished from the real retention forces, the results of the tensile test were compared to results from earlier studies that assessed implant removal forces for comparable surface modifications. Park et al. have shown enhanced removal torque forces for $TiAl_6V_4$ alloy implants incorporating strontium in comparison to implants without strontium.[174] Likewise, Maïmoun et al. have shown that orally administered Sr-ranelate improved Ti-implant osseointegration in rats and showed significantly increased pull-out strength and increased bone to implant contact.[175] These findings could not be confirmed in this study. Although Sr coated implants appeared to show marginally increased tensile removal forces after 8 weeks in this study, the difference to the SBAE surface was not statistically significant. Stenport et al. concluded that EMD did not contribute to peri-implant bone formation for titanium implants as no increase in removal torque was detected in a rabbit study.[176] These findings were comparable to the findings of this study that showed no difference in tensile removal force for EMD coated implants. The moderately rough SBAE surface already showed comparably high functional attachment. Thus, the model itself may be challenged for use with moderately rough surfaces. As the biomolecule is released from the surface, an effect of the biomolecule must not necessarily be an increase in functional attachment but in bone formation itself. The motivation for biomedical modification of the implant surface was to enlarge the patient group that may be eligible for an endosseous dental implant. As patients who are not yet eligible for an endosseous dental implant most often suffer from poor bone quality or scarce bone quantity, the aim of the surface coating was to create a bioactive surface that may have an osseoinductive effect. This is also the reason why the tensile removal force test was not included in Paper V, as it may have been misleading and have led to incorrect conclusions regarding the bio-response to the surface coating.

6 CONCLUSION

The results presented in this thesis suggested that a hydrogen-rich, SBAE surface provides an appropriate substrate for attaching charged biomolecules to titanium based materials in a cathodic polarization process. The SBAE surface decreased the time required for the polarization process in comparison to an unmodified surface. The produced hydride layer acted as an intermediate layer for linker-free attaching biomolecules to the surface while maintaining the original surface micro-topography in a range that is desired for implant materials. The EMD and Sr attached to the implant surfaces were bio-available, intact, and had maintained their bioactivity. The *in vitro* results suggested that the surface coatings had improved bioactive properties over non-coated surfaces. Although the biological response *in vivo* could not benefit from these bioactivated surfaces, the coated surfaces performed as well as the unmodified surface.

In summary, the results presented in this thesis supported the general hypothesis. Moreover, the specific sub-hypothesis that such a coated surface can be used for improving implant performance could be supported by the improved performance observed in the cell study. Since the surface performed as well as the non-coated surface *in vivo*, a bioactive response to the coated surfaces could neither be supported nor confuted.

7 FUTURE WORK: REMAINING AND NEW CHALLENGES

Based on the results presented in paper Paper II, more work should be done on explaining the mechanism involved in the formation of the nano-nodules, their chemical composition, or any details about the effect of the surfaces` modification on their biocompatibility.

Based on the results presented in Paper V, a modified animal model that would provide non-healthy bone may potentially reveal a beneficial effect of the surface coating compared to the SBAE surface. Such a model would mimic the patient group that is not yet eligible for a dental implant.

Endosseous dental implants with a bioactive surface coating may provide a key component for providing implants to patients who are not eligible for an endosseous dental implant today by enhancing or even inducing bone growth at implantation sites with poor bone quality or bone quantity. Anyhow, other influences on the success of a dental implant like the surgical procedure, unique patient variables and mechanical loading of the implant will remain a challenge that cannot be approached by a bioactive surface coating alone.[11-14] In addition, a bioactive surface coating may even require modifications to the surgical procedure in order to maintain the bioactivity of a coated surface. Although coatings like the Sr-coating presented in this thesis should be exempt from influences of temperature and light during storage, this may present a challenge for coatings with proteins or other organic compounds. A complex surface coating like the EMD-coated surface presented in this thesis demands storage and handling that are specific to the demands of EMD. Thus, the EMD-coated surface may be improved in terms of its bioactivity by investigating and defining suitable parameters. The following questions must be answered in order to define suitable handling and storage of EMD-coated surfaces:

- How long, in which medium (water or else?) and by which means (supportive brush or ultrasound?) should the surface be washed immediately after the coating?
- Is a dry or a wet storage, like the 0.9% NaCl (aq) that is used for SLActive® surfaces, preferable?
- If a dry storage were chosen, how would this influence the reactivity of the surface and its bioactivity? Should a protective cover gas be used and which one?
- If a wet storage were chosen, which medium would be ideal in terms of the stability of EMD and possible oxidation or detachment from the surface? How important would the pH of the storage medium be with regard to the solubility of EMD?
- How light sensitive is the EMD-coating and how would this affect the packing?
- How temperature sensitive is the coating? How long is the shelf life before the surface coating degrades?

Besides the remaining challenges concerning handling, package and storage of a coated surface, a special patient compliance may also be necessary so that the biomolecule can unfold its full potential in supporting bone healing. Factors like a special diet, supplementary medication or to discontinue smoking may be critical for the success of a coated-surface. A novel surface may also require new maintenance procedures in the chase of intricacies with the implant.

Alongside the definition of suitable handling and storage standards, the results of this thesis evidence that this process can be used for commercially available implant surfaces and should thus be transferred from coin-shaped samples to screw-shaped implants. Although the general parameters for the coating process can be defined right away by taking into account the enlarged surface area of a screw compared to a coin, there might be influences of the form factor that require adjustments specific to the individual shape. Influences like the previously mentioned homogeneity of the electric field require an adjustment of the counter electrode. Moreover, the sample holder has to be adjusted to the different form-factor of the coated sample.

Coating of screw-shaped samples may allow an implementation of the coating process into the industrial production process of a dental implant. Considering the production of the SBAE surface, as it has been described previously, a bioactive surface coating may be inserted into the production process before the implants are stored in saline solution. If the implants were directly transferred from acid-etching to electro-coating, the surface may even provide a larger potential for attaching biomolecules as it has not been exposed to water or air in between. This would prevent the formation of an oxide layer and allow immediate modulation of the hydride layer. In case of EMD-coating, the EMD may even be provided alongside the acetic acid used for the coating as EMD is dissolved in acidic acid during the production of EMD.

In addition to the challenges faced when transferring the coating process from coin-shaped samples to screw-shaped samples, it must remain possible to confirm the integrity and a homogeneous distribution of the biomolecules after coating. In this regard, the analytical methods must be adjusted alongside the process in order remain in control of the process.

Considering that EMD-coating was done with a buffer made of sodium acetate and acetic acid, the sodium acetate can easily be replaced by strontium acetate in order to create a combined surface coating with EMD and Sr. Such a coating has not been evaluated during the experiments conducted for this thesis and thus remains to be shown. If a combined EMD+Sr coating can be done, it may combine the beneficial characteristics of both biomolecules and is hence worthy of being investigated in future studies.

8 REFERENCES

1. Westbroek P, Marin F. A marriage of bone and nacre. Nature, 1998, 392, 861-862.
2. Brånemark P, Breine U, Adell R, Hansson B, Lindström J, Ohlsson Å. Intra-osseous anchorage of dental prostheses: I. Experimental studies. Scand J Plast Recons, 1969, 3, 81-100.
3. Brånemark PI, Gröndahl K, Brånemark BK. How human applications began. Why osseointegration would work and how it did in the first patients treated. Basic facts and philosophical thoughts. The osseointegration book: from calvarium to calcaneus., 2005, xvii, 19.
4. Cibirka RM, Razzoog M, Lang BR. Critical evaluation of patient responses to dental implant therapy. J Prosthet Dent, 1997, 78, 574-581.
5. Walker A, Maltby T. Active ageing: A strategic policy solution to demographic ageing in the European Union. Int J Soc Welf, 2012, 21, S117-S130.
6. Hille GH. Titanium for Surgical Implants. J Mater, 1966, 1, 373-&.
7. Bernhard N, Berner S, De Wild M, Wieland M. The binary TiZr Alloy – a newly developed Ti alloy for use in dental implants. Forum Implantol, 2009, 5, 30–39.
8. Ferreira EA, Rocha-Filho RC, Biaggio SR, Bocchi N. Corrosion resistance of the Ti-50Zr at.% alloy after anodization in different acidic electrolytes. Corr Sci, 2010, 52, 4058-4063.
9. Williams DF. Definitions in biomaterials: proceedings of a consensus conference of the European Society for Biomaterials. 1986 March 3-5, 1986; Chester, England.
10. Wintermantel E, Shah-Derler B, Bruinink A, Petitmermet M, Blum J, Ha SW. Biokompatibilität. Medizintechnik Life Science Engineering: Springer, 2009, pp 67-104.
11. Zhang F, Yang GL, He FM, Zhang LJ, Zhao SF. Cell response of titanium implant with a roughened surface containing titanium hydride: an in vitro study. J Oral Maxillofac Surg, 2010, 68, 1131-1139.
12. Le Guehennec L, Soueidan A, Layrolle P, Amouriq Y. Surface treatments of titanium dental implants for rapid osseointegration. Dent Mater, 2007, 23, 844-854.
13. Kasemo B. Biological surface science. Surf Sci, 2002, 500, 656-677.
14. Puleo DA, Nanci A. Understanding and controlling the bone–implant interface. Biomaterials, 1999, 20, 2311-2321.
15. Albrektsson T, Zarb G, Worthington P, Eriksson AR. The long-term efficacy of currently used dental implants: a review and proposed criteria of success. Int J Oral Maxillofac Implants, 1986, 1, 11-25.
16. Alsaadi G, Quirynen M, Komarek A, van Steenberghe D. Impact of local and systemic factors on the incidence of late oral implant loss. Clin Oral Implants Res, 2008, 19, 670-676.
17. Atala A, Lanza R. Handbook of stem cells, Access Online via Elsevier, 2012.
18. Haugen HJ, Monjo M, Rubert M, Verket A, Lyngstadaas SP, Ellingsen JE, Rønold HJ, Wohlfahrt JC. Porous ceramic titanium dioxide scaffolds promote bone formation in rabbit peri-implant cortical defect model. Acta Biomater, 2013, 9, 5390-5399.
19. Monjo M, Rubert M, Wohlfahrt JC, Ronold HJ, Ellingsen JE, Lyngstadaas SP. In vivo performance of absorbable collagen sponges with rosuvastatin in critical-size cortical bone defects. Acta Biomater, 2010, 6, 1405-1412.
20. Monjo M, Rubert M, Ellingsen JE, Lyngstadaas SP. Rosuvastatin promotes osteoblast differentiation and regulates SLCO1A1 transporter gene expression in MC3T3-E1 cells. Cell Physiol Biochem, 2010, 26, 647-656.
21. Marie PJ. Osteoblasts and Bone Formation. Adv Organ Biol: Elsevier, 1998, pp 445-473.
22. Kushida K, Takahashi M, Kawana K, Inoue T. Comparison of markers for bone formation and resorption in premenopausal and postmenopausal subjects, and osteoporosis patients. J Clin Endocrinol Metab, 1995, 80, 2447-2450.
23. Teitelbaum SL. Bone Resorption by Osteoclasts. Science, 2000, 289, 1504-1508.

24. Tilg H, Dinarello CA, Mier JW. IL-6 and APPs: anti-inflammatory and immunosuppressive mediators. Immunol Today, 1997, 18, 428-432.

25. Davies JE. Understanding peri-implant endosseous healing. J Dent Edu, 2003, 67, 932-949.

26. Shah-Derler B, Wintermantel E, Ha SW. Gewebe. Medizintechnik Life Science Engineering: Springer, 2008, pp 155-170.

27. Palma-Carrio C, Maestre-Ferrin L, Penarrocha-Oltra D, Penarrocha-Diago MA, Penarrocha-Diago M. Risk factors associated with early failure of dental implants. A literature review. Med Oral Patol Oral Cir Bucal, 2011, 16, e514-517.

28. Moy PK, Medina D, Shetty V, Aghaloo TL. Dental implant failure rates and associated risk factors. Int J Oral Maxillofac Implants, 2005, 20, 569-577.

29. Heitz-Mayfield LJ. Peri-implant diseases: diagnosis and risk indicators. J Clin Periodontol, 2008, 35, 292-304.

30. Rønold HJ, Lyngstadaas SP, Ellingsen JE. Analysing the optimal value for titanium implant roughness in bone attachment using a tensile test. Biomaterials, 2003, 24, 4559-4564.

31. Boyan BD, Hummert TW, Dean DD, Schwartz Z. Role of material surfaces in regulating bone and cartilage cell response. Biomaterials, 1996, 17, 137-146.

32. Buser D, Schenk RK, Steinemann S, Fiorellini JP, Fox CH, Stich H. Influence of surface characteristics on bone integration of titanium implants. A histomorphometric study in miniature pigs. J Biomed Mater Res, 1991, 25, 889-902.

33. Wong M, Eulenberger J, Schenk R, Hunziker E. Effect of surface topology on the osseointegration of implant materials in trabecular bone. J Biomed Mater Res, 1995, 29, 1567-1575.

34. Lamolle SF, Monjo M, Rubert M, Haugen HJ, Lyngstadaas SP, Ellingsen JE. The effect of hydrofluoric acid treatment of titanium surface on nanostructural and chemical changes and the growth of MC3T3-E1 cells. Biomaterials, 2009, 30, 736-742.

35. Rønold HJ. The Effect of Surface Micro Structure on Titanium Implant Attachment to Bone, Doctoral thesis, Faculty of Dentistry, University of Oslo, 2002.

36. Buser D, Broggini N, Wieland M, Schenk RK, Denzer AJ, Cochran DL, Hoffmann B, Lussi A, Steinemann SG. Enhanced bone apposition to a chemically modified SLA titanium surface. J Dent Res, 2004, 83, 529-533.

37. Donos N, Hamlet S, Lang NP, Salvi GE, Huynh-Ba G, Bosshardt DD, Ivanovski S. Gene expression profile of osseointegration of a hydrophilic compared with a hydrophobic microrough implant surface. Clin Oral Implants Res, 2011, 22, 365-372.

38. Lu X, Wang Y, Yang X, Zhang Q, Zhao Z, Weng LT, Leng Y. Spectroscopic analysis of titanium surface functional groups under various surface modification and their behaviors in vitro and in vivo. J Biomed Mater Res A, 2008, 84, 523-534.

39. Wennerberg A, Albrektsson T. Current challenges in successful rehabilitation with oral implants. J Oral Rehabil, 2011, 38, 286-294.

40. Kasemo B. Biocompatibility of titanium implants: surface science aspects. J Prosthet Dent, 1983, 49, 832-837.

41. Choi JW, Heo SJ, Koak JY, Kim SK, Lim YJ, Kim SH, Lee JB. Biological responses of anodized titanium implants under different current voltages. J Oral Rehabil, 2006, 33, 889-897.

42. Park K, Heo S, Koak J, Kim S, Lee J, Kim S, Lim Y. Osseointegration of anodized titanium implants under different current voltages: a rabbit study. J Oral Rehabil, 2007, 34, 517-527.

43. Wang G, Cheng X. The preliminary study on the oxide film of pure titanium treated by anodic oxidation. Zhonghua Kou Qiang Yi Xue Za Zhi, 2001, 36, 427-430.

44. Taxt-Lamolle S. Surface structure, chemistry and bio-performance of titanium implants modified by hydrofluoric acid, Doctoral thesis, Faculty of Dentistry, University of Oslo, 2010.

45. Szmukler-Moncler S, Bischof M, Nedir R, Ermrich M. Titanium hydride and hydrogen concentration in acid-etched commercially pure titanium and titanium alloy implants: a comparative analysis of five implant systems. Clin Oral Implants Res, 2010, 21, 944-950.

46. Conforto E, Caillard D. A fast method for determining favourable orientation relationships and interface planes: Application to titanium-titanium hydrides transformations. Acta Biomater, 2007, 55, 785-798.

47. Ban S, Iwaya Y, Kono H, Sato H. Surface modification of titanium by etching in concentrated sulfuric acid. Dent Mater, 2006, 22, 1115-1120.

48. Cheng Z, Zhang F, He F, Zhang L, Guo C, Zhao S, Yang G. Osseointegration of titanium implants with a roughened surface containing hydride ion in a rabbit model. Oral Surg Oral Med Oral Pathol Oral Radiol Endod, 2010, 110, e5-12.

49. Perrin D, Szmukler-Moncler S, Echikou C, Pointaire P, Bernard JP. Bone response to alteration of surface topography and surface composition of sandblasted and acid etched (SLA) implants. Clin Oral Implants Res, 2002, 13, 465-469.

50. Rupp F, Scheideler L, Olshanska N, de Wild M, Wieland M, Geis-Gerstorfer J. Enhancing surface free energy and hydrophilicity through chemical modification of microstructured titanium implant surfaces. J Biomed Mater Res A, 2006, 76, 323-334.

51. Zhao G, Schwartz Z, Wieland M, Rupp F, Geis-Gerstorfer J, Cochran DL, Boyan BD. High surface energy enhances cell response to titanium substrate microstructure. J Biomed Mater Res A, 2005, 74, 49-58.

52. Gottlow J, Dard M, Kjellson F, Obrecht M, Sennerby L. Evaluation of a New Titanium-Zirconium Dental Implant: A Biomechanical and Histological Comparative Study in the Mini Pig. Clin Implant Dent Relat Res, 2010, 24, 538-545.

53. Al-Nawas B, Bragger U, Meijer HJ, Naert I, Persson R, Perucchi A, Quirynen M, Raghoebar GM, Reichert TE, Romeo E and others. A double-blind randomized controlled trial (RCT) of Titanium-13Zirconium versus Titanium Grade IV small-diameter bone level implants in edentulous mandibles--results from a 1-year observation period. Clin Implant Dent Relat Res, 2012, 14, 896-904.

54. Ellingsen JE, Johansson CB, Wennerberg A, Holmen A. Improved retention and bone-tolmplant contact with fluoride-modified titanium implants. Int J Oral Maxillofac Implants, 2004, 19, 659-666.

55. Cooper L, Zhou Y, Takebe J, Guo J, Abron A, HolmÈn A, Ellingsen J. Fluoride modification effects on osteoblast behavior and bone formation at TiO2 grit-blasted cp titanium endosseous implants. Biomaterials, 2006, 27, 926-936.

56. Ellingsen JE. Pre-treatment of titanium implants with fluoride improves their retention in bone. J Mater Sci-Mater M, 1995, 6, 749-753.

57. Albouy JP, Abrahamsson I, Persson LG, Berglundh T. Spontaneous progression of peri-implantitis at different types of implants. An experimental study in dogs. I: clinical and radiographic observations. Clin Oral Implants Res, 2008, 19, 997-1002.

58. Simonis P, Dufour T, Tenenbaum H. Long-term implant survival and success: a 10-16-year follow-up of non-submerged dental implants. Clin Oral Implants Res, 2010, 21, 772-777.

59. Balshi TJ, Wolfinger GJ. Dental implants in the diabetic patient: a retrospective study. Implant Dent, 1999, 8, 355-359.

60. Javed F, Romanos GE. The role of primary stability for successful immediate loading of dental implants. A literature review. J Dent, 2010, 38, 612-620.

61. Davies JE. Mechanisms of endosseous integration. Int J Prosthodont, 1998, 11, 391-401.

62. Romanos DDSPGE. Present Status of Immediate Loading of Oral Implants. J Oral Impl, 2004, 30, 189-197.

63. Hansson S. The implant neck: smooth or provided with retention elements. A biomechanical approach. Clin Oral Implants Res, 1999, 10, 394-405.

64. Wennerberg A. The importance of surface roughness for implant incorporation. Int J Mach Tool Manu, 1998, 38, 657-662.

65. Bo GA, Bergfelt DR, Brogliatti GM, Pierson RA, Adams GP, Mapletoft RJ. Local versus systemic effects of exogenous estradiol-17β on ovarian follicular dynamics in heifers with progestogen implants. Anim Reprod Sci, 2000, 59, 141-157.

66. Leong KW, Langer R. Polymeric controlled drug delivery. Adv Drug Deliver Rev, 1988, 1, 199-233.

67. Wintermantel E, Ha S. Medizintechnik Life Science Engineering, Springer-Verlag Berlin Heidelberg, 2009.

68. JARCHO M. Calcium Phosphate Ceramics as Hard Tissue Prosthetics. Clin Orthop Relat R, 1981, 157, 259-278.

69. Krukowski M, Shively RA, Osdoby P, Eppley BL. Stimulation of craniofacial and intramedullary bone formation by negatively charged beads. J Oral Maxil Surg, 1990, 48, 468-475.

70. Valletregi M. Calcium phosphates as substitution of bone tissues. Prog Solid State Ch, 2004, 32, 1-31.

71. Dorozhkin SV, Epple M. Biological and medical significance of calcium phosphates. Angew Chem Int Ed Engl, 2002, 41, 3130-3146.

72. Xia W, Lindahl C, Lausmaa J, Borchardt P, Ballo A, Thomsen P, Engqvist H. Biomineralized strontium-substituted apatite/titanium dioxide coating on titanium surfaces. Acta Biomater, 2009, 6, 1591-1600.

73. García C, Ceré S, Durán A. Bioactive coatings deposited on titanium alloys. J Non-Cryst Solids, 2006, 352, 3488-3495.

74. Liu YL, Hunziker EB, Layrolle P, De Bruijn JD, De Groot K. Bone morphogenetic protein 2 incorporated into biomimetic coatings retains its biological activity. Tissue Eng, 2004, 10, 101-108.

75. Liu Y, de Groot K, Hunziker EB. BMP-2 liberated from biomimetic implant coatings induces and sustains direct ossification in an ectopic rat model. Bone, 2005, 36, 745-757.

76. Morra M. Biochemical modification of titanium surfaces: peptides and ECM proteins. Eur Cell Mater, 2006, 12, 1-15.

77. Reyes CD, Petrie TA, Burns KL, Schwartz Z, García AJ. Biomolecular surface coating to enhance orthopaedic tissue healing and integration. Biomaterials, 2007, 28, 3228-3235.

78. Lyngstadaas SP, Ellingsen JE, Astra Tech AB. Medical Prosthetic Devices and implants having improved biocompatibility patent no WO Patent: WO/2002/045,764, 2002.

79. Videm K, Lamolle S, Monjo M, Ellingsen JE, Lyngstadaas SP, Haugen HJ. Hydride formation on titanium surfaces by cathodic polarization. Appl Surf Sci, 2008, 255, 3011-3015.

80. Ellingsen JE, Videm K, Opsahl L, Rønold HJ. Implants with modified surfaces for increased biocompatibility and method for production thereof patent no WO/2000/038753, 2000.

81. Brookes SJ, Robinson C, Kirkham J, Bonass WA. Biochemistry and molecular biology of amelogenin proteins of developing dental enamel. Arch Oral Biol, 1995, 40, 1-14.

82. Hammarström L. Enamel matrix, cementum development and regeneration. J Clin Periodontol, 1997, 24, 658-668.

83. Hammarstrom L, Heijl L, Gestrelius S. Periodontal regeneration in a buccal dehiscence model in monkeys after application of enamel matrix proteins. J Clin Periodontol, 1997, 24, 669-677.

84. Grandin HM, Gemperli AC, Dard M. Enamel matrix derivative: a review of cellular effects in vitro and a model of molecular arrangement and functioning. Tissue Eng Part B Rev, 2012, 18, 181-202.

85. Cattaneo V, Rota C, Silvestri M, Piacentini C, Forlino A, Gallanti A, Rasperini G, Cetta G. Effect of enamel matrix derivative on human periodontal fibroblasts: proliferation, morphology and root surface colonization. An in vitro study. J Periodontal Res, 2003, 38, 568-574.

86. Miron RJ, Oates CJ, Molenberg A, Dard M, Hamilton DW. The effect of enamel matrix proteins on the spreading, proliferation and differentiation of osteoblasts cultured on titanium surfaces. Biomaterials, 2010, 31, 449-460.

87.   Iqbal MK, Bamaas N. Effect of enamel matrix derivative EMDOGAIN® upon periodontal healing after replantation of permanent incisors in Beagle dogs. Dent Traumatol, 2001, 17, 36-45.

88.   Lyngstadaas SP, Wohlfahrt JC, Brookes SJ, Paine ML, Snead ML, Reseland JE. Enamel matrix proteins; old molecules for new applications. Orthod Craniofac Res, 2009, 12, 243-253.

89.   Gestrelius S, Lyngstadaas SP, Hammarström L. Emdogain–periodontal regeneration based on biomimicry. Clin Oral Invest, 2000, 4, 120-125.

90.   Sommer B, Bickel M, Hofstetter W, Wetterwald A. Expression of matrix proteins during the development of mineralized tissues. Bone, 1996, 19, 371-380.

91.   Haze A, Taylor AL, Blumenfeld A, Rosenfeld E, Leiser Y, Dafni L, Shay B, Gruenbaum-Cohen Y, Fermon E, Haegewald S and others. Amelogenin expression in long bone and cartilage cells and in bone marrow progenitor cells. Anat Rec, 2007, 290, 455-460.

92.   Gestrelius S, Andersson C, Johansson AC, Persson E, Brodin A, Rydhag L, Hammarstrom L. Formulation of enamel matrix derivative for surface coating. Kinetics and cell colonization. J Clin Periodontol, 1997, 24, 678-684.

93.   Hammarström L, Heijl L, Gestrelius S. Periodontal regeneration in a buccal dehiscence model in monkeys after application of enamel matrix proteins. J Clin Periodontol, 1997, 24, 669-677.

94.   Heijl L. Periodontal regeneration with enamel matrix derivative in one human experimental defect. A case report. J Clin Periodontol, 1997, 24, 693-696.

95.   Heijl L, Heden G, Svärdström G, Östgren A. Enamel matrix derivative (Emdogain) in the treatment of intrabony periodontal defects. J Clin Periodontol, 1997, 24, 705-714.

96.   Zetterström O, Andersson C, Eriksson L, Fredriksson A, Friskopp J, Heden G, Jansson B, Lundgren T, Nilveus R, Olsson A and others. Clinical safety of enamel matrix derivative (EMDOGAIN®) in the treatment of periodontal defects. J Clin Periodontol, 1997, 24, 697-704.

97.   Lagerström-fermér M, Nilsson M, Bäckman B, Salido E, Shapiro L, Pettersson U, Landegren U. Amelogenin signal peptide mutation: correlation between mutations in the amelogenin gene (AMGX) and manifestations of X-linked amelogenesis imperfecta. Genomics, 1995, 26, 159-162.

98.   Iwata T, Yamakoshi Y, Hu JC, Ishikawa I, Bartlett JD, Krebsbach PH, Simmer JP. Processing of ameloblastin by MMP-20. J Dent Res, 2007, 86, 153-157.

99.   Zilm PS, Bartold PM. Proteomic identification of proteinase inhibitors in the porcine enamel matrix derivative, EMD((R)). J Periodontal Res, 2011, 46, 111-117.

100.   Aoba T, Fukae M, Tanabe T, Shimizu M, Moreno EC. Selective Adsorption of Porcine-Amelogenins onto Hydroxyapatite and Their Inhibitory Activity on Hydroxyapatite Growth in Supersaturated Solutions. Calcif Tissue Int, 1987, 41, 281-289.

101.   Premarket Approval of Biora AB Emdogain®. doi, US Food and Drug Administration; 1996.

102.   Marie PJ, Felsenberg D, Brandi ML. How strontium ranelate, via opposite effects on bone resorption and formation, prevents osteoporosis. Osteoporos Int, 2011, 22, 1659-1667.

103.   Marie PJ, Ammann P, Boivin G, Rey C. Mechanisms of action and therapeutic potential of strontium in bone. Calcif Tissue Int, 2001, 69, 121-129.

104.   Grynpas MD, Hamilton E, Cheung R, Tsouderos Y, Deloffre P, Hott M, Marie PJ. Strontium increases vertebral bone volume in rats at a low dose that does not induce detectable mineralization defect. Bone, 1996, 18, 253-259.

105.   Predel B. Ti-Zr (Titanium-Zirconium), In: Madelung O, editor.

106.   Earle MD. The electrical conductivity of titanium dioxide. Phys Rev, 1942, 61, 56-62.

107.   Beck TR. Electrochemistry of freshly-generated titanium surfaces—II. Rapid fracture experiments. Electrochim Acta, 1973, 18, 815-827.

108.   Solovan MN, Maryanchuk PD, Brus VV, Parfenyuk OA. Electrical and optical properties of TiO2 and TiO2:Fe thin films. Inorg Mater, 2012, 48, 1026-1032.

109.   Ito M, Setoyama D, Matsunaga J, Muta H, Kurosaki K, Uno M, Yamanaka S. Electrical and thermal properties of titanium hydrides. J Alloy Compd, 2006, 420, 25-28.

110.   Wang XY, Li DY. Application of an electrochemical scratch technique to evaluate contributions of mechanical and electrochemical attacks to corrosive wear of materials. Wear, 2005, 259, 1490-1496.

111.   Wang L, Chen SH, Yuan BY, Meng FJ, Wang JQ, Wang C, Li L. Digital holographic reconstruction detection of localized corrosion arising from scratches. J Serb Chem Soc, 2010, 75, 505-512.

112.   Hossain SM, Das J, Chakraborty S, Dutta SK, Saha H. Electrode design and planer uniformity of anodically etched large area porous silicon. Semincond Sci Technol, 2002, 17, 55.

113.   Feynman RP, Leighton RB, Sands M, Treiman SB. The Feynman Lectures on Physics. Phys Today, 1964, 17, 45-46.

114.   Walter MS, Frank MJ, Rubert M, Monjo M, Rønold HJ, Lyngstadaas P, Haugen HJ. Bioactive implant surface with electrochemically bound Doxycycline promotes in vivo gene expression of bone markers. in Submissiondoi; 2013.

115.   Murakami T, Tsuzuki K. Electrolytic etching method and apparatus, USA patent no US 7,691,241, 2010.

116.   Lamolle SF, Monjo M, Lyngstadaas SP, Ellingsen JE, Haugen HJ. Titanium implant surface modification by cathodic reduction in hydrofluoric acid: surface characterization and in vivo performance. J Biomed Mater Res A, 2009, 88, 581-588.

117.   Sensofar-Tech AG. Product Brochure Optical Imaging Profiler PLμ 2003. doi. Terrassa, Spain; 2006.

118.   Petzold C, Gomez-Florit M, Lyngstadaas SP, Monjo M. EPA covalently bound to smooth titanium surfaces decreases viability and biofilm formation of Staphylococcus epidermidis in vitro. J Orthop Res, 2012, 30, 1384-1390.

119.   Cameca S.A.S. IMS 7f High Performance Universal Magnetic Sector SIMS, 2006.

120.   Van Vaeck L, Adriaens A, Gijbels R. Static secondary ion mass spectrometry (S-SIMS) Part 1: methodology and structural interpretation. Mass Spectrom Rev, 1999, 18, 1-47.

121.   Kimura A, Nakatani Y, Yamada K, Suzuki T. Hydrogen detection in CVD diamond films by elastic recoil detection analysis. Diam Relat Mater, 1999, 8, 37-41.

122.   Kamruddin M, Ajikumar PK, Dash S, Tyagi AK, Raj B. Thermogravimetry-evolved gas analysis-mass spectrometry system for materials research. B Mater Sci, 2003, 26, 449-460.

123.   Bogdanović B, Felderhoff M, Germann M, Härtel M, Pommerin A, Schüth F, Weidenthaler C, Zibrowius B. Investigation of hydrogen discharging and recharging processes of Ti-doped NaAlH4 by X-ray diffraction analysis (XRD) and solid-state NMR spectroscopy. J Alloy Compd, 2003, 350, 246-255.

124.   Umezawa K, Kuroi T, Yamane J, Shoji F, Oura K, Hanawa T, Yano S. Quantitative hydrogen analysis by simultaneous detection of $1H(19F, \alpha\gamma)16O$ at 6.46 MeV and 19F-ERDA. Nucl Instrum Meth B, 1988, 33, 634-637.

125.   Binnig G, Rohrer H. Scanning tunneling microscopy. Surf Sci, 1983, 126, 236-244.

126.   Suzuki S, Fukui K-i, Onishi H, Iwasawa Y. Hydrogen Adatoms on TiO_{2}(110)-(1×1) Characterized by Scanning Tunneling Microscopy and Electron Stimulated Desorption. Phys Rev Lett, 2000, 84, 2156-2159.

127.   Moulder JF, Stickle WF, Sobol PE, Bomben KD. Handbook of X-ray photoelectron spectroscopy, Physical Electronics Inc., 1995.

128.   Lozano GA, Ranong CN, von Colbe JMB, Bormann R, Hapke J, Fieg G, Klassen T, Dornheim M. Optimization of hydrogen storage tubular tanks based on light weight hydrides. Int J Hydrogen Energ, 2012, 37, 2825-2834.

129.   Fadley CS, Baird RJ, Siekhaus W, Novakov T, Bergstro.Sa. Surface Analysis and Angular-Distributions in X-Ray Photoelectron-Spectroscopy. J Electron Spectrosc, 1974, 4, 93-137.

130.   Gunter PLJ, Gijzeman OLJ, Niemantsverdriet JW. Surface roughness effects in quantitative XPS: magic angle for determining overlayer thickness. Appl Surf Sci, 1997, 115, 342-346.

131.   Toney MF. X-ray diffraction, In: Brundle CR, Evans CA, Wilson S, editors. Encyclopedia of materials characterization: surfaces, interfaces, thin films: Gulf Professional Publishing, 1992.

132.   Riksen EA, Petzold C, Brookes S, Lyngstadaas SP, Reseland JE. Human osteoblastic cells discriminate between 20-kDa amelogenin isoforms. Eur J Oral Sci, 2011, 119 Suppl 1, 357-365.

133.   Jagtap RN, Ambre AH. Overview literature on matrix assisted laser desorption ionization mass spectroscopy (MALDI MS): Basics and its applications in characterizing polymeric materials. B Mater Sci, 2005, 28, 515-528.

134.   Tamburstuen MV, Reseland JE, Spahr A, Brookes SJ, Kvalheim G, Slaby I, Snead ML, Lyngstadaas SP. Ameloblastin expression and putative autoregulation in mesenchymal cells suggest a role in early bone formation and repair. Bone, 2011, 48, 406-413.

135.   Saeves R, Reseland JE, Kvam B-M, Sandvik L, Nordgarden H. Saliva in Prader–Willi syndrome: Quantitative and qualitative characteristics. Arch Oral Biol, 2012, 57, 1335-1341.

136.   Socrates G, Socrates G. Infrared and Raman characteristic group frequencies: tables and charts, Wiley Chichester, UK, 2001.

137.   Almeida CM, Vasconcelos MTSD. ICP-MS determination of strontium isotope ratio in wine in order to be used as a fingerprint of its regional origin. J Anal At Spectrom, 2001, 16, 607-611.

138.   Peters K, Unger R, Kirkpatrick CJ. Biocompatibility Testing, In: Narayan R, editor. Biomed Mater: Springer US, 2009, pp 261-292.

139.   Quarles LD, Yohay DA, Lever LW, Caton R, Wenstrup RJ. Distinct proliferative and differentiated stages of murine MC3T3-E1 cells in culture: an in vitro model of osteoblast development. J Bone Miner Res, 1992, 7, 683-692.

140.   Oreffo ROC, Triffitt JT. In vitro and in vivo methods to determine the interactions of osteogenic cells with biomaterials. J Mater Sci-Mater M, 1999, 10, 607-611.

141.   Brakefield AC, Prieto EM, Guelcher SA. A Characterization of Three Groups of MC3T3-E1 Pre-Osteoblastic Cells to Aid in Testing of Polyurethane-Bone Scaffolds for Wound Healing. Young Sci, 2011, 1.

142.   Rønold HJ, Ellingsen JE. The use of a coin shaped implant for direct in situ measurement of attachment strength for osseointegrating biomaterial surfaces. Biomaterials, 2002, 23, 2201-2209.

143.   Wohlfahrt JC, Monjo M, Rønold HJ, Aass AM, Ellingsen JE, Lyngstadaas SP. Porous titanium granules promote bone healing and growth in rabbit tibia peri-implant osseous defects. Clin Oral Implan Res, 2010, 21, 165-173.

144.   Khadra M, Rønold HJ, Lyngstadaas SP, Ellingsen JE, Haanæs HR. Low-level laser therapy stimulates bone–implant interaction: an experimental study in rabbits. Clin Oral Implan Res, 2004, 15, 325-332.

145.   Rønold HJ, Lyngstadaas SP, Ellingsen JE. A study on the effect of dual blasting with TiO2 on titanium implant surfaces on functional attachment in bone. J Biomed Mater Res-A, 2003, 67A, 524-530.

146.   Rønold H, Ellingsen J, Lyngstadaas S. Tensile force testing of optimized coin-shaped titanium implant attachment kinetics in the rabbit tibiae. J Mater Sci-Mater M, 2003, 14, 843-849.

147.   Ellingsen JE, Lyngstadaas SP. Increasing Biocompatibility by Chemical Modification of Titanium Surfaces. Bio-Implant Interface: Improving Biomaterials and Tissue Reactions: CRC, 2003, pp 323.

148.   Wang X, Mabrey JD, Agrawal CM. An interspecies comparison of bone fracture properties. Bio-Med Mater Eng, 1998, 8, 1-9.

149.   Pearce AI, Richards RG, Milz S, Schneider E, Pearce SG. Animal models for implant biomaterial research in bone: a review. Eur Cell Mater, 2007, 13, 1-10.

150. Castaneda S, Largo R, Calvo E, Rodriguez-Salvanes F, Marcos ME, Diaz-Curiel M, Herrero-Beaumont G. Bone mineral measurements of subchondral and trabecular bone in healthy and osteoporotic rabbits. Skeletal Radiol, 2006, 35, 34-41.

151. Newman E, Turner AS, Wark JD. The potential of sheep for the study of osteopenia: Current status and comparison with other animal models. Bone, 1995, 16, 277S-284S.

152. Rønold HJ, Lyngstadaas SP, Ellingsen JE. A study on the effect of dual blasting with TiO2 on titanium implant surfaces on functional attachment in bone. J Biomed Mater Res A, 2003, 67, 524-530.

153. Rønold HJ, Ellingsen JE. Effect of micro-roughness produced by TiO2 blasting. Tensile testing of bone attachment by using coin-shaped implants. Biomaterials, 2002, 23, 4211-4219.

154. Franchimont N, Wertz S, Malaise M. Interleukin-6: An osteotropic factor influencing bone formation? Bone, 2005, 37, 601-606.

155. Lee AZ, Jiang J, He J, Safavi KE, Spangberg LSW, Zhu Q. Stimulation of cytokines in osteoblasts cultured on enamel matrix derivative. Oral Surg Oral Med Oral Pathol Oral Radiol Endod, 2008, 106, 133-138.

156. McAdams HH, Arkin A. Stochastic mechanisms in gene expression. Proc Natl Acad Sci USA, 1997, 94, 814-819.

157. Raser JM, O'Shea EK. Noise in gene expression: origins, consequences, and control. Science, 2005, 309, 2010-2013.

158. Morra M, Cassinelli C, Cascardo G, Cahalan P, Cahalan L, Fini M, Giardino R. Surface engineering of titanium by collagen immobilization. Surface characterization and in vitro and in vivo studies. Biomaterials, 2003, 24, 4639-4654.

159. Gestrelius S, Andersson C, Johansson A-C, Persson E, Brodin A, Rydhag L, Hammarström L. Formulation of enamel matrix derivative for surface coating. J Clin Periodontol, 1997, 24, 678-684.

160. Fincham AG, Moradian-Oldak J. Amelogenin post-translational modifications: carboxy-terminal processing and the phosphorylation of bovine and porcine "TRAP" and "LRAP" amelogenins. Biochem Biophys Res Commun, 1993, 197, 248-255.

161. Mumulidu A, Hildebrand B, Fabi B, Hammarstrom L, Cochran DL, Dard M, Lemoult S. Purification and analysis of a 5kDa component of enamel matrix derivative. J Chromatogr B Analyt Technol Biomed Life Sci, 2007, 857, 210-218.

162. Rubert M, Ramis JM, Vondrasek J, Gaya A, Lyngstadaas SP, Monjo M. Synthetic Peptides Analogue to Enamel Proteins Promote Osteogenic Differentiation of MC3T3-E1 and Mesenchymal Stem Cells. J Biomater Tissue Eng, 2011, 1, 198-209.

163. Reseland JE, Reppe S, Larsen AM, Berner HS, Reinholt FP, Gautvik KM, Slaby I, Lyngstadaas SP. The effect of enamel matrix derivative on gene expression in osteoblasts. Eur J Oral Sci, 2006, 114 Suppl 1, 205-211; discussion 254-206, 381-202.

164. Iqbal MK, Bamaas N. Effect of enamel matrix derivative (EMDOGAINR) upon periodontal healing after replantation of permanent incisors in Beagle dogs. Dent Traumatol, 2001, 17, 36-45.

165. Rodrigues TL, Marchesan JT, Coletta RD, Novaes AB, Jr., Grisi MF, Souza SL, Taba M, Jr., Palioto DB. Effects of enamel matrix derivative and transforming growth factor-beta1 on human periodontal ligament fibroblasts. J Clin Periodontol, 2007, 34, 514-522.

166. Ha S-W, Wintermantel E. Biokompatible Metalle, In: Wintermantel E, Ha S-W, editors. Medizintechnik Life Science Engineering: Springer Berlin Heidelberg, 2009, pp 191-217.

167. Moradian-Oldak J, Paine ML, Lei YP, Fincham AG, Snead ML. Self-assembly properties of recombinant engineered amelogenin proteins analyzed by dynamic light scattering and atomic force microscopy. J Struct Biol, 2000, 131, 27-37.

168. He X, Li W, Habelitz S. The cooperative self-assembly of 25 and 23kDa amelogenins. J Struct Biol, 2008, 164, 314-321.

169. Moradian-Oldak J, Goldberg M. Amelogenin supra-molecular assembly in vitro compared with the architecture of the forming enamel matrix. Cells Tissues Organs, 2005, 181, 202-218.

170.   Simmer JP, Fukae M, Tanabe T, Yamakoshi Y, Uchida T, Xue J, Margolis HC, Shimizu M, DeHart BC, Hu C-C and others. Purification, Characterization, and Cloning of Enamel Matrix Serine Proteinase 1. J Dent Res, 1998, 77, 377-386.

171.   Paine ML, Luo W, Zhu D-H, Bringas P, Snead ML. Functional Domains for Amelogenin Revealed by Compound Genetic Defects. J Bone Miner Res, 2003, 18, 466-472.

172.   Moradian-Oldak J, Bouropoulos N, Wang L, Gharakhanian N. Analysis of self-assembly and apatite binding properties of amelogenin proteins lacking the hydrophilic C-terminal. Matrix Biol, 2002, 21, 197-205.

173.   Kmetko J, Yu C, Evmenenko G, Kewalramani S, Dutta P. Organic-template-directed nucleation of strontium fluoride and barium fluoride: Epitaxy and strain. Phys Rev B, 2003, 68, 085415.

174.   Park J-W, Kim H-K, Kim Y-J, Jang J-H, Song H, Hanawa T. Osteoblast response and osseointegration of a Ti-6Al-4V alloy implant incorporating strontium. Acta Biomater, 2010, 6, 2843-2851.

175.   Maimoun L, Brennan TC, Badoud I, Dubois-Ferriere V, Rizzoli R, Ammann P. Strontium ranelate improves implant osseointegration. Bone, 2010, 46, 1436-1441.

176.   Stenport VF, Johansson CB. Enamel matrix derivative and titanium implants. J Clin Periodontol, 2003, 30, 359-363.

9 ERRATA

Chapter (Page)	Originally submitted version	Revised version
(II)	ISBN 000-00-00000-00-0	ISBN 978-82-91757-85-8
(VII)	Paper II:	Paper II:
	Revised manuscript re-submitted to Applied Surface Science (Ms. Ref. No.: APSUSC-D-12-05470)	*Revised version accepted in Applied Surface Science, DOI: 10.1016/j.apsusc.2013.04.059.*
(VII)	Paper III:	Paper III:
	Submitted to Acta Biomaterialia (Ms. Ref. No.: AB-13-372)	*In submission.*
(VII)	Paper IV:	Paper IV:
	Submitted to Journal of Materials Science: Materials in Medicine (Ms. Ref. No.: JMSM5667)	*Revised version accepted in Materials Science: Materials in Medicine, DOI: 10.1007/s10856-013-5007-1; 2013.*
1.1 (1)	[…] and to generate new bone thereafter. Both cells derive from mesenchymal stem cells through different signaling pathways the expression of different genes. This is where biomolecules can influence bone formation and bone remodeling by promoting specific cell differentiation. This is where biomolecules can influence bone formation and bone remodeling by promoting specific cell differentiation. Moreover, the gene expression can be assessed in order to determine the influence of a biomaterial on cell differentiation. Moreover, the gene expression can be assessed […]	[…] and to generate new bone thereafter. While osteoblasts derive from mesenchymal stem cells, osteoclasts derive from hematopoietic stem cells.[17] By influencing the signaling pathways during the expression of different genes, biomolecules can influence bone formation and bone remodeling by promoting specific cell differentiation. Moreover, the gene expression can be assessed […]
8. (54)		Additional reference added, order of subsequent references adjusted accordingly:
		17. Atala A, Lanza R. Handbook of stem cells, Access Online via Elsevier, 2012.

II

III

IV

Bioactive coating of metal implant materials with strontium

Matthias J. Frank[1,2], Martin S. Walter[1,2], Hanna Tiainen[1], Marina Rubert[3], Marta Monjo[1,3], S. Petter Lyngstadaas[1] and Håvard J. Haugen[1]

[1]*Department of Biomaterials, Institute for Clinical Dentistry, University of Oslo, PO Box 1109 Blindern, NO-0317 Oslo, Norway*

[2]*Institute of Medical and Polymer Engineering, Chair of Medical Engineering, Technische Universität München, Boltzmannstrasse 15, 85748 Garching, Germany*

[3]*Department of Fundamental Biology and Health Sciences, Research Institute on Health Sciences (IUNICS), University of Balearic Islands, ES-07122 Palma de Mallorca, Spain.*

Corresponding author:
Håvard J. Haugen
E-mail: h.j.haugen@odont.uio.no
Phone: +47 22 85 21 70
Fax: +47 22 85 23 51
URL: http://www.biomaterials.no

Abstract

The aim of this study was to show that cathodic polarization can be used for coating commercial implant surfaces with an immobilized but functional and bioavailable surface layer of strontium (Sr). Moreover, this study assessed the effect of fluoride on Sr-attachment. XPS revealed that addition of fluorine (F) to the buffer during coating increased surface Sr-amounts but also changed the chemical surface composition by adding SrF_2 alongside of SrO whereas pre-treatment of the surface by pickling in hydrofluoric acid appeared to hinder Sr-attachment. Assessment of the bio-availability hinted at a positive effect of Sr on cell differentiation given that the surface reactivity of the original surface remained unchanged. Additional SrF_2 on the surface appeared to reduce undesired surface contamination while maintaining the surface micro-topography and micro-morphology. Anyhow, this surface modification revealed to create nano-nodules on the surface.

Keywords

1   Introduction

Titanium based endosseous dental implants have shown steady improvements of their clinical performance over the recent years [1]. Most dental implants available on the market today feature a moderately rough, sand-blasted and acid-etched (SBAE) surface [2]. Despite the improved performance of such moderately rough endosseous dental implants, long-term bone resorption is still an issue with current commercially available the implant systems [2, 3]. Moreover, patients who suffer from bone loss or generally poor bone quality are often not eligible for an endosseous dental implant [4-6]. Thus, the focus of current research in the field of endosseous dental implants is directed towards creating a bioactive surface that may help patient who cannot be treated with dental implants today. The desired implant should actively support peri-implant bone healing in order to allow the formation of strong, mature bone at the bone-implant interface that facilitates the necessary mechanical interlocking but also provides long term stability in the alveolar bone. Coating of the surface with bioactive components that support bone healing appears a promising way of creating such a surface. Successful biochemical surface modifications with e.g. peptides, extracellular matrix proteins, hydroxyapatite, calcium phosphate, and fluorine (F) have shown promising results in supporting bone healing [7-11]. Yet, none of these modifications has shown sufficient evidence for long term success. A variety of studies has shown the positive effect of strontium (Sr) on bone healing [12-16]. A recently published review article by Marie et al. summarized how strontium affects bone resorption and bone formation by activating pre-osteoblast replication as well as osteoblast differentiation and survival [12]. At the same time Sr was reported to reduce pre-osteoclast differentiation in addition to osteoclast function and survival, thus preventing bone resorption [12]. The described properties made Sr an interesting candidate for a surface coating that could combine the mechanical properties of a titanium-based implant with a moderately rough surface with the positive effects of Sr on bone healing. Lyngstadaas and Ellingsen suggested to use a polarization process to attach charged biomolecules to the surface in order to stimulate bone healing [17]. As Sr may easily be ionized, it appeared to be a well suited candidate for use in such a coating process.

The aim of this study was to show that cathodic polarization can be used for coating commercially available implant surfaces of grade IV titanium and titanium-zirconium alloy with a moderately rough, hydrogen rich sand-blasted and acid-etched surface with an immobilized but functional and bioavailable surface layer of Sr.

During a series of experiments preceding this study (unpublished data) we observed a possible beneficial influence of fluorine on the amount of Sr that may be coated to a surface. It appeared as if fluorine supported the attachment of Sr to the surface by cathodic polarization. Hence, a further aim of this study was to explore the effect of additional fluorine on the coating-process. This was done either by adding additional sodium-fluoride to the process or by pre-treatment of the samples by pickling in hydrofluoric acid. This study used XPS to examine the surface coverage and to evaluate the chemical composition and the binding states of the surface components. Bio-availability was assessed by evaluation of the gene expression levels of collagen-1 (Coll-1), alkaline phosphatase (ALP), and osteocalcin (OC) of osteoblastic MC3T3-E1 cells to Sr-coated surfaces.

2   Materials and methods

2.1   Samples

This study used coins shaped samples made of grade IV titanium (Ti) and a titanium-zirconium alloy (TiZr) containing 13% to 17% zirconium [18]. Surfaces were sand-blasted with large-grit (0.25mm–0.5mm) aluminum oxide particles and acid etched in a mixture of hydrochloric and sulfuric acid at 125°C–130°C for 5 minutes (SBAE). The samples were handled under nitrogen cover gas and stored in 0.9% NaCl solution to obtain a surface comparable with the commercially available SLActive® surface (Institut Straumann AG, Basel, Switzerland). This surface modification has been previously described in other studies [19, 20].

Coin-shaped samples with a diameter of 4.5 mm and a height of 2 mm were used for evaluating the feasibility of the coating, the effect of fluorine on the surface, and the effect of the modification on the surface. The setup used for cathodic polarization of these coins consisted of a power supply (Protek Dual DC power, Korea) connected to the sample cathode and a platinum anode, a datalogger (NI DAQPad, National Instruments, Asker, Norway) and a magnetic stirrer with heating (IKA-RET Control Visc C, VWR, Kaldbakken, Norway). The platinum electrode had a cylindical shape and the samples were always placed in the center of the Pt-electrode to ensure an equal horizontal and vertical distance between the two electrodes for all samples. The pH was monitored by a pH electrode (Schott N62, SCHOTT Instruments GmbH, Mainz, Germany), which was driven by a power supply (Xantrex XDL 56-4P, Burnaby, Canada). The temperature was measured by a Pt100 device (Pt100, IKA Labortechnik, Staufen, Germany). The coating of TiZr SBAE with Sr was done for 60 minutes while the output current density was set to 0.54 mA/cm^2. Ti SBAE was coated with Sr for 60 at a current density of 1.3 mA/cm^2. The electro-coating was done in a buffer made of 0.25M strontium-acetate and acetic acid at pH 5 at a temperature of 21°C. Ultra-pure, 99.995 % trace metal free strontium-acetate (Sigma Aldrich, Prod. # 437883-5G) was used for reducing the effect of trace elements on the process. Two groups used a modified version of this Sr-buffer. One group contained an additional 0.1 M of sodium-chloride (Sr+NaCl) in the buffer and a second group contained an additional 0.1 M of sodium-fluoride (Sr+NaF) in the buffer. This was done to monitor the effect of Na-ions on the process independently of the fluoride. The last group used modified SBAE samples that were pickled in 0.2% hydrofluoric acid (Sr+HFp) for 2 minutes prior to electro-coating in the regular Sr-buffer. After the coating process the coins were rinsed in deionized water for 10 seconds and then air-dried in a laminar flow cabin. Thereafter the samples were stored in eppendorf tubes prior to further usage. Five groups with different surface modifications were included in the first part of this study. Besides the unmodified SBAE surface of both materials, this study included a group that was only polarized using a buffer made of sodium-acetate and acetic acid. This kind of polarization has been used in our previous study and has been shown to alter the surface hydrogen levels and the surface micro- and nano-morphology [21]. Thus, a polarized only surface was added to assess the effect the different Sr-coatings on the biological response independent of the surface modifications induced by the polarization itself. An overview of the different groups and the coating conditions is provided in Table 1.

2.2   Chemical characterization

The X-ray photoelectron spectroscopy (XPS) analysis was carried out on an Axis Ultra[DLD] XP spectrometer (Kratos Analytical Limited, Manchester, United Kingdom). The instrument resolution was 1.1 eV for the survey scans and 0.55 eV for the detail scans for the employed settings, determined by measuring of the full width at half maximum (FWHM) of the Ag $3d_{5/2}$ peak obtained on sputter cleaned silver foil. The emission of the photoelectrons from the sample was 90° (normal to sample surface), and the incidence angle of the X-rays was 33.3° (or 56.7° between X-ray incidence direction and captured photoelectron emission direction). For the survey spectra, a hybrid lens mode was used with slot aperture at 80 eV pass energy. The survey scan was executed at between 0 eV and 1100 eV binding energy. For the detail spectra, a hybrid lens mode with slot aperture was used at a pass energy of 20 eV. A detail spectrum was recorded for Sr 3d. The energy shift due to surface charging was below 1 eV based on the C 1s peak position relative to the established BEs, therefore the experiment was performed without charge compensation. All samples were referenced to C 1s at 284.5 eV.

An ion selective electrode (Orion Fluoride ISE with Orion 4-Star Plus Benchtop pH/ISE Meter, Thermo Scientific, Beverly, MA, USA) was used to assess the amount of free F-ions in the Sr+NaF buffer before and during coating.

2.3   Surface topography and morphology characterization

All scanning electron microscope (SEM) images in this study were taken by a Quanta 200 FEG (FEI Hillsboro, Oregon, USA) field-emission SEM. Its Schottky field emission gun (FEG) allowed high spatial resolution. All samples were sputtered with platinum for one minute prior to imaging and mounted on the sample holder with conductive carbon tape.

2.4   Cell study

An *in vitro* cell study was performed to compare the performance of the polarized and Sr-coated groups with the respective SBAE groups. The murine osteoblastic cell line MC3T3-E1 was obtained from the German Collection of Microorganisms and Cell Cultures (DSMZ, Braunschweig, Germany). MC3T3-E1 cells were routinely cultured at 37°C in a humidified atmosphere of 5% CO_2, and maintained in α-MEM supplemented with 10% fetal calf serum (FCS) and antibiotics (50 IU penicillin/ml and 50 µg streptomycin/ml). Cells were subcultured 1:5 before reaching confluence using PBS and trypsin/EDTA. All experiments were performed in the same passage of the MC3T3-E1 cells. The coins were placed in a 96-well plate (4.5 mm well) and 7x103 cells were seeded on each well to study cell differentiation after 14 days and lactate dehydrogenase (LDH) activity after 24 h. This study used a group size of n=8 samples per group for all groups. The same number of cells was cultured in parallel in plastic culture dishes during all experiments as a reference. Trypan blue stain was used to determine total and viable cell number. For the experiments, MC3T3-E1 cells were maintained for 14 days on the implants in α-MEM supplemented with 10% FCS and antibiotics. Culture media was changed every other day. To study cell differentiation, cells were harvested after 14 days and collagen 1 (Coll-1), alkaline phosphatase (ALP) and osteocalcin (OC) gene expression were analyzed using real-time RT-PCR. The detailed methods used for LDH activity, RNA isolation, Real-time RT-PCR, the

sequences of sense and antisense primers were exactly the same as they have been described by Satué et al.[22].

2.5 Statistical analysis

Data were compared by a two way ANOVA in SigmaPlot 11 (Systat Software, San José, California, USA). A normality test was performed; once this was passed, all samples were compared in pairs using the Holm-Sidak method. ANOVA was performed on ranks when the normality test failed, using the Tukey test for pairwise comparison. The results of the cell study were compared by the student's t-test using the program SPSS® 19 (IBM Corporation, Armonk, NY, USA) for Windows®. Significance levels were set to significant *$p \leq 0.05$ and highly significant **$p \leq 0.01$. The spearmen rank correlation study between Sr and F levels from the XPS analysis was performed by the same software package. The results were interpreted as follows: no correlation if $|r| < 0.3$, correlation if $0.3 \leq |r| < 0.5$, and strong correlation if $0.5 \leq |r| \leq 1$ [23]. A negative r indicated a negative correlation while a positive r indicated a positive correlation. Significance levels were set to significant *$p \leq 0.05$ and highly significant **$p \leq 0.01$. All data were displayed as arithmetic mean values with standard deviation when the data were distributed normally and as median values with interquartile range when the data were not distributed normally.

3 Results

3.1 Chemical surface characterization

Evaluation of the surface chemistry was done by XPS with particular focus on quantifying the strontium (Sr 3d), fluorine (F 1s), and titanium (Ti 2p) surface ratio of each surface. The complete results of the general surface composition are presented in Table 2. The specific binding-state of strontium was assessed by analysis of the Sr 3d detail spectrum (Fig. 1).

The Sr+NaF groups showed the highest strontium content of all groups at similar concentrations for Ti (4.26at.%) and TiZr (4.08at.%). Although the Sr-groups showed the second highest strontium content for both materials, the total concentration differed over 1at.% between Ti (2.17at.%) and TiZr (3.74at.%). There was no clear trend for an increased strontium content of either the Sr+NaCl group or the Sr+HFp group. Anyhow, it appeared as if fluorine only increased the strontium content of a surface, when it was present in the buffer during polarization. In addition, the spearman rank correlation study revealed no significant correlation between the strontium content and the fluorine content of a sample (Table 2). Although the Sr+NaF group showed the highest fluorine content of all groups, the fluorine content of the other groups appeared rather random as e.g. the Sr+HFp group showed significantly different fluorine levels for Ti and TiZr.

The Sr 3d detail spectra of the Sr+NaF group revealed a second doublet of Sr $3d_{5/2}$ and Sr $d_{3/2}$ peaks that was not observed for any other group (Fig. 1). It was of particular interest that the of Sr $3d_{5/2}$ peak of the first doublet and the Sr $3d_{3/2}$ peak of the second doublet had the same binding energy at 135.0 eV for Ti and at 135.2 eV for TiZr (

Table 3). The second doublet was visible as a shoulder in the detail spectra of the Sr+NaF groups that stretched up to almost 140 eV (Fig. 1 A, C). Anyhow, the Sr 3d detail spectra of Ti Sr+NaF and TiZr Sr+NaF were not identical since TiZr Sr+NaF showed a combined first Sr $3d_{3/2}$ and second Sr $3d_{5/2}$ peak that had a higher intensity than the first Sr $3d_{5/2}$ peak (Fig. 1 C). Moreover, the peak position of the first Sr $3d_{5/2}$ peak of TiZr Sr+NaF appeared to be marginally shifted towards a higher binding energy (133.4 eV) compared to the other TiZr groups.

The detail spectra of the C 1s peak with the adjoined Sr $3p_{1/2}$ peak revealed clearly separated Sr $3p_{1/2}$ peaks for all samples comparable to the peak illustrated for Ti Sr+NaF (Fig. 2 A) except for TiZr Sr+NaF (Fig. 2 B) that showed a shift of the Sr $3p_{1/2}$ peak towards the C 1s peak that led to a merging of the two peaks. In addition to the C 1s peak at 284.5 eV, two C 1s peaks at 285.9±0.2 eV and 288.3±0.5 eV were revealed by Gaussian peak fitting for samples of both materials.

All Sr-coated Ti samples revealed some general trends. The titanium content of the outer surface was about 5 at.% - 6 at.% lower and the oxygen content was reduced by at least 5 at.% to almost 12 at.% compared to Ti SBAE. Minor amounts of the trace elements copper, chloride, silicium and zinc were observed for some groups (results not shown).

3.2   Evaluation of the surface topography and morphology

This study observed the same surfaces for Ti SBAE and TiZr SBAE (results not shown) that have been shown and described in our previous study [24]. The Sr+NaF groups were chosen for SEM imaging because they showed the highest strontium content on the surface and were thus most promising for further analysis.

The micro-structure of the Sr+NaF groups (Fig. 1 A, C) showed the same as Ti SBAE [24] with pointed peaks and sharp-edged rims. At larger magnification (Fig. 1 B, D), both Sr+Na surfaces revealed significantly different nano-structure than observed for the respective SBAE surfaces. The whole surface appeared to be covered with nodules at the nano-meter level that were distributed homogeneously over the whole surface and appeared like a snow covered mountain range. In addition, TiZr Sr+Na revealed the same micro- and nano-nodules that have been described for TiZr SBAE [24].

3.3   In vitro cell study

Assessment of cell viability by LDH activity after 24 h showed no toxic effect of the coating. Only TiZr Sr showed significantly higher LDH activity than TiZr SBAE with an increase of 5.4 % (Fig. 4 A), however this increase was not significant compared to reference cells cultured on plastic without a sample.

Ti Sr+NaF was the only group that showed significant differences compared to Ti SBAE for all markers assessed by having lower gene expression of proliferation marker Coll-1, and higher gene expression of differentiation markers ALP and OC (Fig. 4 B-D). TiZr Sr showed significantly higher Coll-1 and lower ALP gene expression than Ti Sr. TiZr Sr+NaF, TiZr Sr+HFp, and Ti Sr+NaCl only showed significantly lower Coll-1 expression than the respective SBAE group. Ti Sr+NaCl had significantly higher OC expression than TiZr Sr+NaCl.

The Ti pol and Ti Sr+HFp groups only revealed significantly higher ALP expression compared to Ti SBAE, while comparison of Ti SBAE and TiZr SBAE showed no significant differences between the groups for Coll-1, ALP, and OC gene expression.

Comparison of the Sr-content and gene expression by spearman rank correlation study (Table 3) revealed that only Coll-1 expression had a negative correlation to the Sr-content of a sample that was highly significant ($p < 0.01$).

3.4   Fluorine content of the NaF modified buffer

During the preparation of the buffer for the Sr+NaF group, it was observed that the Sr-acetate and acidic acid buffer turned turbid immediately when NaF was added. Moreover, a white substance precipitated from the buffer and sedimented on the bottom of the beaker that contained the buffer. This effect was not observed for any other buffer. Assessment of the Sr+NaF buffer before coating without any curren contained only a minute amount of free F-ions (Table 4). When a current was applied, the F-electrode did not provide a stable reading and thus it could not be determined if the current was influencing the amount of free F-ions or not. A comparable unstable reading as it was observed in the buffer could also be observed when repeating the same experiment in water or saline solution.

4   Discussion

4.1   Strontium attachment and the influence of fluorine

XPS results demonstrated a successful coating of Ti and TiZr with Sr and suggested an effect of the additional F present during the coating process. Moreover, the results suggested that the effect of F during polarization was not random but dependent on how the F was administered. The trends observed for the different groups appeared to be comparable for Ti and TiZr, although there were also some minor differences. When F was present in the buffer during polarization, it appeared to increase the total amount of Sr that was attached to the surface. By contrast, when F was already absorbed to the surface before polarization, it appeared to hinder Sr-attachment. The positive effect of F in the buffer on Sr-uptake during polarization was concluded from Sr+NaF groups, which showed the highest Sr content of all groups after electro-coating. Moreover, this was the only treatment that had F in the buffer. By contrast, the F detected for all other groups either was present on the coin already or must have derived from another source. Only the Sr+HFp group was intentionally doped with F prior to polarization with Sr. Nevertheless, the results revealed the presence of F even for SBAE samples. It was believed that this F derived from handling of the samples by use of PTFE bars during sand-blasting and acid-etching. Likewise, the F for the Sr and Sr+NaCl groups was believed to have derived from the handling bars or was a trace element of the Sr-acetate. Young and Otagawa showed similar F contaminations in presumably pure Sr-rods [25]. F appeared to have no effect on Sr-attachement, as it was confirmed by the correlation study that showed no direct correlation between a surface's Sr-content and F-content. Moreover, Ti Sr showed more Sr than F on the surface and Ti Sr+NaCl showed comparably high F levels and comparably low Sr levels, which indicated that there was no imperative presence of F for binding Sr.

The results of the XPS analysis allowed hypothesizing on the mechanisms involved in binding Sr on the surface during the coating and the role of F in this process. As the results for Sr-coated groups without F in the buffer revealed only a single doublet of Sr peaks (Fig. 1 B, D) at almost identical binding energies, it was concluded that Sr was bound to the surface the same way for these groups. Likewise, the first doublet observed for the Sr+NaF group showed a similar binding energy and was believed to have derived from the same component while the second doublet of this group represented a component that was only present for this treatment. As a multitude of possible bonds has been reported for the specific binding energy of the doublet with Sr $3d_{5/2}$ at 133.5±0.2 eV, the binding energy itself could not be used to define the nature of this component [26]. The results presented by Vasquez et al. for the Sr 3d peak showed a characteristic shift of this peak towards higher binding energies for certain compounds [26]. When comparing the results of the study at hand to the results presented by Vasquez et al., it was believed that the Sr $3d_{5/2}$ at 133.5±0.2 eV was referring to SrO whereas the second doublet with the Sr $3d_{5/2}$ peak at 135.4±0.1 eV was associated to SrF_2. The Sr+NaF group was the only group that had F and Sr present in the buffer. These elements have a natural affinity to form SrF_2, which is highly insoluble in aqueous solution and thus precipitate from the buffer [27]. This was supported by the observations made during the preparation of the buffer that resulted in a turbid buffer solution. Assessment of the F-ion content revealed there was only a negligible amount of ionized F in the Sr+NaF buffer. The turbidity of the buffer and the lack of free F-ions in the buffer supported the hypothesis of SrF_2 formation and precipitation in the Sr+NaF buffer, although an influence of the current on liberating F-ions could not be excluded entirely. The precipitated SrF_2 may have developed a dipole moment that led to adsorption of SrF_2 at the sample's surface during polarization [28]. Alternatively, the precipitated SrF_2 may have developed a surface charge as it is commonly observed for solid particles that are dispersed in polar solutions. In either case, the precipitated SrF_2 was likely bond to the sample's surface due to the charged sample surface and its high surface roughness and the complex surface chemistry that included titanium-hydride and titanium-hydroxide on the surface that may have bond SrF_2 by hydrogen bonds and van der Waals forces. Moreover, the Ti-O-H-Sr film that was developing on the surface simultaneously (lower energy Sr $3d_{5/2}$ doublet) may have further embedded the SrF_2 particles. This may also explain the unusual peak positions observed in the XPS. This hypothesis agreed with the findings of this study as it may explain the positive effect of F in the Sr-buffer on increasing surface Sr-levels while F already present appeared to have no beneficial effect on Sr-binding. Anyhow, the precise mechanism involved in the incorporation of Sr and the role of F in the buffer during in this process remained unknown.

Comparison of the results of this study to the results presented by Young and Otagawa for the analysis of pure strontium after argon ion etching may explain the presence of the additional C 1s peaks at higher binding energies [25]. Their study concluded that a C 1s peak of such a higher binding energy indicated the presence of $SrCO_3$. Moreover, they also concluded that the shift in the Sr $3d_{5/2}$ binding energy was not greater than 1 eV for the SrO to SrF_2 transition and that SrO, $SrCO_3$, and $Sr(OH)_2$ could not be distinguished by the Sr $3d_{5/2}$ peak.

When comparing Ti Sr+NaF to TiZr Sr+NaF, the second doublet with the Sr $3d_{5/2}$ peak at 135.4±0.1 eV was more dominant for TiZr Sr+NaF. It appeared as if the alloying element Zr had a positive effect on adsorbing SrF_2 onto the surface. This finding was supported by the analysis of the C 1s and Sr 3p peaks that also showed a tendency towards higher binding energies.

Apart from the results for Sr and F, the results for Sr-coated samples of both materials revealed some common trends among the different groups. The decreased titanium levels observed for all Sr-coated samples indicated a masking effect of the surface coating. Such a masking effect has previously been described by Morra et al. for a surface coating with collagen [29]. Sr was not the only element that adsorbed on the surface during electro-coating. Trace elements, such as Cu, Na, Cl, Zn, and Si, also attached to the surface during polarization and also masked the surface. These trace elements were believed to have derived from impurities in the acetic acid or from the NaCl the coins were stored in prior to coating. Besides the masking of the original surface, all Sr-coated samples showed a trend towards decreased surface oxygen and increased surface carbon content. The decrease in surface oxygen was believed to have been a direct result of the polarization process, while the increase in carbon may have had two possible sources. The hydrogen-rich, reactive surface created by the polarization process was believed to be more reactive and thus would take up carbon from the surrounding air. Another, more likely carbon source was remaining contaminations from the acetate buffer that had not been removed during the rinsing of the samples due to the high surface roughness. Handling of the samples after coating with nitrile gloves may also have contaminated the surface with carbon. This may also explain the elevation in N observed for most of the coated samples.

4.2   Surface topography and morphology

Sr+NaF surface modification revealed visible changes to the surface nano-topography compared to the SBAE surfaces [24]. XPS analysis that revealed this group had a significant amount of SrF_2, which is usually crystalline [30], on the surface. Thus, it was likely that the observed nano nodules could have been precipitated, crystalline SrF_2. Yet, this could not be confirmed as the resolution of the SEM did not allow a precise analysis of the surface structure itself.

4.3   Assessment of the biological response

The biological response of the osteoblastic MC3T3-E1 cells to Sr-coated Ti and TiZr revealed a positive effect of the surface modification. When comparing the results of the study at hand to the temporal expression presented by Quarles et al. [31] and Monjo et al. [32], it was believed that the Ti pol group tended towards a marginally earlier differentiation of the cells compared to Ti SBAE. By contrast, TiZr pol did not show any significant difference in cell differentiation compared to TiZr SBAE. As the pol groups did not have any Sr on the surface, it was concluded that the surface modification itself had a beneficial effect to the biological response for Ti independent of the Sr. None of the surface modifications was toxic to the cells as the absolute values were comparably low. However, the increased LDH activity of TiZr Sr explains the gene expression profile of this group, with higher gene expression of the proliferative marker Coll-1 and lower expression of the differentiation marker OC. As the treatment resulted in an increased toxicity, the cells cultured on this surface were still in a proliferative stage rather than in a differentiation stage.

The observations made for Sr+NaF modified groups were in accordance with the the findings of Marie et al. who reported that Sr supported bone formation by activating pre-osteoblast replication and osteoblast differentiation and survival [12, 13]. It has been shown that Sr increases ALP and collagen-I gene expression and leads to increased mineralization in MC3T3-E1 cells

[33, 34]. It has been demonstrated that Sr activates the calcium-sensing receptor, calcineurin-NFAT (nuclear factor of activated T cells) and Wnt signalling pathways in the mechanism that controls bone formation [33, 34]. Anyhow, there was only a correlation between expression of Coll-1 and the Sr content of a surface in this study.

It appeared that the surface that had additional SrF_2 alongside a majority of Sr bound as SrO on the surface performed best in terms of cell differentiation as it was concluded from the Ti Sr+NaF group. It was believed that this surface had the best combination of bioavailable SrO and SrF_2. It has been shown for polyacid-modified composite resins that SrF_2 released F-ions in different solutions [35-37]. Thus, the additional SrF_2 did not only provide bioavailable Sr but also F that has also been shown to have a positive effect of cell differentiation [7-11]. Furthermore, it was believed that the unreactive SrF_2 on top of the reactive surface shielded it from undesired contaminations during handling and storage [19, 38, 39]. It has been established that Sr-oxides strongly chemisorb carbon dioxide and water to form surface carbonate and surface hydroxide [25]. XPS analysis supported this conclusion as the Sr+NaF groups had the lowest carbon and nitrogen content of all Sr-coated groups. The maintained reactivity of the surface in combination with bioavailable Sr was likely to have triggered the improved cell differentiation by the aforementioned mechanism. This may also have been the reason why the groups that had SrO but no SrF_2 did not show any significant difference in cell differentiation against the SBAE surface that was already highly reactive [19]. This was supported by the XPS results that also showed comparably lower surface carbon and no nitrogen for the SBAE groups. On the other hand TiZr Sr+NaF had more SrF_2 than SrO on the surface but showed no significantly increased cell differentiation despite its low surface contamination. It appeared that there was an ideal surface ratio of SrO and SrF_2 content that triggered the increased cell differentiation. As this study did not use protective cover gas to prevent surface contaminations after the coating, this may offer a chance to further improve the described surface although it may also make a group without SrF_2 just as reactive while offering bioavailable Sr from the SrO at the same time.

5   Conclusion

It was concluded that F appeared to support the attachment of Sr to the surface, when was present in the buffer during polarization. By contrast, when F was already absorbed to the surface before polarization, it appeared to hinder Sr-attachment. The XPS results and analysis of the buffer suggested that the presence of F in the buffer led to the formation of SrF_2 that attached to the surface. SEM images showed nano-nodules that were homogeneously distributed over the whole surface of Sr+NaF groups and may have been related to the precipitated SrF_2. It was concluded that a combination of bioavailable Sr from the Sr-oxide and a protective SrF_2 layer that maintained the reactive surface while maintaining active amounts of Sr bioavailable from the SrO was most desirable in terms of cell differentiation.

Acknowledgements

References

[1] Albrektsson T, Sennerby L, Wennerberg A. State of the art of oral implants. Periodontol 2000 2008;47:15-26.

[2] Wennerberg A, Albrektsson T. Current challenges in successful rehabilitation with oral implants. J Oral Rehabil 2011;38:286-94.

[3] Albouy JP, Abrahamsson I, Persson LG, Berglundh T. Spontaneous progression of peri-implantitis at different types of implants. An experimental study in dogs. I: clinical and radiographic observations. Clin Oral Implants Res 2008;19:997-1002.

[4] Palma-Carrio C, Maestre-Ferrin L, Penarrocha-Oltra D, Penarrocha-Diago MA, Penarrocha-Diago M. Risk factors associated with early failure of dental implants. A literature review. Med Oral Patol Oral Cir Bucal 2011;16:e514-7.

[5] Moy PK, Medina D, Shetty V, Aghaloo TL. Dental implant failure rates and associated risk factors. Int J Oral Maxillofac Implants 2005;20:569-77.

[6] Heitz-Mayfield LJ. Peri-implant diseases: diagnosis and risk indicators. J Clin Periodontol 2008;35:292-304.

[7] Morra M. Biochemical modification of titanium surfaces: peptides and ECM proteins. Eur Cell Mater 2006;12:1-15.

[8] Taxt-Lamolle SF, Rubert M, Haugen HJ, Lyngstadaas SP, Ellingsen JE, Monjo M. Controlled electro-implementation of fluoride in titanium implant surfaces enhances cortical bone formation and mineralization. Acta Biomater 2010;6:1025-32.

[9] Le Guehennec L, Soueidan A, Layrolle P, Amouriq Y. Surface treatments of titanium dental implants for rapid osseointegration. Dent Mater 2007;23:844-54.

[10] Zhao L, Chu PK, Zhang Y, Wu Z. Antibacterial coatings on titanium implants. J Biomed Mater Res B Appl Biomater 2009;91:470-80.

[11] Petzold C, Gomez-Florit M, Lyngstadaas SP, Monjo M. EPA covalently bound to smooth titanium surfaces decreases viability and biofilm formation of Staphylococcus epidermidis in vitro. J Orthop Res 2012;30:1384-90.

[12] Marie PJ, Felsenberg D, Brandi ML. How strontium ranelate, via opposite effects on bone resorption and formation, prevents osteoporosis. Osteoporos Int 2011;22:1659-67.

[13] Marie PJ, Ammann P, Boivin G, Rey C. Mechanisms of action and therapeutic potential of strontium in bone. Calcif Tissue Int 2001;69:121-9.

[14] Peng S, Zhou G, Luk KD, Cheung KM, Li Z, Lam WM, et al. Strontium promotes osteogenic differentiation of mesenchymal stem cells through the Ras/MAPK signaling pathway. Cell Physiol Biochem 2009;23:165-74.

[15] Tsiridis E, Gamie Z, Conaghan PG, Giannoudis PV. Biological options to enhance periprosthetic bone mass. Injury 2007;38:704-13.

[16] Maimoun L, Brennan TC, Badoud I, Dubois-Ferriere V, Rizzoli R, Ammann P. Strontium ranelate improves implant osseointegration. Bone 2010;46:1436-41.

[17] Lyngstadaas SP, Ellingsen JE, Astra Tech AB. Medical Prosthetic Devices and implants having improved biocompatibility. WO Patent: WO/2002/045,764; 2002.

[18] Bernhard N, Berner S, De Wild M, Wieland M. The binary TiZr Alloy – a newly developed Ti alloy for use in dental implants. Forum Implantol 2009;5:30–9.

[19] Rupp F, Scheideler L, Olshanska N, de Wild M, Wieland M, Geis-Gerstorfer J. Enhancing surface free energy and hydrophilicity through chemical modification of microstructured titanium implant surfaces. J Biomed Mater Res A 2006;76:323-34.

[20] Szmukler-Moncler S, Bischof M, Nedir R, Ermrich M. Titanium hydride and hydrogen concentration in acid-etched commercially pure titanium and titanium alloy implants: a comparative analysis of five implant systems. Clin Oral Implants Res 2010;21:944-50.

[21] Frank MJ, Walter MS, Lyngstadaas SP, Haugen HJ. Polarization of modified titanium and titanium-zirconium creates nano-structures while hydride formation is modulated. Appl Surf Sci (in submission, minor revisions)2013.

[22] Satue M, Petzold C, Cordoba A, Ramis JM, Monjo M. UV photoactivation of 7-dehydrocholesterol on titanium implants enhances osteoblast differentiation and decreases Rankl gene expression. Acta Biomater 2013;9:5759-70.

[23] Borenstein M, Cohen J, Rothstein HR, Pollack S, Kane JM. A Visual Approach to Statistical Power Analysis on the Microcomputer. Behav Res Meth Ins C 1992;24:565-72.

[24] Frank MJ, Walter MS, Lyngstadaas SP, Wintermantel E, Haugen HJ. Hydrogen content in titanium and a titanium–zirconium alloy after acid etching. Mat Sci Eng C 2013;33:1282-8.

[25] Young V, Otagawa T. Xps Studies on Strontium Compounds. Appl Surf Sci 1985;20:228-48.

[26] Vasquez RP. X-Ray Photoelectron-Spectroscopy Study of Sr and Ba Compounds. J Electron Spectrosc Relat Phenom 1991;56:217-40.

[27] Kmetko J, Yu C, Evmenenko G, Kewalramani S, Dutta P. Organic-template-directed nucleation of strontium fluoride and barium fluoride: Epitaxy and strain. Phys Rev B 2003;68:085415.

[28] Beaumont JH, Harmer AL, Hayes W, Spray ARL. Zero-phonon lines in CaF 2 and SrF 2. J Phys C 1972;5:1489.

[29] Morra M, Cassinelli C, Cascardo G, Cahalan P, Cahalan L, Fini M, et al. Surface engineering of titanium by collagen immobilization. Surface characterization and in vitro and in vivo studies. Biomaterials 2003;24:4639-54.

[30] Bochner RA, Abdulrahman A, Nancollas GH. Crystal-Growth of Strontium Fluoride from Aqueous-Solution. J Chem Soc Faraday Trans 1984;80:217-24.

[31] Quarles LD, Yohay DA, Lever LW, Caton R, Wenstrup RJ. Distinct proliferative and differentiated stages of murine MC3T3-E1 cells in culture: an in vitro model of osteoblast development. J Bone Miner Res 1992;7:683-92.

[32] Monjo M, Rubert M, Ellingsen JE, Lyngstadaas SP. Rosuvastatin promotes osteoblast differentiation and regulates SLCO1A1 transporter gene expression in MC3T3-E1 cells. Cell Physiol Biochem 2010;26:647-56.

[33] Takaoka S, Yamaguchi T, Yano S, Yamauchi M, Sugimoto T. The Calcium-sensing Receptor (CaR) is Involved in Strontium Ranelate-induced Osteoblast Differentiation and Mineralization. Horm Metab Res 2010;42:627-31.

[34] Fromigue O, Hay E, Barbara A, Marie PJ. Essential role of nuclear factor of activated T cells (NFAT)-mediated Wnt signaling in osteoblast differentiation induced by strontium ranelate. J Biol Chem 2010;285:25251-8.

[35] Geurtsen W, Leyhausen G, Garcia-Godoy F. Effect of storage media on the fluoride release and surface microhardness of four polyacid-modified composite resins ("compomers"). Dent Mater 1999;15:196-201.

[36] Sales D, Sae-Lee D, Matsuya S, Ana ID. Short-term fluoride and cations release from polyacid-modified composites in a distilled water, and an acidic lactate buffer. Biomaterials 2003;24:1687-96.

[37] Xu X, Burgess JO. Compressive strength, fluoride release and recharge of fluoride-releasing materials. Biomaterials 2003;24:2451-61.

[38] Massaro C, Rotolo P, De Riccardis F, Milella E, Napoli A, Wieland M, et al. Comparative investigation of the surface properties of commercial titanium dental implants. Part I: chemical composition. J Mater Sci Mater Med 2002;13:535-48.

[39] Taborelli M, Jobin M, Francois P, Vaudaux P, Tonetti M, Szmukler-Moncler S, et al. Influence of surface treatments developed for oral implants on the physical and biological properties of titanium. (I) Surface characterization. Clin Oral Implants Res 1997;8:208-16.
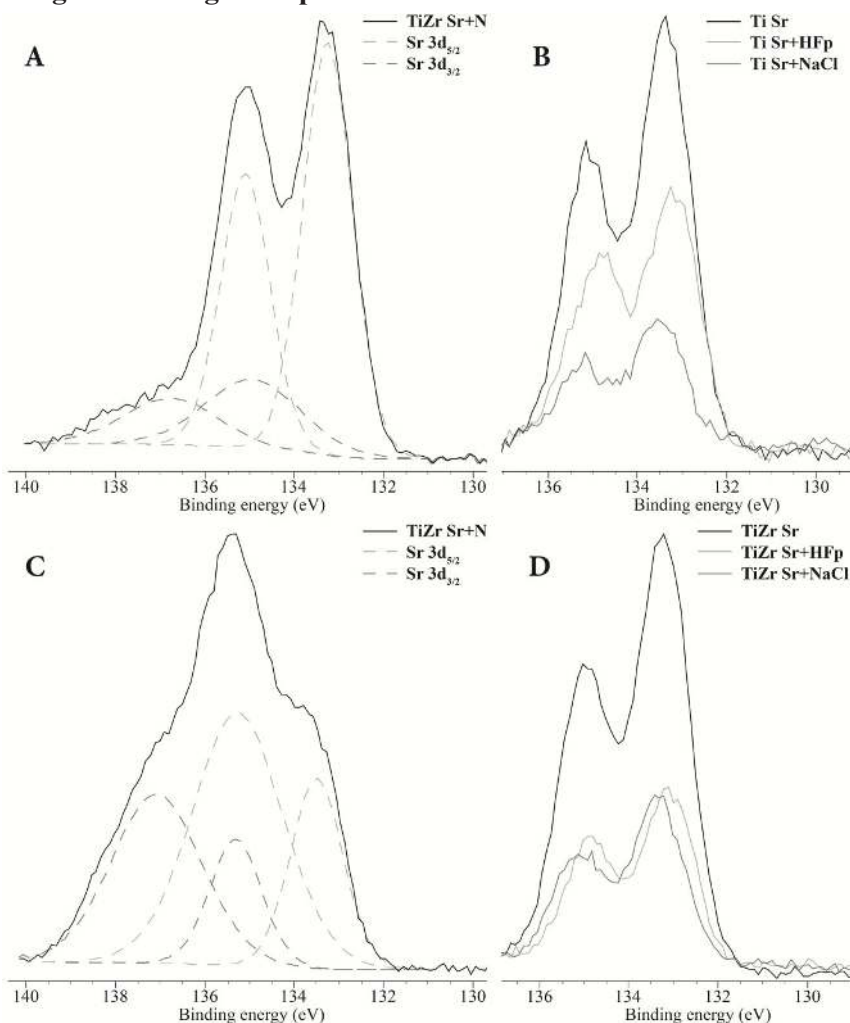
Figures and figure captions

Fig. 1 XPS detail spectra of the Sr 3d peak with the peak position (eV) on the x-axis and the relative peak intensity on the y-axis (a.u.). The groups polarized with Sr+NaF (A, C) revealed a second doublet of Sr $3d_{5/2}$ and Sr $3d_{3/2}$ peaks (dashed lines in A, C), whereas there was only one doublet all other groups (B, D). The precise peak positions were provided in Table 3.
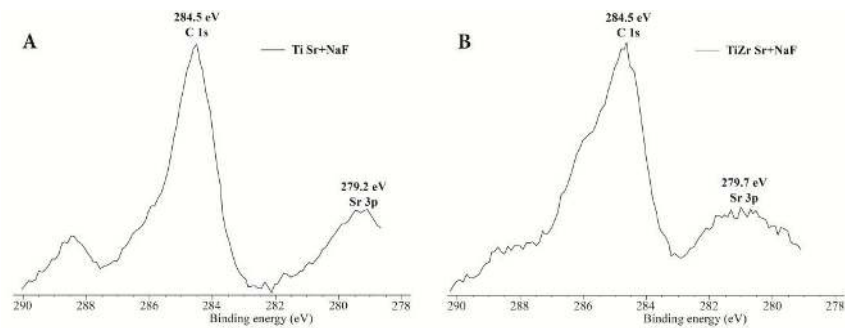
Fig. 2 XPS detail spectra of the C 1s peak and Sr 3p peak with the peak position (eV) on the x-axis and the relative peak intensity on the y-axis (a.u.). The Sr 3p peak of Ti Sr+NaF (A) showed had a peak shape that was comparable for all other groups while TiZr Sr+NaF (B) showed a shift of the Sr 3p peak towards the C 1s peak that resulted in a merging of the peaks.
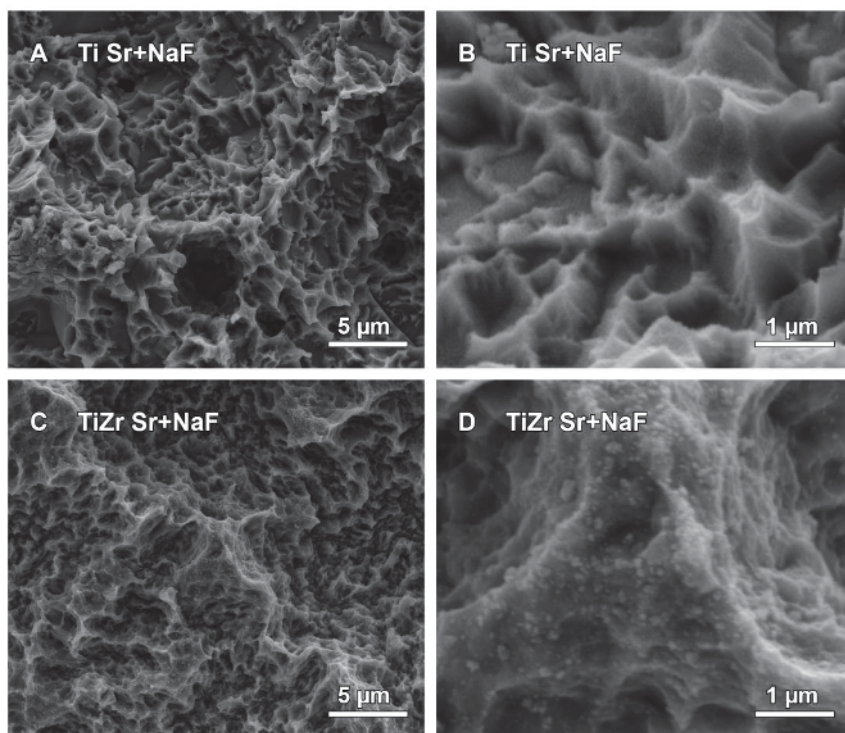

Fig. 3 SEM images of Ti Sr+NaF (A, B) and TiZr Sr+NaF (C, D).

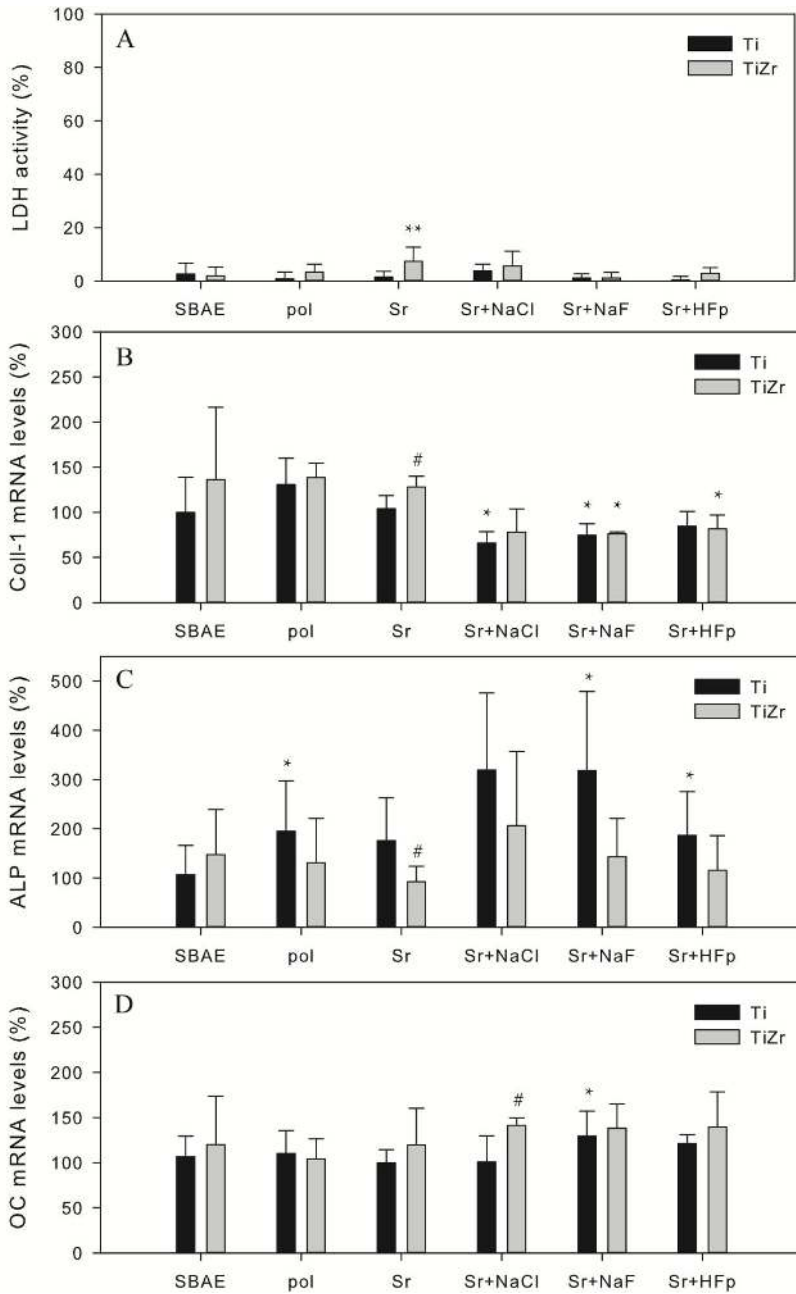Fig. 4 LHD activity (A) was displayed relative to cells cultured on plastic control whereas gene expression of Coll-1 (B), ALP (C), and OC (D) were displayed relative to the Ti SBAE group as the mean values with standard deviation. Student t- test revealed significant (*p≤ 0.05) and highly significant (**p≤ 0.01) differences for (*) electro-coated vs. SBAE samples and for (#) Ti group vs. TiZr group.

Tables and table captions

Table 1 Different surface modification groups used in this study. The given abbreviations were used in combination with the abbreviations Ti and TiZr for the materials used in this study (titanium and titanium-zirconium alloy).

Group	Surface modification
SBAE	Sand-blasted and acid-etched surface that was comparable to the Straumann SLActive® surface
pol	Polarized only group 2 M Acetic acid and sodium-acetate buffer, pH=5
Sr	Sr-coated group 0.25 M Acetic acid and Sr-acetate buffer, pH=5
Sr+NaCl	Sr-coated group with additional NaCl in the buffer 0.25 M Acetic acid and Sr-acetate buffer with 0.1M NaCl, pH=5
Sr+NaF	Sr-coated group with additional NaF in the buffer 0.25 M Acetic acid and Sr-acetate buffer with 0.1M NaF, pH=5
Sr+HFp	Sr-coated group with pickling in 0.2% HF for 2 min before electro-coating 0.25 M Acetic acid and Sr-acetate buffer, pH=5

Table 2 XPS element analysis for all groups. In addition, minor amounts of the trace elements copper, silicon, nitrogen and zinc were observed for some groups (results not shown).

Name	Ti SBAE (at.%)	Ti Sr (at.%)	Ti Sr +NaCl (at.%)	Ti Sr +NaF (at.%)	Ti Sr HFp (at.%)	TiZr SBAE (at.%)	TiZr Sr (at.%)	TiZr Sr +NaCl (at.%)	TiZr Sr +NaF (at.%)	TiZr Sr HFp (at.%)
O 1s	54.24	45.14	46.98	48.90	42.37	53.73	44.25	44.53	41.74	44.14
C 1s	22.74	31.58	28.42	21.60	25.47	20.72	30.38	28.81	26.39	31.48
Sr 3d		2.17	0.51	4.26	1.14		3.74	1.55	4.08	1.34
F 1s	1.29	2.03	1.87	5.70	4.98	0.78	3.14	1.21	7.43	1.70
Cl 2p		0.23	0.90	0.78	0.78	1.55	1.31	2.18	1.03	0.77
Ti 2p	21.73	16.07	17.89	17.57	17.43	19.43	11.91	12.36	13.06	14.56
Na KLL			1.24	0.85	4.50	0.78		0.86		
Zr 3d						2.9	2.09	2.08	1.94	1.47

Table 3 Binding energies of the Sr $3d_{5/2}$ and Sr $3d_{3/2}$ peaks from the 1st and 2nd doublet acquired by XPS.

Peak	Ti Sr	Ti Sr +NaCl	Ti Sr +NaF	Ti Sr +HFp	TiZr Sr	TiZr Sr +NaCl	TiZr Sr +NaF	TiZr Sr +HFp
1st Sr $3d_{5/2}$	133.3 eV	133.2 eV	133.2 eV	133.1 eV	133.2 eV	133.4 eV	133.4 eV	133.1 eV
1st Sr $3d_{3/2}$	135.0 eV	135.1 eV	135.0 eV	134.8 eV	134.9 eV	135.2 eV	135.2 eV	134.8 eV
2nd Sr $3d_{5/2}$			135.0 eV				135.2 eV	
2nd Sr $3d_{3/2}$			136.5 eV				137.0 eV	

Table 4 Correlation study results. The results were interpreted as follows: no correlation if $|r| < 0.3$, correlation if $0.3 \leq |r| < 0.5$, and strong correlation if $0.5 \leq |r| \leq 1$ [23]. Significance levels were set to significant *$p \leq 0.05$ and highly significant **$p \leq 0.01$. Only results that were correlating and statistically significant were marked.

	Sr vs. F	Sr vs. Coll-1	Sr vs. ALP	Sr vs. OC
r	0.595	-0.368**	0.158	0.268
p	0.102	0.000	0.108	0.006
n	8	109	104	106

Table 5 Assessment of the F-ion concentration in the Sr and Sr+NaF buffer with an ion-selective electrode. When the measurement was done while a current was applied, no stable reading could be recorded and thus the area of the readings was given.

Buffer	Current density (mA/cm²)	F-concentration (M)
Sr buffer	0	0
Sr buffer	0.54	0.0003 – 0.55
Sr buffer	1.30	0.0009 – 0.68
Sr+NaF buffer	0	0.0009
Sr+NaF buffer	0.54	0.0020 – 0.38
Sr+NaF buffer	1.30	0.0026 – 0.41